The Catalysed Activation of *n*-Octane over Iron Modified Hydroxyapatites

Drushan Padayachee

2014

The Catalysed Activation of *n*-Octane over Iron Modified Hydroxyapatites

by

Drushan Padayachee

This thesis has been submitted in fulfillment of the academic requirements for the degree of

Master of Science

In the School of Chemistry and Physics
University of KwaZulu-Natal
Durban
Westville
4000

May 2014

As the candidate's supervisor I have approved this thesis/dissertation for submission.

Signed: _____ Name: Prof. Holger B. Friedrich Date: _____

Signed: _____ Name: Dr. S. Singh Date: _____

Preface

The experimental work described in this thesis was carried out at the School of Chemistry and Physics, College of Agriculture, Engineering and Science, University of KwaZulu-Natal, Durban from February 2012 to February 2014 under the supervision of Professor H. B. Friedrich and Doctor S. Singh.

These studies represented original work by the author and have not otherwise been submitted in any form for any degree or diploma to any tertiary institution. Where use has been made of work done by others, it is duly acknowledged in the text.

Declaration 1 – Plagiarism

I, Drushan Padayachee, declare that:

1. The research reported in this thesis, except where otherwise indicated, is my original research.
2. This thesis has not been submitted for any degree or examination at any other university.
3. This thesis does not contain other persons' data, pictures, graphs or other information, unless specifically acknowledged as being sourced from other persons.
4. This thesis does not contain other persons' writing, unless specifically acknowledged as being sourced from other researchers. Where other written sources have been quoted, then:
    a. Their words have been re-written but the general information attributed to them has been referenced.
    b. Where their exact words have been used, then their writing has been placed in italics and inside quotation marks, and referenced.
5. This thesis does not contain text, graphics or tables copied and pasted from the Internet, unless specifically acknowledged, and the source being detailed in the thesis and in the References sections.

_____

Drushan Padayachee

As the candidate's supervisors we approve this thesis/dissertation for submission

_____ _____

Prof. Holger B. Friedrich Dr. Sooboo Singh

This thesis is dedicated to my late grandparents, Dr. D. N. Padayachee and Mrs. R. Padayachee.

Acknowledgements

My sincere thanks and appreciation are extended to the following people who enabled me to complete this research project successfully:

1. To my financial supporters, SASOL, THRIP and the NRF, I hereby acknowledge with due appreciation

2. Prof. H. B. Friedrich and Dr. S. Singh, my supervisors, for their assistance and guidance.

3. Dr V. D. B. C. Dasireddy, UKZN School of Chemistry and Physics, for his unwavering assistance, pep talks and guidance with my studies and more especially with this project.

4. My friend, Kershen Naicker, for all his assistance with the experimental aspect of the project and words of encouragement.

5. Friends and colleagues at the UKZN Catalysis Research Group, and the UKZN School of Chemistry and Physics for their on-going motivation and assistance during my laboratory work.

6. Alisa Govender from SASOL Research and Development for her assistance with the scanning electron microscopy imaging and energy dispersive X-Ray spectroscopy analysis of the catalysts.

7. My family, Thiag, Fazila and Seryosha, for all their valuable assistance in the proof reading and compilation of this thesis.

8. Santo and Kenzo our family dogs, for providing a distraction when studies became too much to bare.

9. Seryosha, my sister, for the constant encouragement to be the best and for believing that I am very good at what I do.

10. My parents, Thiag and Fazila, for their love, care and words of encouragement that I can be anything I want to, just so long as I believe in myself. Thank you for guiding me and helping me become the well-grounded individual that I am.

‘Obstacles cannot crush me; every obstacle yields to stern resolve’

Leonardo da Vinci

Abstract

This research effort investigated the activation of *n*-octane by oxidative dehydrogenation and dehydrogenation over iron substituted and iron supported on hydroxyapatite catalysts. Pure hydroxyapatite and iron substituted hydroxyapatite were prepared using a co-precipitation method and the iron supported on hydroxyapatite catalysts were prepared using a single wet impregnation technique. The weight percentages of iron in both the catalyst materials varied between 1 – 9 %. The catalysts were characterized by inductively coupled plasma optical emission spectroscopy, powder X-ray diffraction, Fourier transform infrared spectroscopy, Raman spectroscopy, scanning electron microscopy, energy dispersive X-ray spectroscopy, transmission electron microscopy and temperature programmed reduction and oxidation. The BET surface area and nitrogen adsorption and desorption isotherms were also determined.

The iron supported on hydroxyapatite catalysts existed as bi-phasic materials of which the dominant phase was assigned to non-stoichiometric hydroxyapatite. The second phase was identified as hematite. The iron substituted hydroxyapatite catalysts were found to exist as a single phase non-stoichiometric hydroxyapatite. All the catalyst materials were hexagonally shaped, mesoporous nanoparticles and were stable under the conditions tested. The iron supported on hydroxyapatite catalysts showed the distribution of iron on the surface of the support with an aggregation of hematite clusters at certain locations. The distribution of iron in the iron substituted hydroxyapatite catalysts occurred throughout the hydroxyapatite-like materials. This suggested that calcium cations were substituted with iron cations within the apatite structure.

Catalytic testing was performed in a continuous flow fixed-bed tubular stainless steel reactor, operated in a down-flow mode, using air as the oxidant and nitrogen as the diluent gas. Reactions were carried out over a temperature range of 350 – 550 °C with 50 °C increments. Gas flow rates were varied to attain gas hourly space velocities of 4000, 6000 and 8000 h^{-1}. The carbon to oxygen ratios employed were 8:0, 8:2, 8:4 and 8:6, the first of which corresponded to anaerobic or dehydrogenation conditions. The catalyst bed was maintained at a volume of 1 cm^3 with pellet

sizes ranging between 600 – 1000 μm and 300 – 600 μm. The reaction product stream was analysed using two gas chromatographs, one fitted with a thermal conductivity detector, and the other with a flame ionization detector. A gas chromatograph coupled to a mass spectrometer was also used intermittently for qualitative assays. For blank runs, when the reactor tube was filled with carborundum only, conversions ranging between 1 – 6 % were obtained. Octene isomers, aromatic compounds, cracked products and carbon oxides were identified in the product stream. The product classes targeted in this study were octene isomers, C8 aromatic compounds and C8 oxygenated compounds. The use of the catalysts gave greater conversion and greater selectivity towards desired products when compared to the blank reactor runs. The catalytic performance of hydroxyapatite was improved upon modification with iron. The highest conversion was observed over the 9 % (by weight) iron supported on hydroxyapatite catalyst. However, this catalyst showed low selectivity towards the targeted value added products and showed high selectivity towards undesirable cracked oxygenated compounds (methanol, ethanol, 2-propanol and acetone) ranging between 18 – 46 mol% over the temperature range investigated. The highest selectivity towards C8 value added products was 83 mol% at a conversion of 7 mol% over the 3 wt% iron substituted catalyst.

Conference Contributions

Part of the work discussed in this thesis was presented at the following conferences:

1. 'Synthesis and characterisation of iron hydroxyapatite catalysts for the oxidative dehydrogenation of *n*-octane'
   Drushan Padayachee, Sooboo Singh and Holger B. Friedrich
   CATSA Conference: Langebaan, 2012, poster presentation

2. 'Activation of *n*-octane over iron modified hydroxyapatite catalysts'
   Drushan Padayachee, Holger B. Friedrich and Sooboo Singh
   EUROPACAT Conference: Lyon, France, 2013, poster presentation

3. 'Oxidative dehydrogenation of *n*-octane over iron hydroxyapatite catalysts'
   Drushan Padayachee, Holger B. Friedrich and Sooboo Singh
   CATSA Conference: Wild Coast Sun, KwaZulu-Natal, 2013, poster presentation

Table of Contents

Calculations

The products of the catalysed reactions were expressed as conversion, selectivity and yield. Conversion is a measure of the amount of feed introduced into the reactor that is converted into products:

$$\text{Conversion} = \frac{\text{moles of n-octane reacted}}{\text{moles of n-octane in feed}} \times \frac{100}{1}$$

The selectivity towards a product may be defined as the ratio of that product formed to the total moles of products formed, based on carbon atoms:

$$\text{Selectivity} = \frac{\text{moles carbon of product}}{\text{conversion}} \times \frac{100}{1}$$

The yield is the molar fraction of a particular product formed to the total number of moles of feed introduced:

$$\text{Yield} = \text{selectivity} \times \text{conversion}$$

The gas hourly space velocity (GHSV) was calculated as follows:

$$\text{GHSV} = \frac{\text{total flow rate (mL/h)}}{\text{volume of catalyst (mL)}}$$

Abbreviations

1-COP	-	1% iron (by weight) substituted hydroxyapatite
3-COP	-	3% iron (by weight) substituted hydroxyapatite
9-COP	-	9% iron (by weight) substituted hydroxyapatite
1-WET	-	1% iron (by weight) supported on hydroxyapatite
3-WET	-	3% iron (by weight) supported on hydroxyapatite
9-WET	-	9% iron (by weight) supported on hydroxyapatite
ATR	-	attenuated total reflectance
BSE	-	back scattered electron
C:O	-	carbon to oxygen
CO_x	-	carbon oxides
ER	-	Eley – Rideal
EDX	-	energy dispersive X-Ray spectroscopy
FCC	-	fluid catalytic cracking
FID	-	flame ionisation detector
FTIR	-	Fourier transform infrared spectroscopy
GC	-	gas chromatograph
GC-MS	-	gas chromatograph coupled to a mass spectrometer
GHSV	-	gas hourly space velocity
HAp	-	hydroxyapatite
HPLC	-	high performance liquid chromatography
ICPOES	-	inductively coupled plasma optical emission spectroscopy
MvK	-	Mars and van Krevelen
ODH	-	oxidative dehydrogenation
ppm	-	parts per million
PXRD	-	powder X-Ray diffraction
REDOX	-	reduction and oxidation
SEM	-	scanning electron microscopy
TCD	-	thermal conductivity detector

TEM	-	transmission electron microscopy
TPD	-	temperature programmed desorption
TPO	-	temperature programmed oxidation
TPR	-	temperature programed reduction

List of Figures

List of Tables

Chapter 1

Introduction and Literature Review

A catalyst is often described as a substance that facilitates a chemical reaction. This statement, however, is an oversimplified definition. A catalyst may better be described as a substance that increases the rate of a reaction without itself being consumed [1]. These statements may be further expanded by considering that a catalyst primarily influences changes in the route to equilibrium of a reaction, which further suggests that only the reaction kinetics are affected and the thermodynamics remain unaffected [2].

In industry, catalysis plays a very large role with more than 90 % of modern processes incorporating catalysed reactions [3]. The global catalyst market was expected to exceed $16 billion during 2012 with 33 % of this being allocated to environmental applications [3]. World demand for catalysis is now expected to rise 5.8 % per annum to $19.5 billion in 2016. Catalytic processes have, for many years, been used for the production of bulk commodity chemicals, and of late, are applied to processes in the pharmaceutical, agricultural (pesticides and fertilizers), water treatment and textile manufacturing sectors. Within Africa alone, in excess of six oil refineries exist, all commonly employing catalysed processes. In South Africa, there is an increasing trend in catalysed processes employed by chemical and petrochemical companies such as SASOL, Caltex/Chevron, Engen, SAPREF and PetroSA. The use of catalysis in industry has allowed for greater efficiency and chemical conversion when compared to conventional techniques. In addition to providing energy saving processes coupled with increased production rates, catalysis offers other advantages such as the ability to reuse the catalyst many times over or the ability to regenerate a ‘deactivated’ catalyst. Overall, catalysis provides a cheaper and more efficient alternative pathway in many industrial processes.

Catalysis is a multidisciplinary field. It is imperative that catalysed systems be tailored to give high conversion and simultaneously show high selectivity to desired products. To date this

dilemma remains a challenge to researchers. Very few systems exist that offer high conversion coupled with high selectivity to desired products. One often encounters catalytic systems that show high conversion with low selectivity or vice versa. These observations are generally consistent with the reactivity-selectivity principle. This principle expounds that with high reactivity (with respect to conversion) low selectivity is attained mainly due to the occurrence of unwanted side reactions.

Catalysis may be divided into three categories, namely, heterogeneous, homogenous and biocatalysis. In homogeneous catalysis, the catalyst, reactants and products exist in the same phase. Generally, homogenous catalysis takes place in a liquid phase. However, reactions in the gas phase and solid phase are common. These catalytic systems are commonly employed under relatively mild operating conditions and demonstrate good heat transfer efficiency, generally giving high selectivity towards value added products. A well-known example of an industrial homogeneously catalysed production system is the Monsanto process [4, 5] which has served, for many years, as an alternative to the synthesis of acetic acid through the aerobic action of bacteria on dilute aqueous ethanol [6]. The Monsanto process is based on the carbonylation of methanol, which is catalysed by three group nine metals, namely, cobalt, rhodium and iridium. Major disadvantages of homogeneously catalysed processes include the separation steps involved, catalyst recovery and also the treatment of toxic and/or corrosive waste, post reaction.

Heterogeneously catalysed reactions involve the catalyst, products and reactants existing in different phases. Generally, heterogeneous catalysis involves a solid catalyst material with reactants and products in a gaseous or liquid phase [1]. The majority of large scale industrial catalysed processes fall in this field. These usually employ transition metals, transition metal oxides, zeolites, silica and alumina catalysts [7]. A major advantage of a heterogeneously catalysed reaction is the relative ease of separation of the catalysts, reactants and products. Heterogeneous catalysis is a widely researched field as it plays an important role in modern industry, particularly in the petrochemical and pharmaceutical sectors. Well known catalysed processes involve the use of phosphoric acid in the polymerisation of alkanes, gold in the decomposition of hydrogen peroxide, iron for ammonia synthesis, nickel for the

hydrogenation of benzene, zeolites in the cracking of crude oil, cobalt, nickel, tungsten and molybdenum in the hydro-treatment of crude oil, chromium in the polymerisation of alkenes, and platinum and palladium and rhodium in catalytic converters in the automotive industry [3]. Styrene is commercially produced by the dehydrogenation of the alkyl substituent of ethylbenzene in the presence of a potassium promoted iron catalyst [8]. It is an important monomer of polymers used in the petrochemical industry. In excess of 20 million tons of this aromatic compound is produced world-wide [8, 9]. The deactivation of iron catalysts by coke deposition, as well as changes in oxidation state and physical degradation, are important factors to consider [9] and thus were taken into consideration for this study.

Heterogeneously catalysed reactions may be made complicated by gas-solid or solid-liquid interfaces depending on the phase compositions of the reactants and catalyst. Essentially, a heterogeneously catalysed reaction may be governed by physical and chemical steps [10]. These physical and chemical steps may result from physical adsorption (physisorption) involving interactions between the surface of the catalyst and the substrate, commonly referred to as van der Waals forces, or chemisorption involving the formation of chemical bonds between the catalyst surface atoms and the adsorbed species respectively. A heterogeneously catalysed gas phase reaction initially begins with the adsorption of a reactant molecule on the surface of a catalyst. Upon this interaction, the reactant's intermolecular chemical bonds weaken and may result in bond breakage and radical formation. The activated adsorbed species then undergoes a reaction, which usually consists of several consecutive steps [11]. Finally, the adsorbed products desorb back into the gas phase and lead to the regeneration of the active site. This is not always the case as one often encounters a phenomenon known as coking [12-16]. This generally involves a strong interaction between reaction products and an active site through chemisorption [9]. Coking is one of the many types of catalyst deactivation known to inhibit catalytic performance. The activity of a solid catalyst may be affected by several factors. The most important of which include the available surface area, structural properties of the solid material (this may include the nature of the crystal lattice), pore size, surface geometry, phase composition and electronic structure.

In industry, the key processes involving heterogeneously catalysed reactions are oxidation, oxidative dehydrogenation, cracking, preferential oxidation, dehydrogenation and hydrogenation. This study focused on the preparation and characterisation of iron modified hydroxyapatites and use of these materials as catalysts in the oxidative dehydrogenation of gaseous *n*-octane.

1.1 Principles of alkane oxidative dehydrogenation

As the demand for activated paraffins, functionalised alkanes and aromatics increases, so does the research into alternate sources of feed-stocks [17]. Paraffins are easily obtainable from natural gas and petroleum. They are by-products formed from coal-to-liquid and gas-to-liquid plants, which have seen an increase in number worldwide [18]. In excess of 1 million tons of these paraffins are produced by gas-to-liquid plants worldwide per annum. Thus the need to activate these relatively inert paraffins has become an increasingly interesting field.

Paraffins or alkanes are saturated hydrocarbons with a general formula of C_nH_{2n+2}. They are generally considered as relatively unreactive compounds when compared to alkenes and alkynes, both respectively characterised by double or triple bonds composed of strong σ bonds and weak π bonds [19]. The relatively unreactive nature of alkanes is primarily due to the presence of strong σ bonds only. Another contributing factor is the equal sharing of electrons in their C-H and C-C covalent bonds. This results in these compounds having no significant charge and rendering them incapable of attracting either nucleophiles or electrophiles [19, 20]. These properties have created the need for extreme reaction conditions for their activation. A generally accepted trend in the homologous series of alkanes is a decrease in the energy required for activation with an increase in chain length. This inverse relationship makes higher alkanes, such as *n*-octane, easier to work with.

Alkenes are unsaturated hydrocarbons with a general formula of C_nH_{2n} and are more reactive than alkanes. Their higher reactivity is attributed to the nucleophilic nature of these compounds, created by the presence of weak π bond interactions involved in the C=C bonds, which increase the electronegativity of these compounds [20]. The high reactivity or ease of

activation makes alkenes viable starting materials for many industrial processes. The catalysed formation of ethylene and propylene has for several decades been achieved through the dehydrogenation of their respective alkanes and has served as an alternative to the pyrolysis process or steam cracking [21, 22]. These endothermic reactions operate under high temperatures and produce low yields of targeted products due to associated thermodynamic limitations [23]. Another disadvantage of dehydrogenation is catalyst deactivation. The use of an oxidant, commonly gaseous oxygen, alters the thermodynamics of dehydrogenation reactions by creating an exothermic process and subsequently eliminating most of the limitations brought on by thermodynamic constraints and reduced coke formation on the surface of the catalysts tested [24-26]. This catalysed process is called oxidative dehydrogenation (ODH). The ODH of alkanes is now the preferred route for the formation of alkenes and other valorised products. However, the ODH of alkanes does have disadvantages in that activated alkenes tend to be more reactive than their alkane precursors and tend to undergo further reactions that ultimately result in the formation of carbon oxides (CO_x). This obviously has a negative impact on the selectivity towards valorised products. Therefore, the optimization of reaction conditions to minimize subsequent reactions of targeted products is essential [27]. In an ODH reaction, the initial step involves the extraction of a hydrogen atom from an organic molecule, which is followed by a second elimination of a hydrogen atom from a neighbouring carbon atom resulting in a π double bond formation, with the consecutive desorption of water (H_2O). This is termed the 'activation' of the alkane and results in the formation of an alkene shown by equation 1:

$$C_nH_{2n+2} + 0.5O_2 \rightarrow C_nH_{2n} + H_2O \quad (1)$$

Catalytic oxidation reactions that lead to oxygen insertion reactions are categorised as electrophilic and nucleophilic oxidation reactions. The ODH of alkanes to alkenes is best described as a nucleophilic oxidation reaction. On the other hand, electrophilic oxidation occurs through the attack on the double bond, of an alkene for example, by activated oxygen resulting in an oxygenated compound.

Catalysts used in an ODH process must possess reduction and oxidation (REDOX) potentials. For this reason, ODH reactions are often catalysed by bulk metal oxide and supported metal oxide catalysts, which almost always include transition metals. Oxygen plays an important role in catalytic ODH reactions. These reactions undergo the Mars and van Krevelen (MvK) mechanism (Figure 1.1) which involves the breakage of C-H bonds and the participation of lattice oxygen species [28].

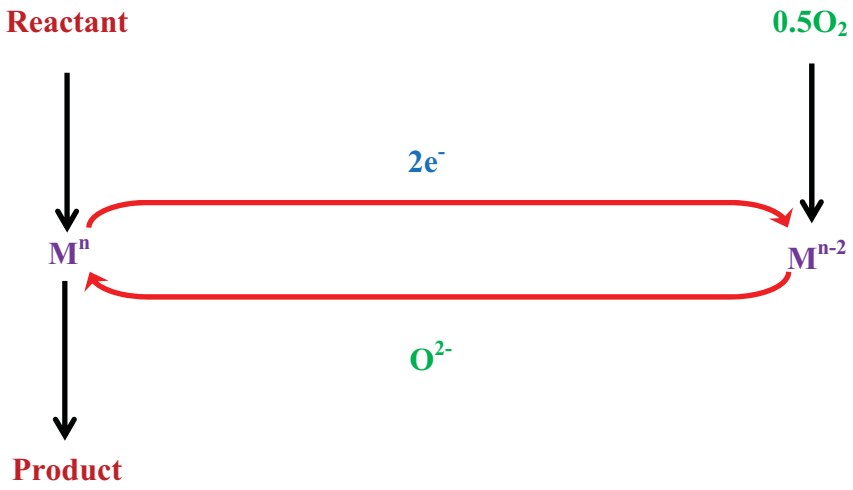

Figure 1.1: Scheme of the Mars and van Krevelen mechanism

The MvK mechanism involves the nucleophilic addition of oxygen to an activated alkyl radical, accompanied by the removal of a hydrogen atom. Thus, the participation of lattice oxygen is crucial and a catalyst capable of supplying this is essential [29]. Activated gaseous oxygen, formed by the interaction of a co-feed with the surface of the catalyst, replenishes depleted lattice oxygen and prevents catalyst deactivation.

The MvK mechanism does have its limitations in that it fails to explain the ODH of alkanes catalysed by materials without rapid redox properties such as Fe-ZSM5 zeolites [30]. In cases like these, the acid-base properties of supports or isolated cations capable of activating C-H bonds are important [31-34]. Thus, it can be said that supports with variable acid-base properties are advantageous for the ODH of alkanes.

1.2 Review of C4 – C6 alkane activation

Functionalised hydrocarbons are of great interest in the chemical industry [35]. An increased demand for these compounds has created a need for their production. Alkenes serve as important starting materials in a wide range of industrial applications. Their low cost and ability to be easily functionalised make them particularly valuable in the petrochemical industry. The catalysed conversion of even lower cost alkanes to alkenes is a growing research topic because of the increasing availability of alkanes, formed as by-products from coal and gas to liquid plants. With the number of these plants increasing worldwide, these easily available and cheap chemical feed-stocks have sparked considerable interest as substituents of alkene and aromatic feed-stocks [17]. The growing interest in alkane ODH is also driven by the depletion of easily available natural sources and the increased prices of alkenyl compounds [36].

In excess of 60 % of the chemicals produced by catalytic processes are products of oxidation catalysis. A general trend observed amongst these catalysed systems is an inverse relationship between conversion and selectivity towards value added or targeted products. Over time, the fine tuning in terms of catalyst design, co-feeds and reaction conditions have been the topics of several investigations.

The activation of light alkanes, from the homologous series C1 (methane) through to C5 (pentane), has been extensively studied. The selective oxidation of light alkanes has been investigated by Cavani and Trifiro [37]. Their work focused on the chemistry behind the selective oxidative transformation of alkanes and the role of the REDOX nature of modified mixed metal oxide catalysts. Furthermore, the authors paid attention to the influence of homogeneous reactions on non-reducible metal oxides and the heterogeneity associated with the activation of these reactions. In a similar study involving ethane, propane and butane, López-Nieto and co-workers [35, 38-44] showed that the REDOX nature of vanadium based catalysts and supported vanadium catalysts together with its acid-base properties influenced alkane activation. Research into vanadium based catalysts is extensive, partly due to their successful implementation in the commercial conversion of *n*-butane to maleic anhydride.

Work done by Hutchings and co-workers [45-51] also focused on alkane activation over several different catalyst materials incorporating, in some cases, gold, and focussing on the REDOX nature of these nanosized particles. In studies by Corma and co-workers [52-54] on the oxidation of alkanes, particular attention was given to the acid-base nature and particulate properties of the catalysts with respect to their influence on activity and selectivity.

In their earlier work, Friedrich and co-workers [17, 55-57] investigated the activation of C4 – C6 alkanes. The conversion of *n*-butane to maleic anhydride is the only known commercially heterogeneously catalysed oxidative process that uses an *n*-alkane as a feed-stock. Govender *et al*. [57] investigated vanadium-phosphorus-oxide (VPO) catalysts in the activation of *n*-butane. The study involved the effects of cobalt loading as a promoter, temperature and gas hourly space velocity (GHSV). The optimisation of these parameters to enhance catalytic activity and maleic anhydride selectivity was of primary interest. This study found that the best performing catalyst yielded 45 % maleic anhydride at a temperature of 275 °C and a GHSV of 7200 mL g^{-1} h^{-1}, with an *n*-butane conversion of 73 %. Govender *et al*. [17] also investigated the activation of *n*-hexane over magnesium orthovanadate (VMgO) catalysts. This work highlighted problems associated with *n*-alkane activation with respect to voids and catalyst packing in a reactor. *n*-Hexane dilution factors were also found to play an important role. Carborundum was used to fill the voids and was found to influence catalytic conversion of *n*-hexane as opposed to homogeneous radical gas phase conversion that occurred in the presence of voids. Pillay *et al*. [55] studied the activation of *n*-hexane over nickel-molybdenum-oxide ($NiMoO_4$) catalysts. The effects of phase composition of the catalysts and temperature on catalytic activity, with respect to conversion and selectivity, were investigated. This study demonstrated that the most selective catalyst for hexene isomers was pure β-$NiMoO_4$ giving 25 % selectivity to 1-hexene and 10 % selectivity to 2-hexene and 3-hexene at 9 % conversion. Terminal functionalisation of *n*-alkanes is difficult due to the lower reactivity of primary carbons [20] and Pillay *et al*. [55] to some extent overcame this problem. In a separate study, Pillay *et al*. [56] published work directing their studies towards the ODH of *n*-hexane over β-$NiMoO_4$ catalysts below the flammability limits of the hydrocarbon. Variations in contact time and *n*-hexane concentration were investigated to determine their effects on catalytic activity. The highest selectivity to 1-hexene was found to be 27 % with 25 %

selectivity to trans-2-hexene and 2 % to cis-2-hexene at a conversion of approximately 7 %. Naicker and Friedrich [58] investigated the influence of vanadium loading on modified zeolite ZSM-5 catalysts in the oxidation of *n*-hexane. They found that by varying the SiO_2/Al_2O_3 ratio of the ZSM-5 catalysts, the degree of cracking could be controlled. A decrease in cracked product yield was observed from 36 to 8 mol% with an increase in the SiO_2/Al_2O_3 from 100 to 320. The use of a Na-ZSM-5 catalyst, with a SiO_2/Al_2O_3 ratio of 100, eliminated acid cracking completely. After further investigation of the Na-ZSM-5 zeolites and its modification with vanadium (1 wt% loading) Naicker and Friedrich [58] found that the highest selectivity towards terminal functionalised products were found at a conversion of 39 mol%, attained at a temperature of 400 °C, contact time of 1.1 s and a fuel to air ratio of 1.3.

1.3 Review of *n*-octane in heterogeneous catalysis

Oxidation and oxidative dehydrogenation

Catalytic oxidation yields valuable chemical compounds by the auto-thermal treatment of hydrocarbons [59]. Alkenes are generally made from refinery sources. These chemical feed-stocks generally exist as complicated mixtures of linear and branched hydrocarbons as well as aromatic compounds. The oxidation of alkanes, like *n*-octane, has shown that straight chain hydrocarbons produce the highest selectivity towards alkenes [60].

Air has generally been used as the oxidant in the oxidation of *n*-octane with hydrogen peroxide being used in some cases [18, 21, 61-64]. It has been found that the acidic and basic properties, as well as the REDOX characteristics of a catalyst, show an effect on its performance in an ODH reaction [65].

In recent years, research published by Friedrich and co-workers involved the activation of *n*-octane using a variety of catalysts. Elkhalifa and Friedrich [63, 66], Friedrich and Mohamed [18] and Dasireddy *et al*. [21] have all discussed the influence of reaction conditions on the ODH of *n*-octane over different mixed metal oxide catalysts, with key focus on the mechanistic understanding of reaction pathways involved in these reactions. They have

demonstrated that octene formation is the rate determining step of the reaction and that octene isomers serve as reaction intermediates that may influence the formation of C8 aromatic compounds, viz. ethylbenzene, styrene and *o*-xylene, or undergo other reaction pathways that ultimately lead to combustion forming carbon oxides (CO_x). Shi and Davis [67] have shown that the formation of these C8 aromatic compounds occurs via a C_2 and C_7 or C_1 and C_6 dehydrocyclisation mechanism. C8 aromatic compounds are important in industry as these are used in a variety of processes. Ethylbenzene has found applications in chemical manufacturing and as a feed-stock for styrene, formed by the dehydrogenation of ethylbenzene catalysed by potassium promoted iron oxides [8, 68, 69]. Styrene is an important and extensively used monomer in the petrochemical industry. The most well-known polymer derived from this monomer is polystyrene. *o*-Xylene is also an important compound and a well-known process exists that uses *o*-xylene as a precursor to form phthalic anhydride.

Friedrich and Mahomed [18] studied the ODH of *n*-octane to styrene over catalysts derived from hydrotalcite-like precursors containing magnesium and vanadium with varying Mg/V ratios. Investigations were carried out in order to determine the effect of GHSV, temperature and the carbon to oxygen (C:O) molar ratios. A maximum selectivity to styrene was found to be 19 %, corresponding to a yield of 14 %. This was obtained over a catalyst with a Mg/V ratio of 2.3. Their work also suggested that the mechanism of formation of styrene involved octene formation, followed by cyclisation to give ethylbenzene which was further dehydrogenated to form styrene.

Elkhalifa and Friedrich [63] tested VMgO catalysts, with varied vanadium loadings, in the activation of *n*-octane. Vanadium concentration was found to affect both the textural and chemical properties of the catalysts and thus their activity and selectivity. The highest selectivity to 1-octene and styrene were observed over a VMgO catalyst with a vanadium pentoxide (V_2O_5) loading of 15 wt%. In another study, Elkhalifa and Friedrich [66] investigated the effects of varying *n*-octane concentration in the feed. They found that catalytic performance, with regards to conversion and selectivity, were susceptible to changes in the *n*-octane concentration. A maximum in conversion of 80 mol% was observed at 500 °C and 550 °C at a C:O molar ratio of 8:10. Corresponding to the maximum in conversion was

the highest selectivity towards CO_x (80 mol%) over all the C:O molar ratios tested. The VMgO catalysts proved to be stable under the conditions tested as the used catalysts showed no phase changes. Only textural changes were observed.

Narayanappa *et al*. [70] investigated the oxidative activation of *n*-octane over cobalt substituted cerium oxides ($Ce_{1-x}Co_xO_{2-\delta}$). The $Ce_{1-x}Co_xO_{2-\delta}$ catalysts were prepared by a solution-combustion method. This study investigated the effects of varying *n*-octane to oxygen molar ratios and temperature. They showed that activity increased with the hydrocarbon to oxygen molar ratio and an increase in temperature. A maximum in conversion of 50 mol% was observed at temperatures of 500 °C and 550 °C and a C:O ratio of 8:4. This maximum in conversion corresponded to a minimum in CO_x selectivity.

Dasireddy *et al*. [21] studied the effects of supporting varied loadings of V_2O_5 on hydroxyapatite (HAp) and the use of these materials as catalysts in the ODH of *n*-octane. Powder X-ray diffraction and Fourier transform infrared spectroscopy identified the dominant phase as HAp. Inductively coupled plasma optical emission spectroscopy analysis confirmed the vanadium loadings and provided insight on the Ca/P molar ratio of the support, which was characterised as non-stoichiometric HAp. Electron microscopy illustrated the homogeneous distribution of V_2O_5 on the support. V_2O_5 loadings of 2.5 wt% showed good selectivity towards octenes, while V_2O_5 loadings of 15 wt% showed a decrease in the formation of octenes corresponding to an increase in the selectivity towards C8 aromatics, viz. ethylbenzene, styrene and *o*-xylene. The 15 wt% V_2O_5 supported on HAp catalyst showed a conversion of 24 % at 450 °C and selectivity towards octenes of 72 %. A maximum selectivity of 10 % for C8 aromatics was attained at a conversion of 36 % over a 15 wt% V_2O_5 supported HAp catalyst.

A further study involved the activation of *n*-octane over 2.5 and 10 wt% V_2O_5 supported on alkaline earth metal HAps [62]. This work aimed to investigate the effect of different HAp-like supports on the ODH of *n*-octane with varying C:O molar ratios. Here, an additional pyrovanadate phase was identified for the 10 wt% catalysts. They observed aromatics and octenes at a C:O ratio of 8:1 and aromatics and oxygenates at a ratio of 8:4. At a C:O ratio of

8:2 both the 2.5 and 10 wt% V_2O_5 supported on strontium hydroxyapatite (Sr-HAp) catalysts showed the highest conversion over the temperature range tested. A maximum in conversion of 29 mol% for the 2.5 wt% V_2O_5 supported on Sr-HAp catalyst was observed at 550 °C. The 10 wt% V_2O_5 supported on Sr-HAp catalyst showed a maximum conversion of 40 mol% at a temperature of 550 °C and a C:O ratio of 8:2. High selectivity towards octenes was observed for the 2.5 wt% V_2O_5 catalysts. There was a marked decrease in octenes selectivity corresponding to an increase in C8 aromatics selectivity when the 10 wt% V_2O_5 catalysts were used. At an iso-conversion of 27 mol%, the V_2O_5 supported on HAp yielded octenes as the major products. At the same conditions, V_2O_5 supported on Sr-HAp showed the highest yield of C8 aromatics, V_2O_5 supported on magnesium hydroxyapatite (Mg-HAp) yielded predominantly oxygenates and V_2O_5 supported on barium hydroxyapatite (Ba-HAp) yielded predominantly C8 aromatics and oxygenates. The difference in the product profiles was attributed to the acid-base characteristics of the catalyst materials.

To gain a mechanistic insight into *n*-octane activation using vanadium supported alkaline earth metal HAp-like materials, octene isomers and 1,7-octadiene were used as reactants in a series of experiments using the 2.5 and 10 wt% V_2O_5 supported catalysts [64]. Phase composition and C:O molar ratios were contributing factors in the selectivity of desired products. The octene isomers showed the highest selectivity to C8 aromatics and the formation of oxygenates and CO_x also occurred. 2-Octene and 3-octene showed the greatest selectivity to C8 aromatics and a preference for the C_2 and C_7 cyclisation mode, whereas 1-octene and 1,7-octadiene preferred the C_1 and C_6 cyclisation mode.. These catalysed reactions also suggested that the MvK mechanism was followed [28].

The use of zeolites as catalysts in the activation of *n*-octane was investigated by Brillis and Manos [71]. They observed the formation of cracked products. This could have been due to the acidic nature of ZSM5 zeolite materials. Their work has shown that the catalytic oxidation of *n*-octane can produce synthesis gas, octenes, C8 aromatics and cracked products. However, a challenge exists in the ODH of this hydrocarbon as it has a tendency to crack when exposed to the high temperatures required for the reaction [63].

Dehydrogenation

The dehydrogenation of *n*-octane has many industrial applications and is generally achieved over mono-functional or bi-functional catalysts [72]. Long chain alkanes tend to favour dehydrogenation and in order to achieve good yields of valorised products, such as aromatic compounds and oxygenated compounds, relatively high reaction temperatures are required. *n*-Octane can undergo dehydrogenation to form octene isomers which can serve as reaction intermediates for aromatic compounds, cracked products or CO_x formation. The latter depends on the availability of oxygen species in the catalyst used. A key function of a catalysed dehydrogenation reaction is to accelerate the desired reaction while controlling side reactions. An octene isomer is formed through H_2 abstraction from *n*-octane, thereafter terminal ring closure may occur, generally on an acidic site of a catalyst [64, 67, 72]. A problem associated with this is the acid catalysed cracking which generally occurs at faster rates than dehydrogenation reactions. Uniform and even dispersion of the catalytically active phase on the surface of the support has been shown to reduce the relative amount of unwanted side reactions, such as cracking [72]. Méricaudeau *et al*. [73] described the formation of C8 aromatic compounds as initially involving the dehydrogenation of *n*-octane to form an octene, which subsequently undergoes a C_1 and C_6 or C_2 and C_7 cyclisation. Subsequent steps involve the dehydrogenation of the cyclic compounds producing ethylbenzene and *o*-xylene. The formation of styrene can occur through further dehydrogenation of the alkyl substituent of ethylbenzene. Another mechanism involves the stepwise dehydrogenation of *n*-octane into a triene followed by terminal ring closure [74]. An advantage of *n*-octane dehydrogenation is the lower activation energy associated with the relatively longer hydrocarbon molecule. Therefore, these processes are carried out under relatively lower temperatures than when compared to lower alkanes, viz. C1 (methane) through to C7 (*n*-heptane).

1.4 Iron in heterogeneous catalysis

The REDOX properties of iron, particularly its reducibility, has led to its implementation as a Fischer-Tropsch (FT) catalyst [75-80] and its use in ammonia synthesis [81]. These processes utilize magnetite (Fe_3O_4) as a catalyst which undergoes a reduction of the active iron species

and corresponding phase changes ultimately leading to the formation of iron carbides. The implementation of iron oxides as FT catalysts sparked great interest in the REDOX properties of these metal oxides. The REDOX nature of iron oxides has been discussed by Wimmers *et al*. [82] and Liang *et al*. [83]. Although Fe_3O_4 is commonly used as an FT catalyst, their work investigated the reduction behaviour of hematite (α-Fe_2O_3) as it provided a broader understanding of the REDOX nature of iron oxides. The reduction mechanisms were investigated through temperature programmed techniques and showed that the reduction of α-Fe_2O_3 can be controlled by co-feeding water with the reducing agent used. The findings of these studies provided valuable information on the REDOX properties of iron oxides and demonstrated the ability to control their REDOX nature, making them favourable catalyst materials.

Apart from iron being used in the form of iron oxide as a FT catalyst, iron is used to catalyse many industrial processes. Examples of these include Fe-Mo oxides, which are employed in the selective oxidation of methanol to formaldehyde [84], ferrites in the selective ODH of butane to butadiene [85] and ethylbenzene to styrene [86, 87], Fe-Sb oxide catalysts in the ammoxidation of propane to acrylonitrile [88, 89] and Fe-Cr oxides in the water gas shift reaction [90]. Iron oxide may also sometimes be used as a promoter [69].

Kung and Kung [69] have studied the ODH of butane to butadiene over ferrite catalysts to gain insight on some of the reaction parameters that influence catalytic performance. They found that the nature of the transition metal ion influenced the interaction of the hydrocarbon with the catalyst surface and the catalyst's ability to activate gaseous oxygen to form highly reactive surface species. They also suggested that it was the crystal structure of the active phase, α-Fe_2O_3, that played a pivotal role in the REDOX properties of the catalyst. Crystallite size and the orientation of the exposed crystal planes were also suggested to have influenced the selectivity of the catalyst materials. Catalytic performance was found to vary with variations in the presence or absence of gaseous oxygen and the temperature of operation. The presence of oxygen and higher temperatures led to higher conversion at the expense of butadiene selectivity. Sugiyama *et al*. [91] investigated the ODH of propane over α-Fe_2O_3 in the presence and absence of tetrachloromethane (TCM). Their work suggested that TCM

improved the conversion and selectivity in oxygen limited conditions. It was found that the inhibition of the phase change of α-Fe_2O_3 to maghemite (γ-Fe_2O_3) and the formation of active surface and gaseous chlorinated species contributed to activity. Ates *et al*. [30] investigated the ODH of propane, with N_2O, over iron containing zeolite (Fe-ZSM5) catalysts. Catalytic activity and selectivity of propene showed optimum values over the Fe-ZSM5 catalysts with low aluminium loading and thus reduced acidity. This work found that propene yields were greater over the Fe-ZSM5 catalysts as opposed to amorphous iron silicate (Fe-SiO_2) catalysts. This was suggested to have been due to the presence of weak and medium acid sites existing synergistically with oligonuclear iron species and iron oxides on the Fe-ZSM5 materials which were found to enhance N_2O activation. Coke deposition on the surface of the catalysts tends to be prevented by the addition of O_2 as a co-feed and a reduction in the surface acidity of the catalyst materials. These iron containing zeolites were prepared by a solid state method and demonstrated comparable activity and improved selectivity, with respect to catalyst deactivation by coke deposition, when compared to similar catalysts prepared by wet chemical techniques and hydrothermal synthetic methods.

The dehydrogenation of ethylbenzene to styrene over iron oxide supported on alumina catalysts in the presence of CO_2 was investigated by Mimura and Saito [8]. Their work showed that the dehydrogenation of ethylbenzene yields more styrene in the presence of CO_2 as opposed to steam. This catalysed process occurred via a two-step pathway and provided higher equilibrium yields of styrene at a given temperature with less energy requirements than when compared to the present commercial process using steam. An Fe_2O_3 (10 wt%) supported on Al_2O_3 (90 wt%) catalyst prepared by a co-precipitation method proved to be effective in the presence of CO_2 giving a styrene yield of 35 %. Castro *et al*. [92] investigated porous iron based catalysts, with different promoters (Ti, Zr or Al), in the ODH of ethylbenzene with CO_2 for styrene production. The performance of the catalysts proved to be dependent on the structural and textural features of the materials and the nature of the promoter. α-Fe_2O_3 and rutile (TiO_2) were converted, *in-situ*, to $FeTiO_3$, Fe_2TiO_5 and $FeTi_2O_5$. These FeTi catalysts gave styrene yields of up to 50 %. The FeTi catalysts also proved to be more stable than the FeZr and FeAl catalysts. The FeZr and FeAl catalysts suffered deactivation through hard coke deposition on their active sites.

Bonnet *et al*. [93] investigated new approaches in the preparation of iron phosphate catalysts. These new single phase catalysts proved to be very selective and showed good conversion in the ODH of isobutyric acid to methacrylic acid. When these catalysts were compared to a common commercial iron phosphate catalyst they demonstrated improved performance. They also investigated the use of water as a co-feed. Their results suggested that using water as a co-feed seemed to have moved the hydration equilibrium and superficially stabilised the new iron phosphate phase throughout the bulk of the material as opposed to surface stabilisation observed in the commercial catalyst. The activation of ethane over stoichiometric and non-stoichiometric iron phosphate catalysts was carried out by Miller *et al.* [94]. In this study, they found that the unstable iron phosphates tended to convert back to a quartz-like ($FePO_4$) phase or other phases depending on their stoichiometry. The non-stoichiometric phases demonstrated unique activation behaviour, such that both the selectivity and conversion increased with time-on-line. Ethylene yields showed a maximum of approximately 50 % over a catalyst with a P/Fe ratio of 1.2:1. This study suggested that conversion and selectivity resulted from the migration of phosphorus from the bulk of the catalyst to its surface. Nagaraju *et al*. [95] used iron phosphate catalysts for the ammoxidation of 2-methyl pyrazine. The iron phosphate catalysts were prepared by different wet precipitation techniques utilizing different starting materials and contained varying P/Fe ratios. Structurally and texturally, the catalysts differed depending on the reactants used in their synthesis. XRD and Raman spectroscopy identified the dominant phases as a quartz-like ($FePO_4$) phase and precipitation in a basic medium led to an increase in the presence of this phase in the catalyst. An increase in this phase contributed to a decrease in the acidity of the catalysts and hence, nitrile selectivity.

Another study involving iron oxide and iron carbide catalysts found these to be active in the dehydration of tertiary alcohols [96]. This study found that the iron oxide was not reduced nor was the bulk carbide oxidised by the H_2O vapour generated during this process. Secondary alcohols were found to be converted to ketones and hydrogen by both iron oxides and iron carbides with the iron oxide undergoing a reduction from $Fe_2O_3 \rightarrow Fe_3O_4$. Both the iron oxide and iron carbide catalysts were found to dehydrogenate primary alcohols to form the

aldehyde. This aldehyde underwent a subsequent ketonisation producing a symmetrical ketone. This work highlighted the dehydration ability of iron oxide.

Baldi *et al*. [97] investigated the applications of iron oxides and manganese oxides in the combustion of propane. They successfully synthesised Mn_2O_3-Fe_2O_3 catalyst materials by a co-precipitation method to be used as combustion catalysts for propane and propene. They found that in terms of pure phases, the α-Mn_2O_3 phase showed better activity than the α-Fe_2O_3 phase in the combustion of propane and propene. As combustion catalysts, the mixed phase Mn_2O_3-Fe_2O_3 materials proved to be better than the pure phase α-Mn_2O_3. All the catalysts showed good activity in propene oxidation and were very selective towards CO_2. An interesting observation was that α-Fe_2O_3 gave rise to significant selectivity towards propene in the oxidation of *n*-propane. This highlighted the ODH ability of α-Fe_2O_3 on light alkanes. Nogueira *et al*. [98] studied the oxidation of toluene over catalysts prepared by supporting Fe_2O_3 on the surface of a clay material. The catalysts were prepared by wet impregnation and an incipient wetness impregnation technique. After the impregnation of Fe_2O_3 on the surface of the clays, an increase of surface area from 17 to 62 m^2 g^{-1} was observed. The distribution of the iron species was found to be dependent on the preparatory method. Their work found that the catalyst prepared by wet impregnation reached 100 % conversion of toluene at a temperature of 350 °C, compared to that of the catalyst prepared by the incipient wetness impregnation technique, which reached a conversion of 100 % at a temperature of 400 °C. This difference was attributed to higher metal dispersion achieved through the wet impregnation synthesis technique.

Sciré *et al*. [99] investigated the selective oxidation of CO in H_2 rich streams over gold supported on iron oxide catalysts. This study highlighted the effects of catalyst pre-treatment on catalytic performance. CO conversion was found to be dependent on the active phase reduction temperature of the catalysts tested. Selectivity decreased with an increase in temperature and this was found to be independent of the influence of catalyst pre-treatment. Particle size, metal-support interaction, the oxidation state and the phase of iron oxide were all factors that influenced the efficiency of the catalyst.

Zhang *et al*. [100] studied the catalytic performance of iron oxide supported on alumina intercalated laponite clay and the deactivation mechanism for H_2S selective oxidation. These catalysed reactions were proposed to have followed the MvK mechanism. In addition to this finding, it was suggested that the good distribution of iron, the metal-support interaction and the increased number of acid sites on the surface of the clays improved the catalytic performance of these materials.

These investigations highlighted the oxidation, oxidative dehydrogenation and dehydrogenation ability of iron. This together with its unique REDOX properties, were the main reasons that iron was chosen as the active element in this study. It was also clear that different techniques employed during catalyst synthesis influence the behaviour of a catalyst and thus its performance, and this was the rationale behind the use of two different synthetic routes to synthesise the iron modified hydroxyapatite powders in this MSc study.

1.5 Hydroxyapatite

Hydroxyapatite (HAp) is a bifunctional material with acid-base properties that are dependent on its composition. The general chemical formula for HAp is $Ca_{10-x}(HPO_4)_x(PO_4)_{6-x}(OH)_{2-x}$. Stoichiometric HAp has $x = 0$ giving $Ca_{10}(PO_4)_6(OH)_2$, whereas calcium deficient, non-stoichiometric HAp has $0 \leq x \leq 1$. The molar ratio of calcium to phosphorus (Ca/P) varies from 1.2 to 2.0, with the stoichiometric molar ratio of HAp being 1.67. HAp is usually found in a hexagonal unit cell having the $P6_3/m$ space group symmetry with lattice parameters of a = b = 9.342 Å and c = 6.881 Å [101]. The structure of HAp (Figure 1.2) consists of an array of PO_4^{3-} tetrahedra held together by Ca^{2+} ions interspersed among them. The Ca^{2+} ions occur in two markedly different sites.

In site I, Ca^{2+} ions are found in a columnar arrangement where each Ca^{2+} ion is coordinated to nine oxygen atoms from the PO_4^{3-} groups. Ca^{2+} ions occupying site II are hepta-coordinated by six oxygen atoms from five PO_4^{3-} anions and one OH^- group. The Ca^{2+} ions at site II are in equilateral triangles centred on the screw axis. The OH^- groups occupy distorted positions above or below the Ca^{2+} triangles because they are too large to fit in the site II triangles.

Figure 1.2 illustrates the arrangement of the PO_4^{3-}, OH^- and Ca^{2+} ions in the hexagonal unit cell of HAp.

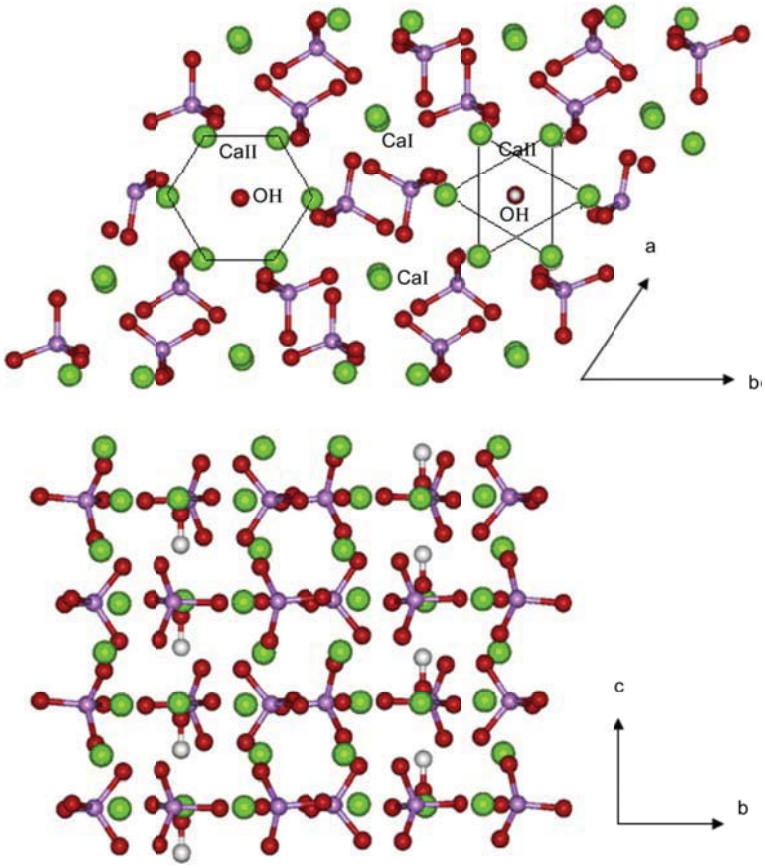

Figure 1.2: Representation of the hydroxyapatite structure perpendicular to the crystallographic *a* and *c* axes. This representation shows the OH^- channels and the different types of calcium ions (Ca = green, O = red, P = purple, H = white) [102] (Redrawn with permission from Elsevier Copyright© 2013)

Although the chemical synthesis of HAp was first achieved several decades ago, the synthetic methodology has been developing over recent years in order to satisfy certain requirements for various applications, including catalysis.

HAp has been used as a basic catalyst for the Michael addition of metacarpenes to chalcone derivatives in an attempt to increase yields [103]. In this study, good conversion and

selectivities to targeted products were obtained with a reduction in side reactions that produced undesirable products. The use of HAp demonstrated an alternative to this homogeneous reaction that uses basic reagents.

The reaction of ethanol over HAp was studied at varying Ca/P ratios and it was found that the distribution of acidic and basic sites varied with the Ca/P ratio, which influenced the yields of products, namely ethylene, 1-butanol and 1,3-butadiene [104]. The oxidation of benzene to phenol over HAp in the presence of air and ammonia demonstrated extremely good selectivity with conversion ranging between 3 – 4 % [105]. The reaction involved the activation of oxygen species on the surface of the catalyst by decomposition of N_2O [105]. The partial oxidation of methane over HAp in the presence of TCM increased selectivity towards carbon oxide and synergistically improved methane conversion and ethylene selectivity [106].

HAp as a support has been used extensively in gas and liquid phase catalysed reactions. HAp has been shown to have good hydrogenation ability in the conversion of quinoline over ruthenium supported HAp. This was attributed to the presence of surface hydroxyl groups which have been shown to interact with the nitrogen atoms of quinoline [107].

The substitution of Ca^{2+} ions by transition metal cations and the supporting of transition metals on the surface of HAp play a significant role in altering the acid-base characteristics of synthetic HAp powders. These changes in the acid-base nature of HAp can be useful in tailoring reactions to optimize both selectivity and conversion.

HAp is commonly employed as a cation-exchange medium because its Ca^{2+} ions can be substituted for various other cations [108, 109]. Bigi *et al*. [110] synthesised strontium substituted HAp solid solutions. The materials were made by a direct synthesis in an aqueous medium using a co-precipitation technique. They found that the substitution of Ca^{2+} ions with Sr^{2+} ions induced a linear increase in the lattice constraints and a linear shift in the FTIR absorption bands of the OH^- and PO_4^{3-} groups. These findings were coherent with the larger ionic radius of Sr^{2+} when compared to Ca^{2+}.

Suchanek *et al*. [111] prepared magnesium substituted HAp powders with different crystallinities using a mechanochemical-hydrothermal method. They characterised the powders by PXRD, FTIR spectroscopy, thermogravimetric and chemical analysis. They found that the Mg substituted HAp powders contained unreacted $Mg(OH)_2$ and subjected them to purification in an ammonium citrate solution at room temperature. The purified powders were found to be pure phase Mg-HAp with 0.24 – 28.4 wt% of Mg. X-ray photoelectron spectroscopy showed the surface concentration of Mg to be lower than that of the bulk of the HAp-like crystals. SEM imaging showed that the Mg-HAp powders consisted of submicron agglomerates of nano-sized grains, less than 20 nm in length. Yasukawa *et al*. [112] prepared Mg substituted HAp solid solutions by a co-precipitation method. The ion-exchange properties of these materials were investigated by immersing the MgCa-HAp particles into solutions containing Ca^{2+} ions under different conditions where Ca^{2+} concentration, immersion period, solution pH and temperature were varied. They found that Mg^{2+} ions in the MgCa-HAp particles were exchanged with Ca^{2+} ions from solution. The ion-exchange equilibrium was attained within 15 – 30 minutes. Ion-exchange was promoted by raising the Ca^{2+} concentration and temperature of solution and by lowering the solution pH. The exchange of Ca^{2+} with Mg^{2+} ions was found to have occurred through a dissolution-precipitation type reaction at the surface of the material.

Yasukawa *et al*. [113] prepared carbonated barium-calcium HAp solid solution particles, with varied Ba content, using a co-precipitation method. They found that the crystal phases and structures of the particles were dependant on the concentration of Ba. With an increasing Ba concentration the products became large spherical agglomerates. Xiu *et al*. [114] prepared Ba-HAp nanoparticles using a citric acid sol-gel combustion method. Pure phase Ba-HAp was formed at 600 °C. The calcined powders showed a nano-scale microstructure with particle sizes of less than 50 nm.

Xu *et al*. [115] studied the sorption of lead on carbonated HAp and charcaterised the materials by PXRD, SEM, SEM-EDX and toxicity leaching procedures. They concluded that the main sorption mechanism is dissolution-precipitation in conjunction with surface sorption. Ellis *et al*. [116] prepared HAp and lead substituted HAp using a co-precipitation method. Using

PXRD and FTIR analysis they determined the polycrystalline materials were single phase HAp. Using DFT analyses they found that lead mainly occupied the site II position of the hexagonal unit cell of HAp.

Stanić *et al*. [117] synthesised copper and zinc doped HAp nanopoarticles using a neutralisation method. This method employed a solution of CuO or ZnO dissolved in H_3PO_4, which was slowly added to a suspension of $Ca(OH)_2$ to obtain a monophasic product. Characterisation of the particles using PXRD, FTIR, SEM and TEM, showed that all the particles were nano-sized and that they did not contain any crystalline impurities. Quantitative elemental analysis in conjunction with the previously mentioned characterisation techniques showed that the copper and zinc ions fully incorporated into the HAp lattice.

The substitution of Zn into HAp was investigated by Ren *et al*. [118]. Nanosized crystals of Zn substituted HAp were synthesised using a co-precipitation method. XRD and Rietveld refinement revealed changes in the apatite lattice parameters and phase changes with Zn substitution. Pure HAp was well crystallised with regular shaped particles, while the Zn substituted HAp crystals became irregular and formed agglomerates. A decrease in the *a*, *b* and *c* lattice parameters was observed with an increase in Zn substitution. Misono and Hall [119] successfully prepared Ni^{2+} and Cu^{2+} substituted HAp powders using a co-precipitation method. They investigated the oxidation-reduction properties of the materials.

Cobalt exchanged HAps (Co/Ca-HAp) were tested in the dehydrogenation of 2-butanol and the ODH of ethane [33]. It was found that an increase in cobalt content led to a decrease in the basicity of the catalysts as inferred from the increase in butanone yield during the dehydrogenation of 2-butanol. In the ODH of ethane, the yield of ethylene showed a maximum of 22 % over a Co/Ca-HAp of 0.96 wt% cobalt. These observations were attributed to the dehydrogenating activity of cobalt brought on by a decrease in the basicity the Co/Ca-HAps with an increase in cobalt loading.

Chromium exchanged HAps were prepared by ion exchange with varying chromium loading, and were tested in the ODH of propane over a temperature range of 300 – 550 ° C. It was

found that these catalyst materials influence the cracking of propane under ODH conditions and this was attributed to the increased acid nature of the chromium modified HAps [120].

The substitution or exchange of Ca^{2+} with other metal cations is controlled by both the size and charge of the substituting cation. Larger cations like Sr^{2+}, Ba^{2+} and Pb^{2+} are preferentially substituted at site II [116, 121], whereas smaller cations have been reported to preferentially substitute Ca^{2+} ions at site I [102]. In certain cases, smaller cations can be substituted at site II but this tends to have a destabilizing effect on the HAp structure, which leads to lattice distortion. Cation substitution by metals with a 3+ charge must follow a charge compensation mechanism or the apatite network collapses. These mechanisms involve the replacement of three Ca^{2+} ions with two M^{3+} ions. Numerous studies on Fe^{3+}, Cr^{3+}, Al^{3+}, La^{3+} and Co^{3+} substituted HAps have suggested that the substitution of Fe^{3+} ions is the most favourable [33, 122-131].

Iron modified hydroxyapatites

Khachani *et al*. [123] prepared hydroxyapatites containing iron, with varied loadings, by the ion exchange method. They identified the existence of iron as isolated Fe^{3+} species distributed in HAp between distorted octahedral and lower coordination sites. These catalysts were tested in the ODH and dehydrogenation of 2-butanol. Tests showed an increase in 2-butanol dehydration which suggested an increase in surface acidity with an increase in iron loading. The catalysts were also tested in propane ODH and demonstrated good propene selectivity with limited conversion between 1 – 20 %. The maximum propene yield was 6.2 % at low iron loading. They found that at low iron loading, the existence of Fe^{3+}-O-Ca^{2+} sites as opposed to Fe^{3+}-O-Fe^{3+} sites that existed at higher iron loading, providing the necessary basicity required for hydrogen abstraction from *n*-propane.

Tanizawa and Sawamura [129] investigated the effects of Fe^{2+} and Fe^{3+} ions on the formation of HAp and calcium phosphates. Their work showed that Fe^{2+} and Fe^{3+} inhibit crystallisation of calcium phosphates during synthesis. They also found that HAp can host within its lattice Fe^{2+} species that are partially oxidised to Fe^{3+} upon interaction with oxygen atoms in solution.

Wakamura *et al*. [130] prepared Al^{3+}, La^{3+} and Fe^{3+} substituted and exchanged HAps using a co-precipitation and ion-exchange immersion method respectively. With respect to the substituted HAps, the exchange ratio of all the metal ions remained below the theoretical value of 1.5. This result verified the exchange with metal hydroxo ions. Infrared spectra of the Al^{3+} substituted and exchanged HAps showed bands representing surface Al-OH groups in addition to surface P-OH bands. The La^{3+} substituted HAps showed no surface La-OH bands. Of the iron modified HAps, only the iron substituted HAps (prepared by co-precipitation) showed surface Fe-OH bands.

Jiang *et al*. [132] investigated the substitution of Fe^{2+} and Fe^{3+} in iron doped HAp. Using electron paramagnetic resonance, Mössbauer spectroscopy and electronic structure calculations, they estimated the local geometries and lattice strain concomitant with the fourfold, fivefold and sixfold iron sites. Their work also discussed the electronic structure associated with the substitution of calcium with Fe^{2+} and Fe^{3+}. Gross *et al*. [124] studied the substitution of calcium with iron in hydroxyapatite-like materials. XRD analysis showed that the iron substituted HAps subjected to heat treatment under an inert atmosphere (nitrogen) eliminated the formation of hematite, observed when the materials were heat treated in air. They stated that the absence of any other iron bearing phase in the XRD patterns of an iron substituted HAp confirmed that the material was successfully synthesised. Anee *et al*. [125] studied the precipitation of iron doped calcium phosphates and iron substituted HAp under physiological pH at various temperatures. XRD revealed no additional iron bearing phases suggesting the formation of a cation substituted HAp. Changes in the intensity and shape of the characteristic *hkl* planes of HAp were observed. These changes were attributed to the incorporation of Fe^{3+} into the HAp lattice framework.

Morrissey *et al*. [126] synthesised and characterised iron containing HAps, for biomedical applications, using a co-precipitation method involving the use of di-ammonium hydrogen orthophosphate, calcium nitrate and ferrous chloride. Their work showed that the apatite structure of the iron substituted HAps had been retained after thermal treatment. Sintering of the materials in air led to the oxidation of Fe^{2+} species to Fe^{3+}, resulting in the formation of hematite (α-Fe2O3). Rietveld refinement of the XRD patterns revealed that the introduction

of iron into the HAp lattice led to an increase in the *a* parameter of the hexagonal HAp lattice. It was also observed that after sintering in air, the *c* parameter increased.

Wu *et al*. [122] prepared iron substituted HAps with varied iron loading by a co-precipitation method. Their characterisation showed that the crystal and molecular structure of the synthesised HAp-like nanoparticles remained unaltered without the collapse of the apatite framework. Rietveld refinement showed that the lattice constants were similar to those of pure HAp. These materials were found to be super-paramagnetic with a size distribution of 20 nm. Wang *et al*. [127] synthesised iron containing HAps from a solution modified to simulate physiological conditions, at low temperatures. They characterised these materials by XRD, Rietveld structural refinement, transmission electron microscopy and UV-VIS photo adsorption spectroscopy. Their characterisation suggested that Ca^{2+} ions were substituted with high spin Fe^{3+} ions within the apatite structure forming a pure HAp like phase.

Li *et al*. [128] prepared Mn^{2+} and Fe^{3+} exchanged HAp nanoparticles using an ion exchange method. XRD analysis showed that all the materials were single phase, non-stoichiometric, B-type carbonated HAp. The ion-exchange synthetic HAp-like materials consisted of elongated spheroids of around 70 nm in length. Energy dispersive X-ray spectroscopy and inductively coupled plasma spectroscopy were respectively used to qualitatively determine and quantify the elemental compositions of the materials. Their work showed that Fe^{3+} ions were more active in replacing Ca^{2+} in the HAp lattice than Mn^{2+} ions.

1.6 Objectives of the study

The commercial production of medium to long chain linear alkanes as by-products from coal and gas to liquid plants has increased significantly over recent years. These abundant and inexpensive alkanes serve as suitable feed-stocks to the more expensive alkene and aromatic compounds in many industrial processes. In this context the dehydrogenation and oxidative dehydrogenation of *n*-octane using iron modified hydroxyapatites as catalysts to provide a viable route for the formation of octene isomers and C8 aromatics was studied.

The main objectives of this study were:

- The preparation and characterisation of hydroxyapatite, iron supported on hydroxyapatite and iron substituted hydroxyapatite.
- To investigate the effect of varying weight percentages of iron of these catalysts in the activation of *n*-octane.
- To investigate the effects of gas hourly space velocity and carbon to oxygen molar ratios on conversion of *n*-octane and selectivity towards octene isomers, C8 aromatic compounds and C8 oxygenated compounds.

References

[1] G. Rothenberg, Catalysis Concepts and Green Applications, Wiley-VCH, Weinheim, 2008.

[2] M. Bowker, The Basics and Applications of Heterogeneous Catalysis, Oxford University Press, USA, Oxford, USA, 1998.

[3] J.N. Armor, Catalysis Today 163 (2011) 3-9.

[4] J.T. Richardson, Principles of Catalyst Development, Plenum Press, New York, 1989.

[5] D. Forster, in: F.G.A. Stone, W. Robert (Eds.), Advances in Organometallic Chemistry, Academic Press, 1979, pp. 255-267.

[6] D.F. Shriver, P.W. Atkins, T.L. Overton, J.P. Rourke, M.T. Weller, F.A. Armstrong, Shriver & Atkins Inorganic Chemistry, 4th ed., Oxford University Press, Oxford, New York, 2006.

[7] G.C. Bond, Heterogeneous Catalysis: Principles and Applications, 2nd ed., Oxford University Press, USA, Oxford, USA, 1987.

[8] N. Mimura, M. Saito, Catalysis Today 55 (2000) 173-178.

[9] G.R. Meima, P.G. Menon, Applied Catalysis A: General 212 (2001) 239-245.

[10] J. Hagen, Industrial Catalysis - A Practical Approach, Wiley - VCH, Federal Republic of Germany, 1999.

[11] P. Atkins, J. de Paula, Physical Chemistry, 8th ed., Oxford University Press, Oxford, USA, 2006.

[12] A.V. Sapre, Chemical Engineering Science 52 (1997) 4615-4623.

[13] J.A. Moulijn, A.E. van Diepen, F. Kapteijn, Applied Catalysis A: General 212 (2001) 3-16.

[14] C.H. Bartholomew, Applied Catalysis A: General 212 (2001) 17-60.

[15] S.T. Sie, Applied Catalysis A: General 212 (2001) 129-151.

[16] P. Forzatti, L. Lietti, Catalysis Today 52 (1999) 165-181.

[17] H.B. Friedrich, N. Govender, M.R. Mathebula, Applied Catalysis A: General 297 (2006) 81-89.

[18] H.B. Friedrich, A.S. Mahomed, Applied Catalysis A: General 347 (2008) 11-22.

[19] J. Clayden, N. Greeves, S. Warren, P. Wothers, Organic Chemistry, Oxford University Press, Oxford, USA, 2001.

[20] P.Y. Bruice, Organic Chemistry, fifth ed., Pearson Prentice Hall, New Jersey, 2007.

[21] V.D.B.C. Dasireddy, S. Singh, H.B. Friedrich, Applied Catalysis A: General 421–422 (2012) 58-69.

[22] S.M. Sadrameli, A.E.S. Green, Journal of Analytical and Applied Pyrolysis 73 (2005) 305-313.

[23] F. Cavani, F. Trifirò, Applied Catalysis A: General 88 (1992) 115-135.

[24] K.A. Williams, L.D. Schmidt, Applied Catalysis A: General 299 (2006) 30-45.

[25] G. Centi, F. Cavani, F. Trifirò, Selective Oxidation by Heterogeneous Catalysis, Springer USA, 2001.

[26] A. de Lucas, P. Sánchez, F. Dorado, M.J. Ramos, J.L. Valverde, Applied Catalysis A: General 294 (2005) 215-225.

[27] E.A. Elkhalifa, On the activation of *n*-octane using vanadium-magnesium oxide catalysts, PhD Thesis, College of Agriculture, Engineering and Science, University of KwaZulu-Natal, Durban, 2010, p. 198.

[28] P. Mars, D.W. van Krevelen, Chemical Engineering Science 3, Supplement 1 (1954) 41-59.

[29] R. Grasselli, Topics in Catalysis 21 (2002) 79-88.

[30] A. Ates, C. Hardacre, A. Goguet, Applied Catalysis A: General 441–442 (2012) 30-41.

[31] L. Lisi, P. Patrono, G. Ruoppolo, Catalysis Letters 72 (2001) 207-210.

[32] K. El Kabouss, M. Kacimi, M. Ziyad, S. Ammar, A. Ensuque, J.-Y. Piquemal, F. Bozon-Verduraz, Journal of Materials Chemistry 16 (2006) 2453-2463.

[33] K. Elkabouss, M. Kacimi, M. Ziyaad, S. Ammar, F. Bozon-Verduraz, Journal of Catalysis 226 (2004) 16-24.

[34] J. Védrine, Topics in Catalysis 21 (2002) 97-106.

[35] T. Blasco, J.M. López-Nieto, Applied Catalysis A: General 157 (1997) 117-142.

[36] Y. Nabae, I. Yamanaka, K. Otsuka, Applied Catalysis A: General 280 (2005) 149-155.

[37] F. Cavani, F. Trifirò, Catalysis Today 51 (1999) 561-580.

[38] P. Botella, A. Corma, J.M. López-Nieto, Journal of Catalysis 185 (1999) 371-377.

[39] P. Botella, E. García-González, J.M. López-Nieto, J.M. González-Calbet, Solid State Sciences 7 (2005) 507-519.

[40] J.M. López-Nieto, J. Soler, P. Concepción, J. Herguido, M. Menéndez, J. Santamaría, Journal of Catalysis 185 (1999) 324-332.

[41] J.M. López-Nieto, A. Dejoz, M.I. Vazquez, W. O'Leary, J. Cunningham, Catalysis Today 40 (1998) 215-228.

[42] A. Corma, J.M. López-Nieto, N. Paredes, M. Pérez, Y. Shen, H. Cao, S.L. Suib, in: P. Ruiz, B. Delmon (Eds.), Studies in Surface Science and Catalysis, Elsevier, 1992, pp. 213-220.

[43] I. Ramli, P. Botella, F. Ivars, W. Pei Meng, S.M.M. Zawawi, H.A. Ahangar, S. Hernández, J.M. López-Nieto, Journal of Molecular Catalysis A: Chemical 342–343 (2011) 50-57.

[44] A. Dejoz, J.M. López-Nieto, F. Márquez, M.I. Vázquez, Applied Catalysis A: General 180 (1999) 83-94.

[45] T.J. Hall, J.S.J. Hargreaves, G.J. Hutchings, R.W. Joyner, S.H. Taylor, Fuel Processing Technology 42 (1995) 151-178.

[46] G.J. Hutchings, R. Higgins, Journal of Catalysis 162 (1996) 153-168.

[47] Y.H. Taufiq-Yap, S.N. Asrina, G.J. Hutchings, N.F. Dummer, J.K. Bartley, Journal of Natural Gas Chemistry 20 (2011) 635-638.

[48] G. Jin, W. Weng, Z. Lin, N.F. Dummer, S.H. Taylor, C.J. Kiely, J.K. Bartley, G.J. Hutchings, Journal of Catalysis 296 (2012) 55-64.

[49] S.H. Taylor, J.S.J. Hargreaves, G.J. Hutchings, R.W. Joyner, C.W. Lembacher, Catalysis Today 42 (1998) 217-224.

[50] S.H. Taylor, G.J. Hutchings, M.L. Palacios, D.F. Lee, Catalysis Today 81 (2003) 171-178.

[51] G.J. Hutchings, R. Higgins, Applied Catalysis A: General 154 (1997) 103-115.

[52] A. Corma, H. Garcia, Catalysis Today 38 (1997) 257-308.

[53] A. Corma, D. Kumar, in: L. Bonneviot, F. Beland, C. Danumah, S. Giasson, S. Kaliaguine (Eds.), Studies in Surface Science and Catalysis, Elsevier, 1998, pp. 201-222.

[54] Y. Pérez, M.L. Ruiz-González, J.M. González-Calbet, P. Concepción, M. Boronat, A. Corma, Catalysis Today 180 (2012) 59-67.

[55] B. Pillay, M.R. Mathebula, H.B. Friedrich, Applied Catalysis A: General 361 (2009) 57-64.

[56] B. Pillay, M.R. Mathebula, H.B. Friedrich, Catalysis Letters 141 (2011) 1297-1304.

[57] N. Govender, H.B. Friedrich, M.J. van Vuuren, Catalysis Today 97 (2004) 315-324.

[58] T. Naicker, H.B. Friedrich, Journal of Porous Materials 20 (2013) 763-775.

[59] G.J. Panuccio, K.A. Williams, L.D. Schmidt, Chemical Engineering Science 61 (2006) 4207-4219.

[60] J.J. Krummenacher, K.N. West, L.D. Schmidt, Journal of Catalysis 215 (2003) 332-343.

[61] G. Süss-Fink, L. Gonzalez, G.B. Shul'pin, Applied Catalysis A: General 217 (2001) 111-117.

[62] V.D.B.C. Dasireddy, S. Singh, H.B. Friedrich, Applied Catalysis A: General 456 (2013) 105-117.

[63] E.A. Elkhalifa, H.B. Friedrich, Applied Catalysis A: General 373 (2010) 122-131.

[64] V.D.B.C. Dasireddy, H.B. Friedrich, S. Singh, Applied Catalysis A: General 467 (2013) 142-153.

[65] B. Grzybowska-Świerkosz, Topics in Catalysis 21 (2002) 35-46.

[66] E.A. Elkhalifa, H.B. Friedrich, Catalysis Letters 141 (2011) 554-564.

[67] B. Shi, B.H. Davis, Journal of Catalysis 157 (1995) 626-630.

[68] M.M. Hossain, L. Atanda, N. Al-Yassir, S. Al-Khattaf, Chemical Engineering Journal 207-208 (2012) 308-321.

[69] H.H. Kung, M.C. Kung, in: D.D. Eley, H. Pines, B.W. Paul (Eds.), Advances in Catalysis, Academic Press, 1985, pp. 159-198.

[70] M. Narayanappa, V.D.B.C. Dasireddy, H.B. Friedrich, Applied Catalysis A: General 447–448 (2012) 135-143.

[71] A. Brillis, G. Manos, Catalysis Letters 91 (2003) 185-191.

[72] S. Jongpatiwut, P. Sackamduang, T. Rirksomboon, S. Osuwan, D.E. Resasco, Journal of Catalysis 218 (2003) 1-11.

[73] P. Meriaudeau, A. Thangaraj, C. Naccache, S. Narayanan, Journal of Catalysis 146 (1994) 579-582.

[74] P. Mériaudeau, C. Naccache, Catalysis Reviews 39 (1997) 5-48.

[75] J.A. Amelse, J.B. Butt, L.H. Schwartz, Journal of Physical Chemistry 82 (1978) 558-563.

[76] G.B. Raupp, W.N. Delgass, Journal of Catalysis 58 (1979) 337-347.

[77] G.B. Raupp, W.N. Delgass, Journal of Catalysis 58 (1979) 348-360.

[78] G.B. Raupp, W.N. Delgass, Journal of Catalysis 58 (1979) 361-369.

[79] J.W. Niemantsverdriet, A.M. Van der Kraan, W.L. Van Dijk, H.S. Van der Baan, Journal of Physical Chemistry 84 (1980) 3363-3370.

[80] T.R. Motjope, H.T. Dlamini, G.R. Hearne, N.J. Coville, Catalysis Today 71 (2002) 335-341.

[81] F. Pinna, T. Fantinel, G. Strukul, A. Benedetti, N. Pernicone, Applied Catalysis A: General 149 (1997) 341-351.

[82] O.J. Wimmers, P. Arnoldy, J.A. Moulijn, Journal of Physical Chemistry 90 (1986) 1331-1337.

[83] M. Liang, W. Kang, K. Xie, Journal of Natural Gas Chemistry 18 (2009) 110-113.

[84] G. Chang, Unsupported catalyst for the oxidation of methanol to formaldehyde, Google Patents, 1974.

[85] K.Y. Cha, D.H. Ko, D.C. Kim, H.S. Nam, D.H. Choi, High yield production method for 1,3-butadiene, Google Patents, 2013.

[86] R. Iezzi, D. Sanfilippo, Process for the dehydrogenation of ethylbenzene to styrene, Google Patents, 2005.

[87] C. Rubini, L. Cavalli, E. Conca, Catalysts for the dehydrogenation of ethylbenzene to styrene, Google Patents, 1997.

[88] H. Hinago, S. Komada, Ammoxidation catalyst for use in producing acrylonitrile or methacrylonitrile from propane or isobutane by ammoxidation, Google Patents, 2000.

[89] G. Blanchard, G. Ferre, Ammoxidation of saturated hydrocarbons, Google Patents, 1994.

[90] G.C. Hinton, R.I. Johnston, J.D. Pach, H.C. Yang, I. Barton, Water gas shift reaction process, Google Patents, 2011.

[91] S. Sugiyama, K. Kastuma, N. Fukuda, T. Shono, T. Moriga, H. Hayashi, Catalysis Communications 2 (2001) 285-290.

[92] A.J.R. Castro, J.M. Soares, J.M. Filho, A.C. Oliveira, A. Campos, É.R.C. Milet, Fuel 108 (2013) 740-748.

[93] P. Bonnet, J.M.M. Millet, C. Leclercq, J.C. Védrine, Journal of Catalysis 158 (1996) 128-141.

[94] J.E. Miller, M.M. Gonzales, L. Evans, A.G. Sault, C. Zhang, R. Rao, G. Whitwell, A. Maiti, D. King-Smith, Applied Catalysis A: General 231 (2002) 281-292.

[95] P. Nagaraju, C. Srilakshmi, N. Pasha, N. Lingaiah, I. Suryanarayana, P.S. Sai Prasad, Catalysis Today 131 (2008) 393-401.

[96] Y. Wang, B.H. Davis, Applied Catalysis A: General 180 (1999) 277-285.

[97] M. Baldi, V.S. Escribano, J.M.G. Amores, F. Milella, G. Busca, Applied Catalysis B: Environmental 17 (1998) L175-L182.

[98] F.G.E. Nogueira, J.H. Lopes, A.C. Silva, R.M. Lago, J.D. Fabris, L.C.A. Oliveira, Applied Clay Science 51 (2011) 385-389.

[99] S. Scirè, C. Crisafulli, S. Minicò, G.G. Condorelli, A. Di Mauro, Journal of Molecular Catalysis A: Chemical 284 (2008) 24-32.

[100] X. Zhang, G. Dou, Z. Wang, L. Li, Y. Wang, H. Wang, Z. Hao, Journal of Hazardous Materials 260 (2013) 104-111.

[101] G. Ma, X.Y. Liu, Crystal Growth & Design 9 (2009) 2991-2994.

[102] D. Laurencin, N. Almora-Barrios, N.H. de Leeuw, C. Gervais, C. Bonhomme, F. Mauri, W. Chrzanowski, J.C. Knowles, R.J. Newport, A. Wong, Z. Gan, M.E. Smith, Biomaterials 32 (2011) 1826-1837.

[103] M. Zahouily, Y. Abrouki, B. Bahlaouan, A. Rayadh, S. Sebti, Catalysis Communications 4 (2003) 521-524.

[104] T. Tsuchida, J. Kubo, T. Yoshioka, S. Sakuma, T. Takeguchi, W. Ueda, Journal of Catalysis 259 (2008) 183-189.

[105] B. Liptáková, M. Hronec, Z. Cvengrošová, Catalysis Today 61 (2000) 143-148.

[106] S. Sugiyama, T. Minami, H. Hayashi, M. Tanaka, N. Shigemoto, J.B. Moffat, Energy & Fuels 10 (1996) 828-830.

[107] Y.-P. Sun, H.-Y. Fu, D.-l. Zhang, R.-X. Li, H. Chen, X.-J. Li, Catalysis Communications 12 (2010) 188-192.

[108] J.C. Elliott, in: J.C. Elliott (Ed.), Studies in Inorganic Chemistry, Elsevier, 1994, pp. v-vii.

[109] P.W. Brown, B. Constantz, Hydroxyapatite and related materials, CRC Press, 1994.

[110] A. Bigi, E. Boanini, C. Capuccini, M. Gazzano, Inorganica Chimica Acta 360 (2007) 1009-1016.

[111] W.L. Suchanek, K. Byrappa, P. Shuk, R.E. Riman, V.F. Janas, K.S. TenHuisen, Biomaterials 25 (2004) 4647-4657.

[112] A. Yasukawa, T. Yokoyama, K. Kandori, T. Ishikawa, Colloids and Surfaces A: Physicochemical and Engineering Aspects 238 (2004) 133-139.

[113] A. Yasukawa, E. Ueda, K. Kandori, T. Ishikawa, Journal of Colloid and Interface Science 288 (2005) 468-474.

[114] Z. Xiu, M. Lü, S. Liu, G. Zhou, B. Su, H. Zhang, Materials Research Bulletin 40 (2005) 1617-1622.

[115] H. Xu, L. Yang, P. Wang, Y. Liu, M. Peng, Journal of Environmental Management 86 (2008) 319-328.

[116] D.E. Ellis, J. Terra, O. Warschkow, M. Jiang, G.B. Gonzalez, J.S. Okasinski, M.J. Bedzyk, A.M. Rossi, J.-G. Eon, Physical Chemistry Chemical Physics 8 (2006) 967-976.

[117] V. Stanić, S. Dimitrijević, J. Antić-Stanković, M. Mitrić, B. Jokić, I.B. Plećaš, S. Raičević, Applied Surface Science 256 (2010) 6083-6089.

[118] R.X. Fuzeng Ren, Xiang Ge, Yang Leng, Acta Biomaterialia 5 (2009) 3141-3149.

[119] M. Misono, W.K. Hall, Journal of Physical Chemistry 77 (1973) 791-800.

[120] C. Boucetta, M. Kacimi, A. Ensuque, J.-Y. Piquemal, F. Bozon-Verduraz, M. Ziyad, Applied Catalysis A: General 356 (2009) 201-210.

[121] S. Sugiyama, T. Shono, E. Nitta, H. Hayashi, Applied Catalysis A: General 211 (2001) 123-130.

[122] H.-C. Wu, T. Wei, J.-S. Sun, W.-H. Wang, F.-H. Lin, Nanotechnology 18 (2007) 9.

[123] M. Khachani, M. Kacimi, A. Ensuque, J.-Y. Piquemal, C. Connan, F. Bozon-Verduraz, M. Ziyad, Applied Catalysis A: General 388 (2010) 113-123.

[124] K.A. Gross, R. Jackson, J.D. Cashion, L.M. Rodriguez-Lorenzo, European Cells and Materials 3 (2002) 114-117.

[125] T.K. Anee, M. Palanichamy, M. Ashok, N.M. Sundaram, S.N. Kalkura, Materials Letters 58 (2004) 478-482.

[126] R. Morrissey, L.M. Rodriguez-Lorenzo, K.A. Gross, Journal of Materials Science 16 (2005) 387-392.

[127] J. Wang, T. Nonami, K. Yubata, Journal of Materials Science: Materials in Medicine 19 (2008) 2663-2667.

[128] Y. Li, J. Widodo, S. Lim, C.P. Ooi, Journal of Materials Science 47 (2012) 754-763.

[129] Y. Tanizawa, K. Sawamura, Journal of the Chemical Society, Faraday Transactions 86 (1990) 1071-1075.

[130] M. Wakamura, K. Kandori, T. Ishikawa, Colloids and Surfaces A: Physiochemical and Engineering Aspects 164 (2000) 297-305.

[131] M. Wakamura, K. Kandori, T. Ishikawa, Colloids and Surfaces A: Physicochemical and Engineering Aspects 142 (1998) 107-116.

[132] M. Jiang, J. Terra, A.M. Rossi, M.A. Morales, E.M. Baggio Saitovitch, D.E. Ellis, Physical Review B 66 (2002) 224107.

Chapter 2
Experimental

2.1 Catalyst preparation

Precipitation is the most frequently used preparatory method for catalyst synthesis. Catalysts that contain more than one component are prepared by co-precipitation. This wet chemical method involves the formation of mixed crystals by adsorption, occlusion or mechanical entrapment. Figure 2.1 illustrates the general flow scheme for the preparation of a precipitated catalyst.

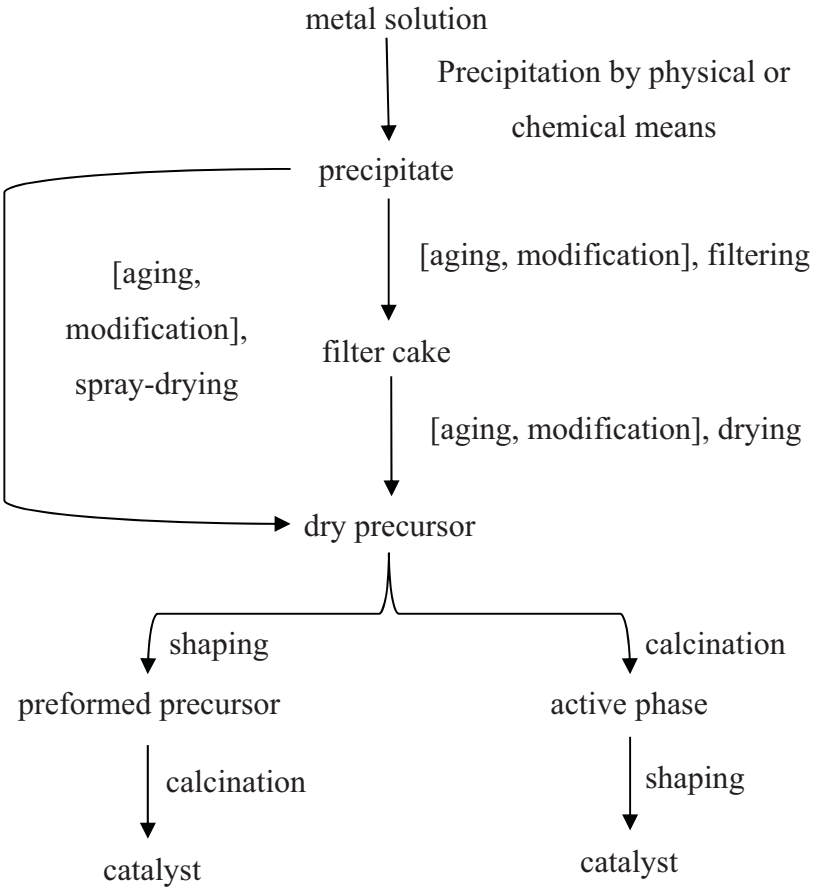

Figure 2.1: Scheme of the preparation of a precipitated catalyst [1]

Co-precipitation is most commonly utilised when a homogenous distribution of catalyst components or precursors with a definite stoichiometry are desired. A nucleus has to form in order for a solid to precipitate out of a homogeneous solution. The formation of a precipitated particle is governed by the free energy of agglomerates of the components of the solution. The total free energy, ΔG, is determined by equation 2:

$$\Delta G = \Delta G_{\text{bulk}} + \Delta G_{\text{interface}} + \Delta G_{\text{others}} \quad (2)$$

where ΔG_{bulk} is the difference of the free energy between solution and solid species, $\Delta G_{\text{interface}}$ is the free energy change related to the formation of the interface and ΔG_{others} summarises all other contributions.

Several possible methods may be used to carry out the precipitation process. In the batch process, the pH and all other parameters, excluding temperature, change continuously during the precipitation due to the consumption of the metal species. The advantage of this method is the simple way in which the product is obtained. A more rigorous process involves the simultaneous addition of the precursors, controlling the pH and the reagent ratios at all times. The control of these parameters prevents phase transitions of the precipitates formed first. This may altogether be avoided by using a continuous process. In the continuous process all the parameters, including temperature, concentration, pH and residence times of the precipitate are kept constant or altered as needed [1].

Hydroxyapatite (HAp) is best prepared by co-precipitation. The characteristics of HAp prepared by this method include high surface area, fine particle size, non-stoichiometry and low crystallinity. These characteristics depend on several factors such as pH, aging time, temperature, and type and concentration of the starting materials. In the precipitation, calcium is supplied as a chloride, nitrate, acetate, hydroxide, carbonate or sulphate salt and phosphorus in the form of ammonium phosphate, phosphoric acid or sometimes sodium and potassium phosphate salts. Nitrates are the preferred metal salts, as NO_3^- ions are not as easily incorporated into the lattice of HAp. Ammonium salts are preferred as a source of phosphorus as opposed to sodium and potassium salts for similar reasons. Maintaining the pH

of the reaction mixture between 9 and 11 is very important as nucleation of HAp occurs in a basic pH range. Adjusting the pH of the solution is best done with ammonia gas or aqueous ammonia as opposed to metal hydroxide salts (such as KOH or NaOH) as this avoids trace contamination of metals that could possibly play a role in the catalysis. The advantage of using an ammonia solution is that NH_4^+ can be removed from the precipitate by decomposition into the gas phase upon heating. It is generally accepted that using a higher pH tends to eliminate the formation of carbonate species in the HAp powders.

Catalyst materials may consist of one or several active components deposited on a high surface area support. The primary advantage of using a support is the optimal dispersion of the catalytically active phase and to stabilise this against sintering. The support used must also be inert. A commonly employed technique used to deposit the active phase on a support is wet impregnation. The impregnation technique involves the inclusion of a precursor into the pore space of the support. The precursor, at this point of the preparation method, is still dissolved in solution and cannot become fixed on the surface. The precursor is generally fixed on the surface by the thermal decomposition of the precursor thus forming the catalytically active phase.

The catalysts used in this study were prepared by two different wet chemical techniques. The techniques chosen were wet impregnation and co-precipitation, because of their simplicity and ease of scale up for industrial applications.

2.1.1 Synthesis of hydroxyapatite

Hydroxyapatite (HAp) was synthesised using a co-precipitation method [2-4]. A solution of diammonium hydrogen orthophosphate, $(NH_4)_2HPO_4$ (5.6 g), (1.00 mol) (Merck, 98.5 %) was adjusted to pH 11.0 using a dilute ammonia solution (Rochelle Chemicals, 25 %) and then diluted to 200 mL with double distilled water. The pH was measured using a pH 211 Microprocessor pH meter (HANNA Instruments). Similarly, a calcium nitrate tetrahydrate, $Ca(NO_3)_2.4H_2O$ (23.7 g), (0.167 mol) (Merck, 98 %) solution was prepared and the pH adjusted to 11.0 and this solution was then diluted to 200 mL using double distilled water.

The $(NH_4)_2HPO_4$ solution was added drop-wise to the $Ca(NO_3)_2.4H_2O$ solution with constant and vigorous stirring at room temperature over a period of 1 hour. The pH of the mixture was maintained between 9.50 and 11.0 throughout, using diluted ammonia. The resultant white gelatinous precipitate was heated to and maintained at 85 °C for 1.5 hours and then allowed to cool to room temperature. Thereafter, the precipitate was filtered under vacuum and washed repeatedly until the filtrate was neutral, thus having ensured the removal of excess diluted ammonia. The HAp was then dried in an oven overnight at 120 °C and thereafter, calcined at 550 °C (reached from room temperature at a ramp rate of 1.5 °C min^{-1}) for 6 hours.

2.1.2 Synthesis of the iron supported on hydroxyapatite catalyst

Iron in the form of iron oxide, α-Fe_2O_3, was supported on the surface of HAp using a wet impregnation technique [2]. A 1 wt% loading of iron supported on Hap catalyst was synthesised by a single impregnation of the support (HAp) with a ferric nitrate, $Fe(NO_3)_3.9H_2O$ (Merck, 97 %), solution. The $Fe(NO_3)_3.9H_2O$ (0.19 g) was dissolved in 20 mL of double distilled water and added drop-wise to the HAp (2.0 g) with continuous stirring. The mixture was left to stir for 6 hours after which excess water was removed by gentle heating and the resultant compound was dried overnight at 120 °C. The powdered form of the catalyst material was calcined at 550 °C at a ramp rate of 1.5 °C min^{-1} for 6 hours. Similarly 3 and 9 wt% iron supported on HAp catalysts were prepared. The catalysts were denoted 1-WET, 3-WET and 9-WET where the number denoted the loadings of 1, 3, and 9 wt% iron respectively.

2.1.3 Synthesis of iron substituted hydroxyapatite catalyst

Weight percentage loadings of 1, 3 and 9 wt% iron substituted HAps were prepared using a co-precipitation method [4-6]. The metal nitrate precursor solution was prepared by adding calculated masses of $Ca(NO_3)_2.4H_2O$ (46.7 g) and $Fe(NO_3)_3.9H_2O$ (1.2 g) to 60 mL of double distilled water. This solution was then diluted to 200 mL with double distilled water. A 100 mL solution of $(NH_4)_2HPO_4$ (11.3 g) was then prepared and adjusted to pH 11.0. This phosphorus containing solution was then diluted to 160 mL using double distilled water. The

metal nitrate solution was added drop-wise to the phosphate solution over a period of 1 hour with constant and vigorous stirring at room temperature. The pH was maintained at 11.0. A brown gelatinous precipitate that formed was heated to and maintained at 80 °C for 1.5 hours to ensure removal of NH_4^+ in solution. The precipitate was then filtered under vacuum and washed thoroughly to ensure the removal of excess unreacted precursor ions. The precipitate was then dried overnight in an oven at 120 °C and then powdered. The powdered catalyst material was calcined at a temperature of 550 °C at a ramp rate of 1.5 °C min^{-1} for 6 hours. The 3 and 9 wt% iron substituted Hap catalysts were prepared in a similar manner.

2.2 Catalyst characterisation

Various characterisation techniques were employed to investigate the physical and chemical properties of the synthesised catalyst materials.

2.2.1 Inductively coupled plasma optical emission spectroscopy

Quantitative elemental analyses were performed by inductively coupled plasma optical emission spectroscopy (ICPOES) using a Perkin Elmer Optima 5300 DV spectrometer. Sample preparation involved the digestion of 30 mg of powdered catalyst in 10 mL of aqua regia. The acid digested samples were transferred to a 100 mL volumetric flask and diluted to the mark with double distilled water. Instrument calibration was performed using separate standards of Ca and Fe (Fluka Chemica, 1000 ppm in 0.5 M HNO_3) and P (Fluka Chemica, 1000 ppm in H_2O).

2.2.2 Powder X-ray diffraction

Powder X-ray diffraction (PXRD) patterns were obtained using a Bruker D8 Advance diffractometer equipped with a graphite monochromator operated at 40 kV and 40 mA. The radiation source was a CuKα X-ray source with λ = 1.5406 Å. Data was collected at a step of 0.021 ° and at a scanning speed of 0.454 ° s^{-1}. The 2θ range covered was between 10 ° to 70 °. For *in situ* PXRD analyses, the instrument was fitted with a XRK 900 reaction chamber and a

TCU 750 temperature control unit. Measurements were taken over the temperature range of 100 – 750 °C at 50 °C increments under reducing and oxidising conditions. For reduction, a gaseous mixture of 5 % H_2 in N_2 was used and oxidation was carried out by flowing air through the reaction chamber.

2.2.3 Fourier transform infrared spectroscopy

Analyses were carried out at room temperature using a Perkin Elmer Spectrum 100 FTIR spectrometer fitted with a Universal Attenuated Total Reflectance (ATR) sampling accessory. The data was processed using Spectrum® software. A small amount of the powdered catalyst was placed onto the ATR crystal and a pressure of 120 psi was applied to ensure contact between the crystal and the catalyst material.

2.2.4 Raman spectroscopy

Raman spectra were measured using a Delta Nu Advantage 532 instrument fitted with a 532 nm laser source (green) and operated by NuSpec® software. Laser intensity and the integration time of the scans were varied until each sample gave clear and reproducible spectra. All analyses were carried out at room temperature with the powdered sample loaded in quartz tubes.

2.2.5 Nitrogen physisorption analysis

Surface area, pore volume and N_2 adsorption-desorption measurements were obtained by N_2 physisorption isotherms at 77 K using the Micromeritics Tristar II Surface Area and Porosity Analyser. The powdered catalysts were degased at 200 °C under a flow of N_2 for 16 hours prior to analysis using a Micromeritics Flow Prep 060 Instrument. Approximately 200 mg of powdered sample was measured into the sample holder. Analyses were carried out in the presence of liquid N_2 at 153 K, over the pressure range, p/p_o = 30 – 790 mmHg.

2.2.6 Electron microscopy

Transmission electron microscopy

Transmission electron microscopy (TEM) was performed on a JEOL JEM 1010 Transmission Electron Microscope operated at a voltage of 100 μm. A small quantity of the powdered catalyst material was dispersed in a 50 % acetone in water solution by sonication for 2 minutes. Copper grids were immersed in these solutions and after drying were viewed under the microscope.

Scanning electron microscopy and energy dispersive X-ray spectroscopy

Surface morphology was investigated by this technique. Scanning electron microscopy (SEM) sample preparation involved the mounting of a powdered catalyst on an aluminium stub with the aid of double sided carbon tape. The samples were sputter coated with Au-Pd and transferred into the Zeiss ULTRA 55 (field emission tungsten hairpin filament with a ZrO reserve as an electron source) and secondary electron imaging was performed.

Sample preparation for energy dispersive X-ray spectroscopy (EDX) mapping involved the mixing of a small amount of the sample with resin in a plastic mould. After the curing period, the sample block was removed and the surface where the catalyst particles had settled was polished with diamond paste to obtain a smooth and flat surface. The polished sample was then coated with carbon and transferred directly into the microscope for analysis. The Zeiss EVO 40 (fitted with a tungsten filament) was used for the back scattered electron (BSE) imaging and EDX analysis. EDX data was interpreted using Bruker Esprit software. The EDX analysis was performed at accelerated voltages of 20 kV, a take-off angle of 35.0 ° and a sample tilt of 0.0 °. A working distance of 14 mm was used so that the EDX detector was directly in line with the point on the sample where the electron beam made contact.

2.2.7 Temperature programmed techniques

Temperature programmed techniques were performed using a Micromeritics 2920 Autochem II Chemisorption Analyser.

Temperature programmed reduction and oxidation

For the temperature programmed reduction (TPR) and temperature programmed oxidation (TPO) experiments, approximately 50 mg of powdered sample was loaded into a quartz u-shaped reactor tube, sandwiched between two layers of quartz wool. Sample preparation involved heating the catalyst to 400 °C under a flow of Ar, followed by gradual cooling to 80 °C. For TPR analysis, the procedure involved the gradual heating of the sample to 950 °C at a rate of 10 °C min^{-1} under a steady flow of 5 % H_2 in Ar. The reduced sample was cooled under a flow of Ar to 80 °C and then subjected to a TPO analysis with the same temperature program but under a steady flow of air. After the TPO analysis the sample was cooled to 80 °C under a flow of Ar and then subjected to a TPR analysis if required.

Temperature programmed desorption

CO_2 temperature programmed desorption (CO_2-TPD) experiments used approximately 30 mg of powdered sample. The samples were pre-treated at 350 °C under a flow of He for 1 hour. The sample was then allowed to cool down to 80 °C. Thereafter a mixture of 5 % CO_2 in He was passed over the catalyst at a flow rate of 30 mL min^{-1} for 1 hour. The excess CO_2 was removed by purging with He for 30 minutes. The temperature was then gradually raised to 950 °C by ramping at 10 °C min^{-1} under a flow of helium and desorption data was recorded.

2.3 Catalytic testing

For catalytic testing, the reactor was set up such that air could be used as an oxidant, while N_2 was delivered as a diluent gas in appropriate amounts so as to achieve the desired gas hourly

space velocity (GHSV). All the reactions were performed with an *n*-octane (Merck, >98 %) concentration in the gaseous mixture (v/v) above the upper flammability limit.

2.3.1 Reactors in heterogeneous catalysis

Three types of reactors exist for heterogeneously catalysed reactions, viz. fluidised-bed, stirred-tank and fixed-bed reactors.

Fluidised-bed reactors involve the catalyst particles suspended in the reactant gas allowing for excellent dispersion of the catalyst into the gaseous reactants, efficient temperature control and heat transfer. The upwards gaseous flow facilitates the fluidised state of the reactor. The design and implementation of such reactors on a laboratory scale are difficult and expensive. Industrial applications of fluidised-bed reactors include fluid catalytic cracking, where solid acid catalysts are generally rapidly deactivated by coke formation. The catalyst is continuously discharged from the reactor and regenerated in an air fluidized generator.

Stirred-tank reactors are generally used in homogeneous catalysis and have the advantage of good contact between the reactants and catalyst. These reactors offer applications in both batch and continuous reactor modes. Disadvantages of these reactors is that they afford lower conversion, by-passing and channelling is possible but with poor agitation normally due to size limitation by motor size, shaft length and weight. In addition catalyst separation and reuse post reaction may be made complicated by the homogeneity of the reactant, product and catalyst.

Fixed-bed reactors are classified as plug-flow closed systems. Catalysed reactions involve the gas phase reactant being fed continuously downwards into the reactor. Fixed-bed reactors can be operated either adiabatically or isothermally depending on the required conditions. The most convenient and generally the cheapest way of carrying out laboratory scale heterogeneously catalysed gas phase reactions are by employing a continuous flow fixed-bed reactor system.

2.3.2 Fixed-bed reactor set up

All catalytic testing was performed in a continuous flow fixed-bed reactor, operated in a down-flow mode. The reactor scheme is shown in Figure 2.2.

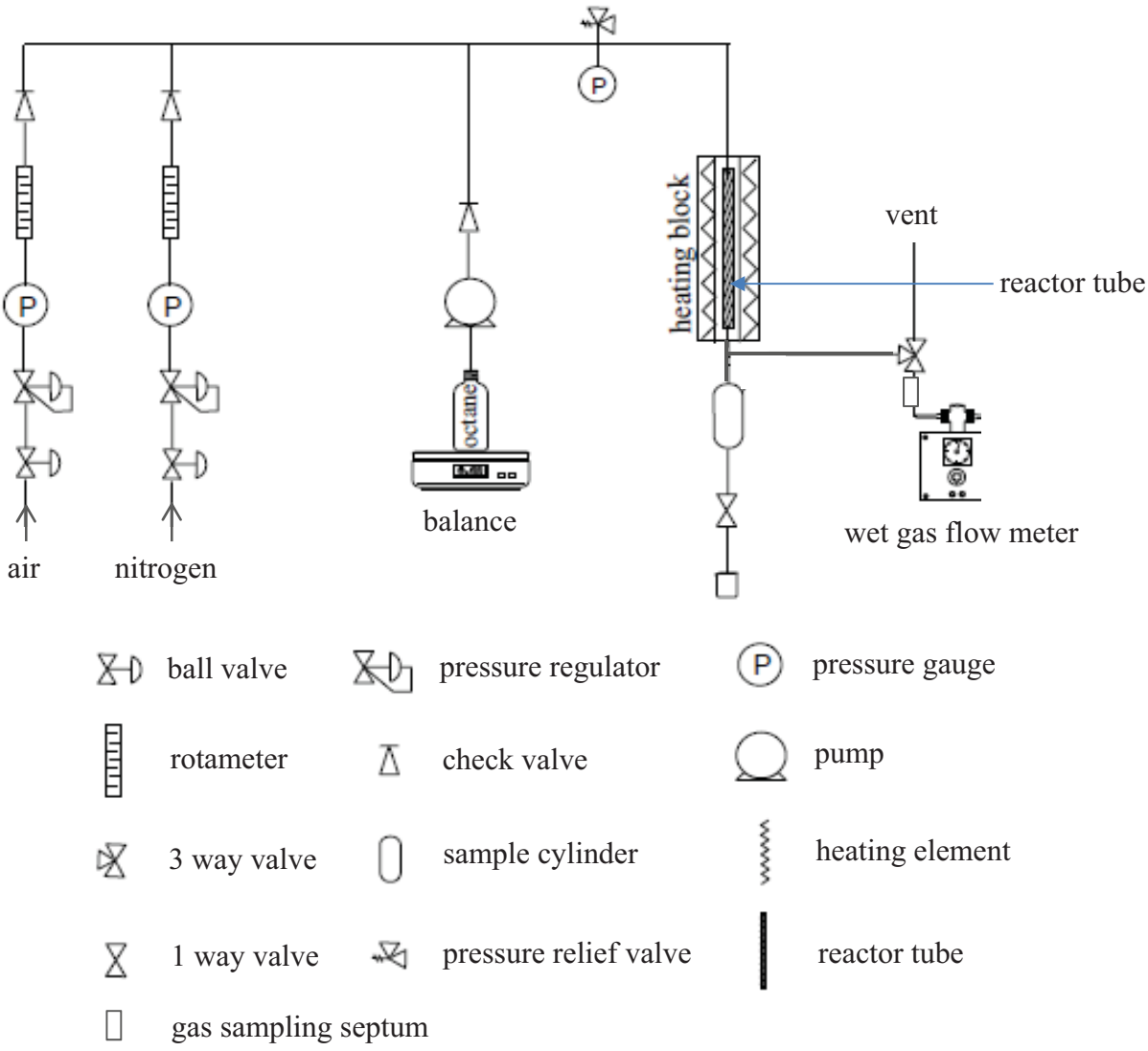

Figure 2.2: Scheme of the fixed-bed reactor set up

The gases were fed into the system via stainless steel tubing (Swagelock grade 316). Gas pressure was regulated at 100 kPa using mini-regulators while the individual flow rates were controlled using calibrated rotameters. The feed, *n*-octane, was introduced using a calibrated Lab Alliance Series II HPLC Pump and the mass delivered was measured by difference using

an electronic balance. In order to maintain the feed in gaseous phase, the feed lines after the point of introduction were heated, using heating tape to 200 °C. The temperature was maintained at 200 °C using a CB-100 RK temperature control unit with internal relay and monitored using K-type thermocouples.

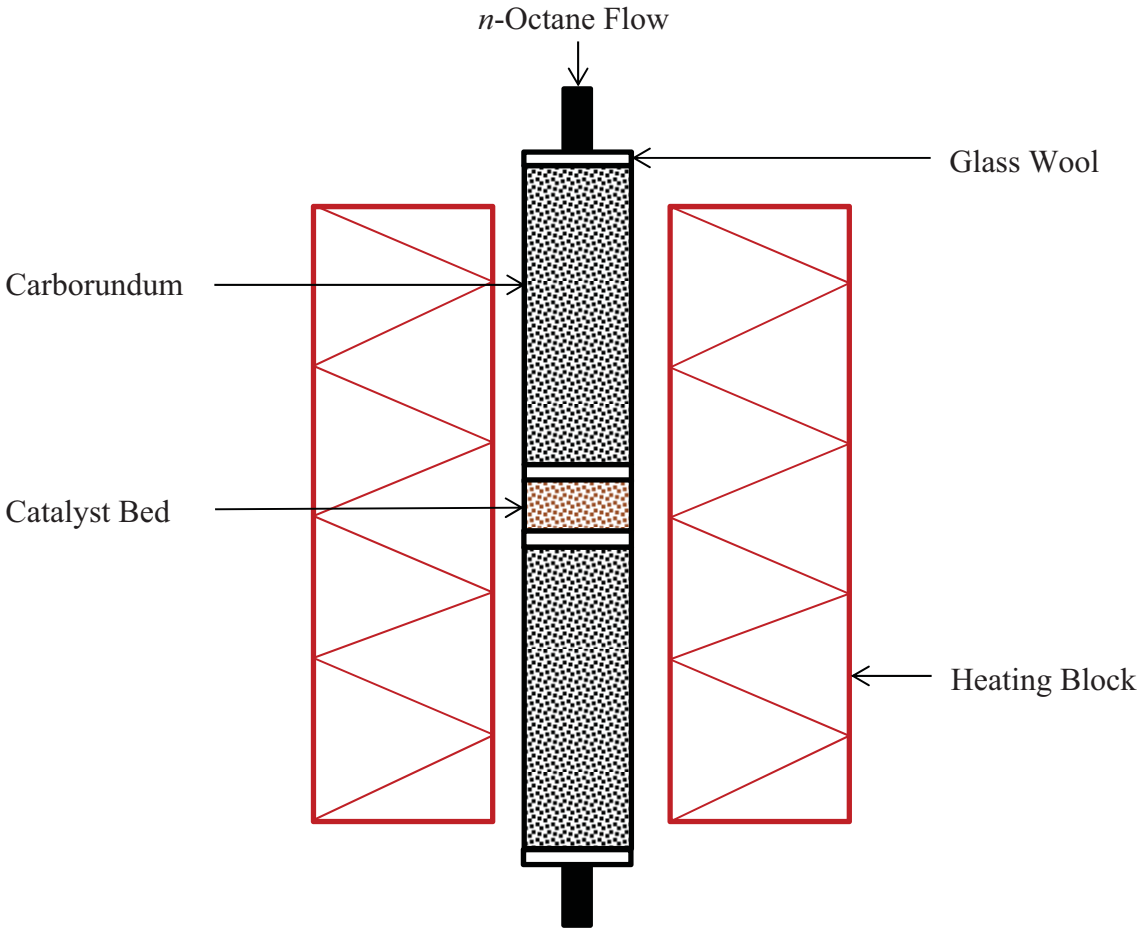

Figure 2.3: Cross sectional diagram of reactor tube

The reactor tube (Figure 2.3) in which the catalysts were loaded was a ½ " (outer diameter) grade 316 stainless steel tube supplied by Swagelok and cut to 34 cm in length. Suitable Swagelok stainless steel fittings were used to reduce the reactor tube down to the ¼ " tubing used in the construction of the rest of the reactor. In all reactions, the reactor tube was packed with 1 cm^3 of pelletised catalyst sandwiched between two layers of glass wool and positioned at the hotspot of the calibrated reactor heating block. The spaces in the reactor tube were packed with 24 gritt carborundum and stoppered at either end with glass wool. This ensured

that the catalyst and carborundum remained in the reactor tube and also reduced free head space within the reactor tube thus inhibiting gas phase cracking of the feed [7]. Total flow rates of the gaseous products were measured using a Ritter type wet gas flow meter (WGFM). Gaseous samples for gas chromatography (GC) analyses were drawn, using a gas tight syringe, through a septum fitted into a stainless steel grade 316 T-piece located on the gas vent. All liquid products and unreacted feed were collected in a cylindrical stainless steel vessel (sample cylinder) that was cooled to ≈ 1.0 °C by means of a FHM Instruments refrigeration chilled unit.

Prior to catalytic testing the reactor was pressurised and monitored for leaks. Thereafter, air and N_2 flow rates were set to the desired values using the relevant rotameters (summarised in Table A1, in Appendix A). The flow of each gas was verified using a Perkin Elmer PE 1000 Electronic Flowmeter. Sampling was done once steady state was achieved, usually after one hour at each temperature. Catalytic testing was carried out in duplicate and in some cases triplicate. Conversion and selectivity of the replicate runs data varied within ± 5 mol%. The carbon balances of the reactions varied within a range of 95 – 105 %.

2.3.3 Product analysis

The components of the product streams were separated and quantified by GC and GC coupled to mass spectrometry (GC-MS). Gaseous products were analysed utilizing a Perkin Elmer Clarus 400 GC fitted with a 30 m × 530 µm Supelco Carboxen 1006 PLOT column and a thermal conductivity detector (GC-TCD). With injection volumes of 0.2 mL, the separation and quantification of carbon oxides (CO_x) were achieved. The remaining gaseous products (0.2 mL injection volumes), liquid products and unreacted feed (0.2 µL injection volume drawn in a 1.0 µL glass syringe, supplied by SGE) were analysed on a Perkin Elmer Clarus 480 GC fitted with a 50 m × 200 µm PONA capillary column and flame ionisation detector (GC-FID). GC-MS analyses were performed on a Perkin Elmer Clarus 500 GC fitted with a 50 m PONA column and was used to qualitatively determine the compounds present in the product stream. The spread sheets used to calculate conversion, selectivity and carbon balance are shown in Appendix A.

References

[1] F. Schüth, K. Unger, in: G. Ertl, H. Knözinger, J. Wietkamp (Eds.), Handbook of Heterogeneous Catalysis, 1st ed., VCH Verlagsgesellschaft, Weinheim, Federal Republic of Germany, 1997, pp. 72-85.

[2] V.D.B.C. Dasireddy, S. Singh, H.B. Friedrich, Applied Catalysis A: General 421-422 (2012) 58-69.

[3] M. Khachani, M. Kacimi, A. Ensuque, J.-Y. Piquemal, C. Connan, F. Bozon-Verduraz, M. Ziyad, Applied Catalysis A: General 388 (2010) 113-123.

[4] M. Wakamura, K. Kandori, T. Ishikawa, Colloids and Surfaces A: Physiochemical and Engineering Aspects 164 (2000) 297-305.

[5] M. Wakamura, K. Kandori, T. Ishikawa, Colloids and Surfaces A: Physicochemical and Engineering Aspects 142 (1998) 107-116.

[6] D. Laurencin, N. Almora-Barrios, N.H. de Leeuw, C. Gervais, C. Bonhomme, F. Mauri, W. Chrzanowski, J.C. Knowles, R.J. Newport, A. Wong, Z. Gan, M.E. Smith, Biomaterials 32 (2011) 1826-1837.

[7] H.B. Friedrich, A.S. Mahomed, Applied Catalysis A: General 347 (2008) 11-22.

Chapter 3

Catalyst Characterisation

3.1 Elemental analysis

Inductively coupled plasma optical emission spectroscopy (ICPOES) was used to quantify the elemental compositions of the iron modified hydroxyapatite (HAp) catalysts (Table 3.1). This analytical technique also provided insight on the metal to phosphate molar ratios of the synthetic powders.

Table 3.1: Elemental analysis of HAp and the iron modified HAp catalysts

Catalyst	Fe loading/ wt%	[1]M/P	[2]Ca/P	[3]Fe/P
HAp	-	1.63	1.63	-
1-WET	0.98	1.64	1.61	0.03
3-WET	2.89	1.68	1.58	0.10
9-WET	8.91	1.90	1.61	0.29
1-COP	0.92	1.67	1.64	0.03
3-COP	2.68	1.68	1.58	0.10
9-COP	8.78	1.86	1.56	0.30

[1]metal to phosphate molar ratio, [2]calcium to phosphate molar ratio, [3]iron to phosphate molar ratio

The iron supported on HAp catalysts were denoted as 1-WET, 3-WET and 9-WET respectively. The numbers 1, 3 and 9 represented the nominal weight percentage of iron in the catalysts and was confirmed by the elemental analysis. Similarly, the iron substituted HAps were denoted 1-COP, 3-COP and 9-COP respectively and their nominal iron weight percentages confirmed by elemental analysis.

The metal to phosphorus molar ratios of the iron substituted HAps showed calcium deficiency in all the catalysts. A slight decrease in the calcium content was observed and corresponded to an increase in the iron content. The limited range of Ca/P molar ratio suggested that the formation of the apatite structure with a substitution of calcium cations with iron cations was favourable.

3.2 Powder X-ray diffraction analysis

The powder X-ray diffraction (PXRD) patterns of all the iron supported on HAp catalysts (Figure 3.1) showed reflections characteristic of HAp in the 2θ range of 20 – 70 °.

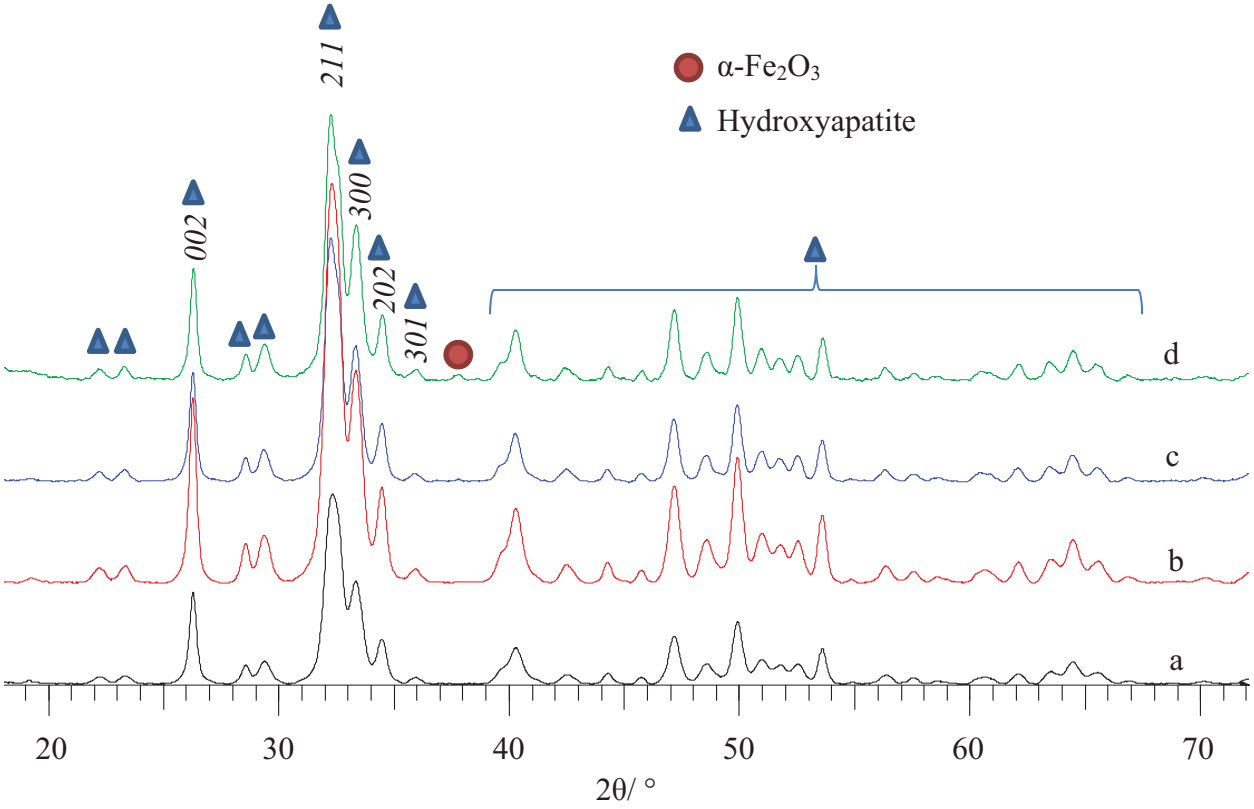

Figure 3.1: PXRD patterns of (a) HAp, (b) the 1-WET catalyst, (c) the 3-WET catalyst and (d) the 9-WET catalyst

The close correlation of these patterns to that of the reference pattern of HAp (JCPDS file no. 9-930) provided strong evidence that the synthesis of HAp was successful and that its structure had been retained after iron oxide was supported on its surface. There were no

significant changes in the d-spacing of the characteristic HAp reflections observed in any of the iron supported on HAp catalysts. This implied that the HAp lattice remained unaffected during the wet impregnation process and subsequent thermal treatment. For the 1-WET and 3-WET catalysts, i.e. the catalysts with weight loadings of 1 wt% and 3 wt% iron, no additional phases corresponding to iron were detected. A mixture of several phases which are poorly crystalline or in a state of fine division, often lead to the weakening or broadening of diffraction reflections, which may overlap [1]. The distribution of iron throughout the surface of the support could have been a contributing factor to this with respect to the limit of detection of the instrument, or the amorphous nature of iron oxide may have led to its presence in a poorly crystalline state [1, 2]. Another contributing factor would have been the significant peak overlap between reflections characteristic of HAp and α-Fe_2O_3. The PXRD pattern of 9-WET showed an additional phase of low intensity that corresponded to α-Fe_2O_3 (JCPDS file no. 33-0664) with a d-spacing of 2.39 and 2θ of 37.66 °. The presence of this phase confirmed that the wet impregnation technique used for the synthesis of these catalysts was successful and suggested that iron was supported, as α-Fe_2O_3, on the surface of HAp.

An estimation of the degree of crystallinity (X_c) (Table 3.2) of the catalysts was calculated using equation 3:

$$X_c = 1 - (V_{112/300} \div I_{300}) \quad (3)$$

where $V_{112/300}$ is the intensity of the shoulder between the (112) and (300) diffraction peaks and I_{300} is the intensity of the (300) peak. The average crystallite sizes (X_s) (Table 3.2) of the powders were estimated from the peak broadening of the XRD patterns using the Scherrer equation (equation 4):

$$X_s = \frac{0.9\lambda}{(FWHM \times Cos\theta)} \quad (4)$$

making use of the *002* reflection of HAp [3]. The estimated X_c values of the iron supported on HAp catalysts showed a slight decrease with increased iron loading, probably due to the amorphous nature of α-Fe_2O_3.

The X_s of the iron supported on HAp catalysts showed no significant change with an increase in iron loading. This result also suggestes that the HAp lattice was not affected by the wet impregnation synthetic technique and that the supported α-Fe_2O_3 did not disturb or distort the apatite lattice.

Table 3.2: Estimated crystallite size (X_s) and degree of crystallinity (X_c) of HAp and the iron modified HAp catalysts

Catalyst	X_s**/ nm**	X_c
HAp	0.6	0.5
1-WET	0.6	0.5
3-WET	0.5	0.4
9-WET	0.6	0.4
1-COP	0.5	0.4
3-COP	0.4	0.3
9-COP	1.1	0.3

The PXRD patterns of the iron substituted HAp catalyst materials (Figure 3.2) showed characteristic reflections of HAp (JCPDS file no. 9-930). This result, together with absence of reflections corresponding to any iron containing phase even at relatively high iron loading (9-COP), suggests that the substitution of calcium with iron in the HAp lattice was achieved. There was no observed shift in the d-spacing of the reflections. The estimated X_c (Table 3.2) of the iron substituted catalysts showed a decreasing trend with an increase of iron substituted into the lattice of HAp as reflected by the decrease and broadening of peaks in the PXRD patterns. The estimated X_s (Table 3.2) of the powdered materials showed no significant difference at low iron loading. However, the 9-COP catalyst showed significant increase in crystallite size (X_s). The structure of many catalytic phases exhibit numerous crystal defects of substitution or displacement with respect to a perfect lattice, due to poorly defined stoichiometry [1]. The increase in X_s at higher iron loading (9-COP) may be attributed to changes in the apatite-like lattice.

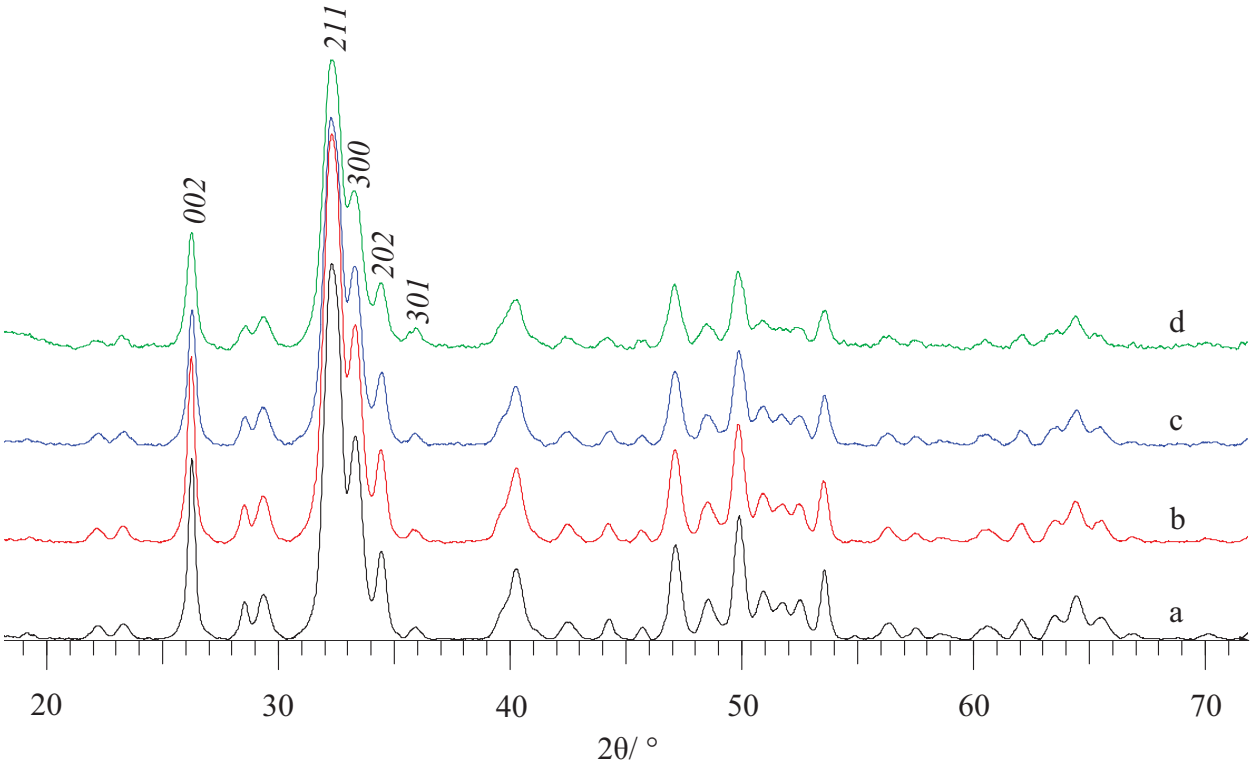

Figure 3.2: PXRD patterns of (a) HAp, (b) the 1-COP catalyst, (c) the 3-COP catalyst and (d) the 9-COP catalyst

X-ray line broadening analysis employing the Scherrer equation provided mean crystallite size estimations. The breadth of an X-ray reflection on the lattice planes of crystallites (small single crystals) depends upon the characteristics of the crystallites, more specifically with respect to size and lattice defects, and instrumental factors.

3.3 *In situ* powder X-ray diffraction analysis

A simple room temperature scan of a powdered catalyst material is sometimes not enough to understand the phase composition of a catalyst under reaction conditions. *In situ* experimentation allowed determination of phase changes under varying redox conditions. The reduction profiles of the 3-COP catalyst (Figures 3.3 and 3.4) showed the formation of an iron(II) pyrophosphate phase that was oxidised back to iron substituted HAp. This result proved promising as they reflected the ability of these catalyst materials to undergo a key step in an ODH reaction, a reduction and re-oxidation (REDOX) cycle. HAp has been shown to be

stable up to a temperature of 900 °C [4]. Thus, changes in the catalyst material were assumed to be caused by the influence of the iron species.

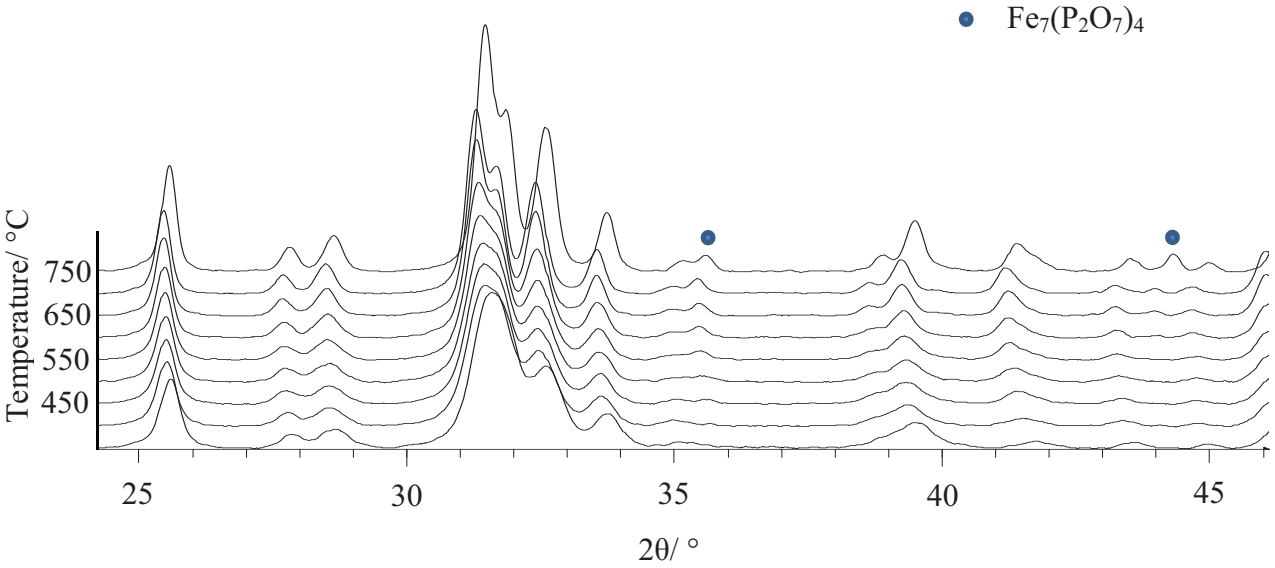

Figure 3.3: *In situ* PXRD patterns of the 3-COP catalyst in a reducing environment, 5 % H_2 in nitrogen

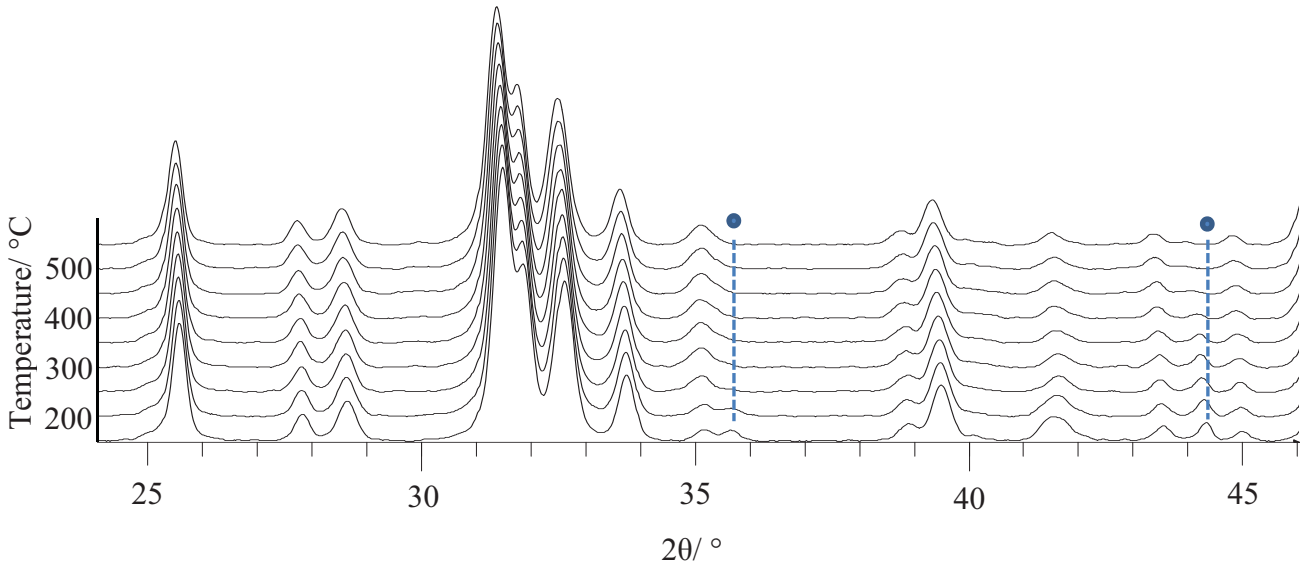

Figure 3.4: *In situ* PXRD patterns of the 3-COP catalyst in an oxidizing environment, air

3.4 Fourier transform infrared spectroscopy

The Fourier transform infrared (FTIR) spectra of all the catalysts showed characteristic peaks of the functional groups of HAp. This indicated that the HAp structure had been retained. The assignments of the bands observed in the FTIR spectra of the catalysts are summarised in Table 3.3 and were in accordance with the assignments of Nyquist and Kagel [5].

Table 3.3: Summarised assignments of observed FTIR bands for the iron supported on HAp catalysts

Wavenumber/ cm^{-1}	**Assignments**
3300 - 3430 broad	OH---O
3575	OH^-
1630	H_2O structural
1080	$(PO_4)^{3-}$
1020	$(PO_4)^{3-}$
875	$(HPO_4)^{2-}$ [P-OH]
620	$(OH)^-$
600	$(PO_4)^{3-}$
560	$(PO_4)^{3-}$
472	$(PO_4)^{3-}$

The broad band in the range of 3300 – 3430 cm^{-1} was attributed to the hydroxide (OH^-) stretching of adsorbed water (H_2O) on the surface of HAp. The absorption band observed at 3575 cm^{-1} was attributed to the stretching vibration mode of lattice or structural OH^- groups and was in accordance with that observed by Wu *et al.* [6]. The band in the range 625 – 635 cm^{-1} was also assigned to the structural OH^- group of HAp. The symmetric v_1 and asymmetric v_3 phosphate (PO_4^{3-}) bands lay in the region of 900 – 1200 cm^{-1}. These along with the v_4 (PO_4^{3-}) adsorption bands in the region of 500 – 700 cm^{-1} were reported as characteristic for HAp [7]. (The FTIR spectra of HAp and the 1-WET, 3-WET and 9-WET catalysts are shown in Figure B1, Appendix B).

The FTIR spectrum of HAp (Figure 3.5 a) showed a band at a wavenumber of 620 cm^{-1}. The intensity of this band observed in the spectrum of the iron substituted HAp catalysts decreased (Figure 3.5 b, c and d). This was caused by the substitution of iron cations into the lattice of HAp. The incorporation of iron into the structural lattice of HAp led to a shift in the wavenumber of the bands at around 620 cm^{-1} attributed to the symmetric vibrations (v_5) of the structural OH^- groups [8]. This trend was observed when the spectra of the iron substituted HAps were compared to the spectrum of HAp and was in accordance with the observations of Bigi *et al.* [9].

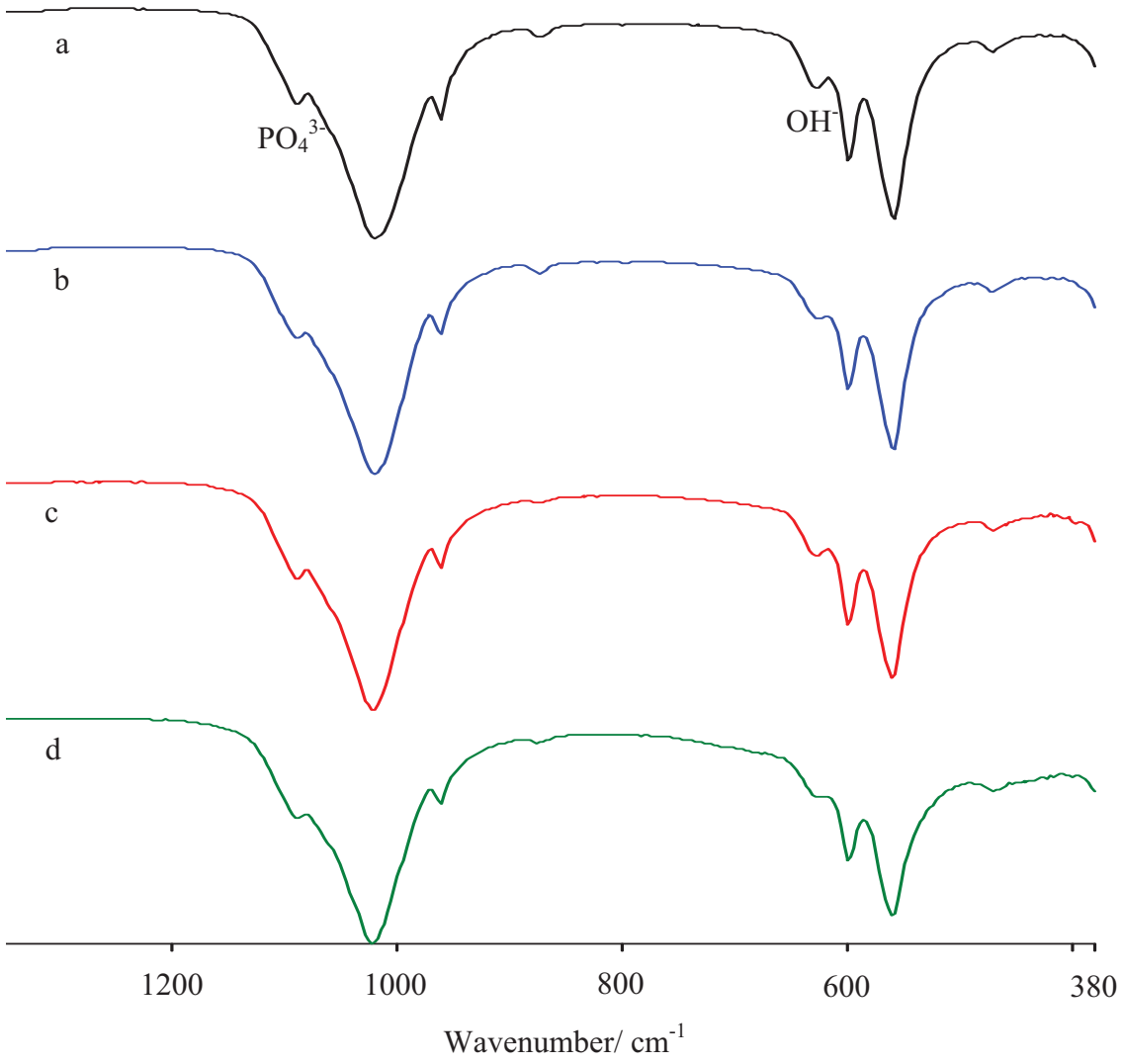

Figure 3.5: FTIR spectra of (a) HAp, (b) the 1-COP catalyst, (c) the 3-COP catalyst and (d) the 9-COP catalyst

A similar trend was observed for the bands attributed to the symmetric stretching (v_1) and bending (v_4) modes of the PO_4^{3-} groups. It has been reported that the shifts in the PO_4^{3-} group frequencies are caused by a decreased anion-anion repulsion concomitant with an increased anion-anion separation upon substitution of a metal cation into the HAp lattice [9-11]. A decrease in M---OPO_3 and M---OH bond distances, where M denotes any metal with a smaller ionic radius than Ca^{2+}, was observed by Laurencin *et al*. [12]. Fe^{3+} ions have smaller ionic radii than Ca^{2+}. Thus, the shift in the OH^- group and PO_4^{3-} band frequencies of iron substituted HAps can be attributed to distortions in the internal HAp lattice brought on by the incorporation of iron into its structure.

Khachani *et al*. [13] have attributed the shift in position and decrease in intensity of the structural OH^- bands to a loss of the proton, an effect of a charge compensation mechanism that accompanied the substitution of calcium cations with iron cations. The remnant O^{2-} species are stabilised within the structural tunnels of the apatite framework and may play a role in catalytic activity. These O^{2-} species have been shown to function as basic sites [14].

3.5 Raman spectroscopy

All bands observed in the Raman spectra of HAp and the iron modified HAp catalysts belonged to the tetrahedral PO_4^{3-} groups of the HAp lattice. The bands observed in the spectra of the iron supported on HAp catalysts are summarised in Table 3.4.

Table 3.4: Summarised assignments of tetrahedral PO_4^{3-} bands observed from the Raman spectra of the iron supported on HAp catalysts

Wavenumber/ cm^{-1}	**Assignments**
462	v_2
600	v_4
960	v_3
1050	v_1

The spectra were dominated by the v_1 (PO_4^{3-}) stretching vibration of HAp corresponding to the asymmetric stretching of P-O bonds. This PO_4^{3-} band is generally the most intense peak observed in a HAp spectrum [15, 16]. The remaining vibration bands, viz. v_2, v_3, and v_4 were attributed to the doubly degenerate O-P-O bending modes, asymmetric P-O stretching and P movement, and triply degenerate T_2 modes of O-P-O bending character of the structural PO_4^{3-} tetrahedra of the HAp lattice respectively [17-19].

Cusco *et al.* [19] stated that distortions in the PO_4^{3-} tetrahedra present in crystalline fields of molecular crystals such as HAp influence changes in the intra-tetrahedral bond lengths and angles, giving rise to shifts and splitting of the PO_4^{3-} normal modes. Thus, internal PO_4^{3-} bands depend on the crystallographic structure of a material. In addition, Khalid *et al*. [20] showed that the intensity of these characteristic bands is dependent on the crystalline nature of synthetic HAp. The more amorphous in nature, the less intense these bands appear until they become indistinguishable from the base line. In the case of strontium, Zhai *et al.* [21] showed that upon strontium substitution into the lattice of HAp a decrease in the wavenumber of the characteristic bands occurs. It can thus be assumed that upon the substitution of calcium with any metal cation with a different ionic radius, a change in the wavenumber of its characteristic bands will occur.

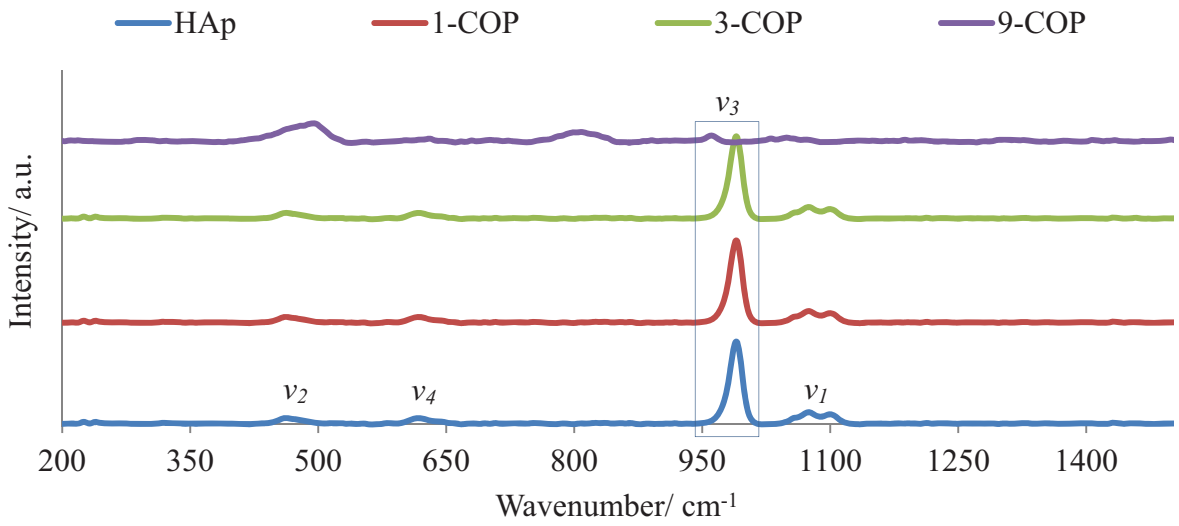

Figure 3.6: Raman spectra of HAp and the iron substituted HAp catalysts reflecting PO_4^{3-} vibration and stretching modes

Figure 3.6 illustrates a decrease in the intensity and position of the v_3 (PO_4^{3-}) band which was observed with an increase in iron content. Both observations were consistent with increased iron substitution into the lattice of HAp. An additional band was observed in the spectrum of the 9-COP catalyst, due to Fe-O-P bonds of the iron substituted into the HAp lattice.

3.6 Nitrogen physisorption analysis

The determined surface areas (Table 3.5) of the iron supported on HAp catalysts showed a decrease upon iron loading when compared to HAp.

Table 3.5: BET surface area and pore volume of HAp and the iron modified HAp catalysts

Catalyst	Surface Area/ $m^2\ g^{-1}$	Pore Volume/ $cm^3\ g^{-1}$
HAp	69	0.30
1-WET	61	0.28
3-WET	53	0.25
9-WET	56	0.29
1-COP	71	0.36
3-COP	70	0.39
9-COP	86	0.43

This was caused by the blockage of narrow pores along the surface of HAp by the dispersion of α-Fe_2O_3 on the support making these inaccessible to the nitrogen (N_2) molecules. Similar results have been reported in literature for metal oxides supported on HAp [7, 22]. The decrease in surface area from a 1 wt% iron loading (1-WET) to a 3 wt% iron loading (3-WET) was attributed to an increase in the amount of iron supported on the surface of HAp. There was a slight increase in the surface area of the 9-WET catalyst when compared to the 3-WET catalyst. This was attributed to the possible aggregation of amorphous α-Fe_2O_3 clusters on the surface of HAp. Pore size distribution plots (Figure 3.7), obtained by plotting the derivative of pore volume as a function of pore diameter illustrated a small decrease in the pore size of the catalysts with an increase of iron loading. This suggested that some of the α-Fe_2O_3 particles were located in the pores of the support (HAp).

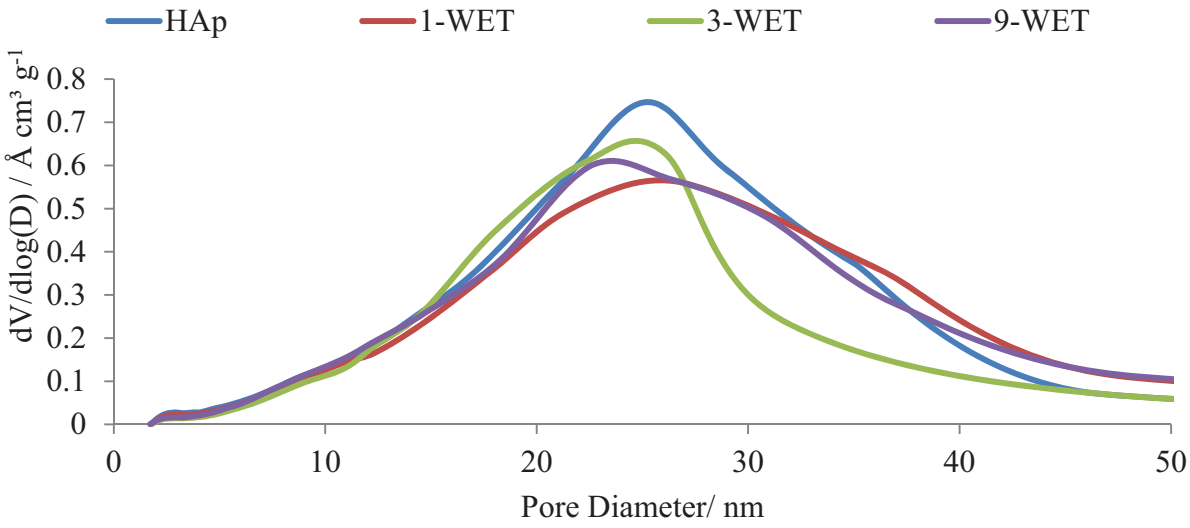

Figure 3.7: Pore size distributions of HAp and the iron supported on HAp catalysts

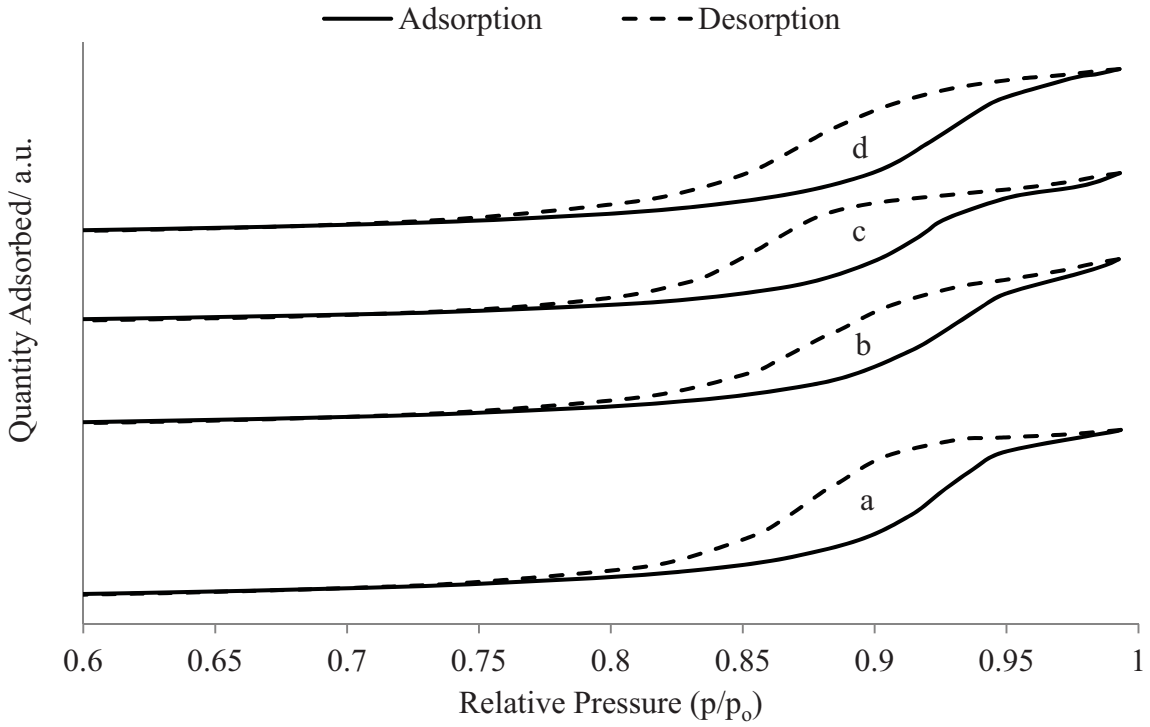

Figure 3.8: Nitrogen adsorption-desorption isotherms of (a) HAp, (b) the 1-WET catalyst, (c) the 3-WET catalyst and (d) the 9-WET catalyst

From Figure 3.8, all the iron supported on HAp catalysts displayed a hysteresis loop characteristic of a type IV (IUPAC) isotherm in the p/p_o range of 0.75 – 0.98. This feature of

the N_2 adsorption-desorption isotherms demonstrated the mesoporous nature of these catalyst materials [23]. A step increase observed between a p/p_o range of 0.90 – 0.99, characteristic of all the iron supported on HAp catalysts, may have been a result of the macropores of the materials caused by particle-particle porosity. This suggested that all the catalysts had a highly ordered and regular pore structure. Another contributing factor to the step increase would have been the filling of inter-particle macropores of the catalyst materials with N_2 [24].

The surface areas obtained for the iron substituted HAp catalysts (Table 3.5) showed no significant difference at low iron content, viz. the 1-COP and 3-COP catalysts. However, the 9-COP catalyst showed a significantly greater surface area, which suggested lattice distortion [13].

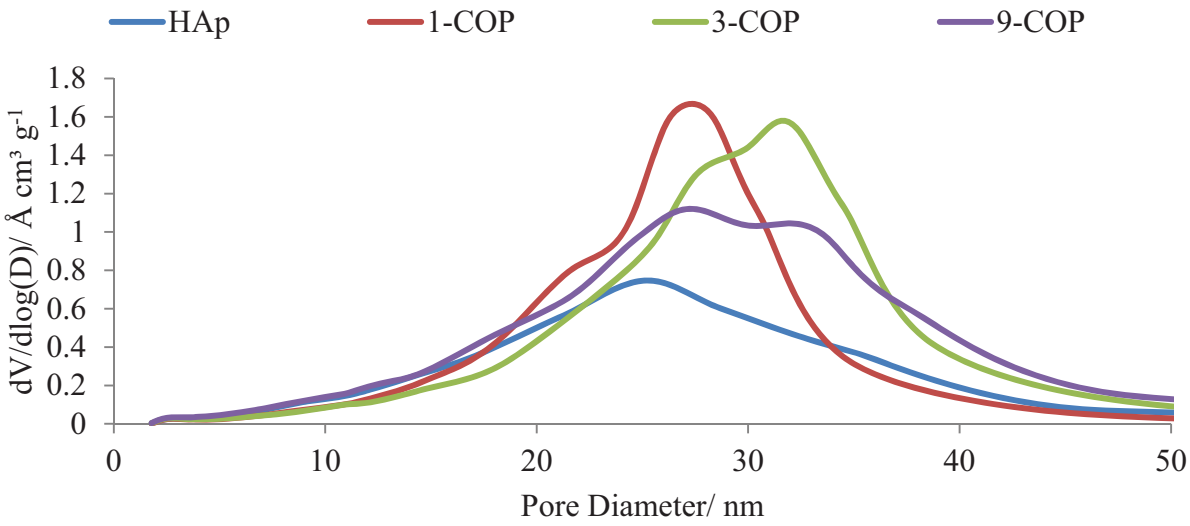

Figure 3.9: Pore size distributions of HAp and the iron substituted HAp catalysts

An increase in pore volume with increased iron content was observed. Pore size distribution plots of the iron substituted HAps (Figure 3.9) showed drastic increases in volume and size with increased cation substitution. The increase in pore volume and size was attributed to changes in the pore structure induced by lattice distortions [13]. The ionic radius of Fe^{3+} (0.064 nm) is smaller than that of Ca^{2+} (0.099 nm). Thus substitution of calcium with iron cations may have led to changes in the inter-atomic lattice bond distances. Changes in the Ca-

OPO_3 and Ca-OH bond distances have been reported through substitution of Ca^{2+} with other metal cations [12]. A similar increase in surface area and pore volume was observed by Morrissey *et al.* [25] and Gross *et al.* [26] upon substitution of Ca^{2+} with Fe^{2+} or Fe^{3+} ions in HAp using a similar co-precipitation technique. The smaller ionic radius of Fe^{3+} may have aided in the nucleation or prevented crystal growth and resulted in fine crystallite formation [26].

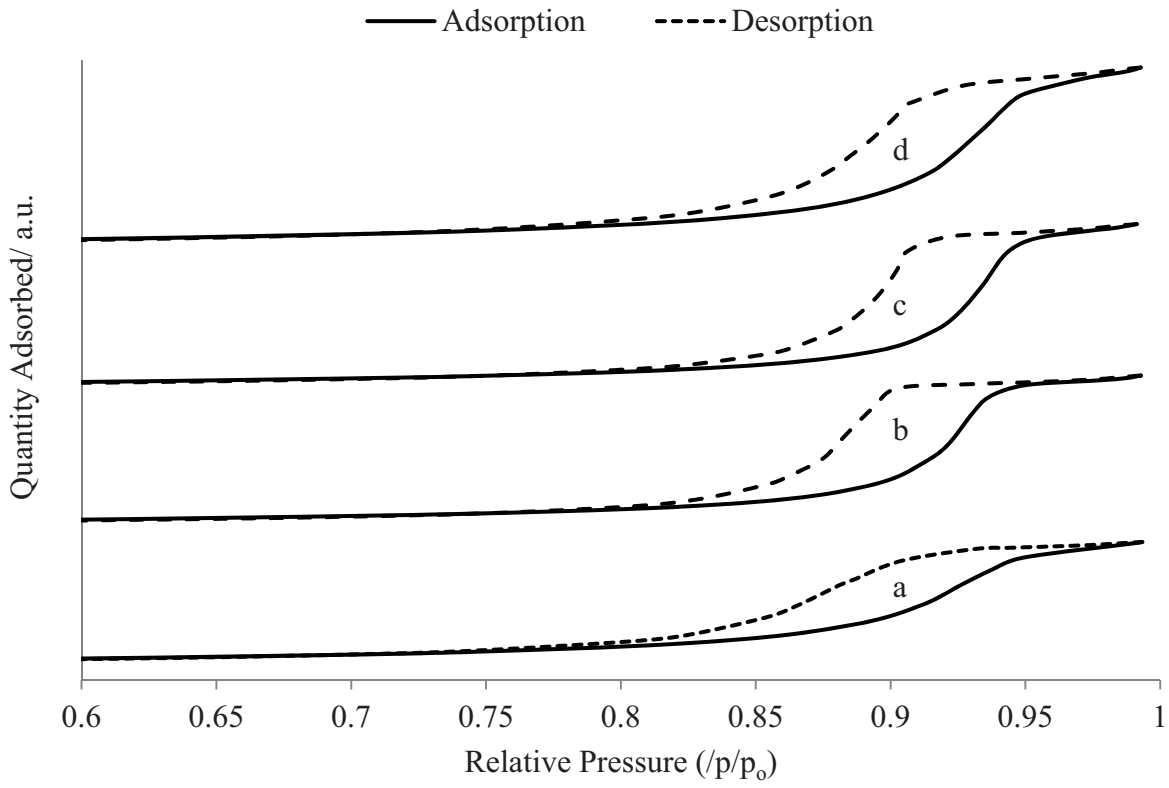

Figure 3.10: Nitrogen adsorption-desorption isotherms of (a) HAp, (b) the 1-COP catalyst, (c) the 3-COP catalyst and (d) the 9-COP catalyst

From Figure 3.10, N_2 adsorption-desorption plots of the iron substituted HAp catalysts showed type IV (IUPAC) isotherms displaying a hysteresis loop formed within a relative pressure (p/p_o) range of 0.70 – 0.99, demonstrating the mesoporous nature of the catalysts [23]. The isotherms showed a stepped increase between a p/p_o range of 0.85 – 0.99 which was attributed to the filling of inter-particle macropores of the catalyst material with gaseous N_2 [24].

Both the N_2 adsorption-desorption isotherms and pore size distribution plots (Figure 3.9) showed a non-uniform distribution of pore size in the iron substituted HAps when compared to HAp. This result supported the argument that iron replaced calcium cations in the lattice of the HAp. Distortions in the lattice of HAp, as a result of cation substitution, may have resulted in a change in the pore shape of the materials and thus resulted in a varied pore size distribution. The numerical increase in pore volume observed with an increase in iron loading is shown in Table 3.5.

3.7 Electron microscopy

Transmission electron microscopy

The transition electron microscopy (TEM) micrograph of HAp (Figure 3.11) showed rod shaped particles with sizes ranging between 70 – 100 nm in length.

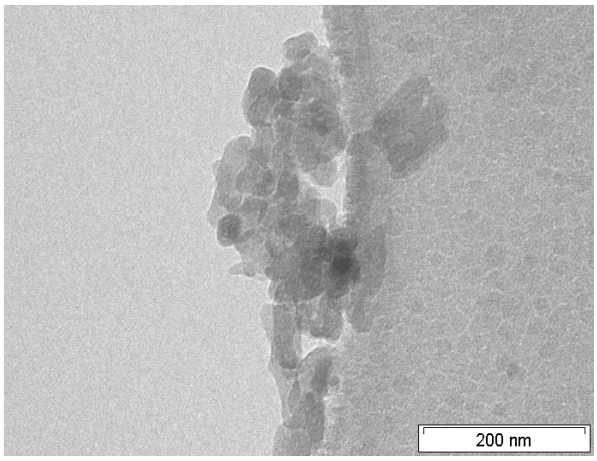

Figure: 3.11: TEM micrograph of HAp

The TEM micrographs of the iron supported on HAp catalysts are shown in Figure 3.12. The size of particles of the iron supported on HAp catalysts showed no significant changes when compared to the HAp particles (Figure 3.11). A deformation of the hexagonal shaped rods observed for HAp occurred for these catalysts. This was probably due to the exposure of HAp to the acidic iron precursor solution, whose pH was ≈ 2.3 during the wet impregnation

procedure. It proved difficult to distinguish between the iron and HAp particles due to the poor mass contrast between the two phases.

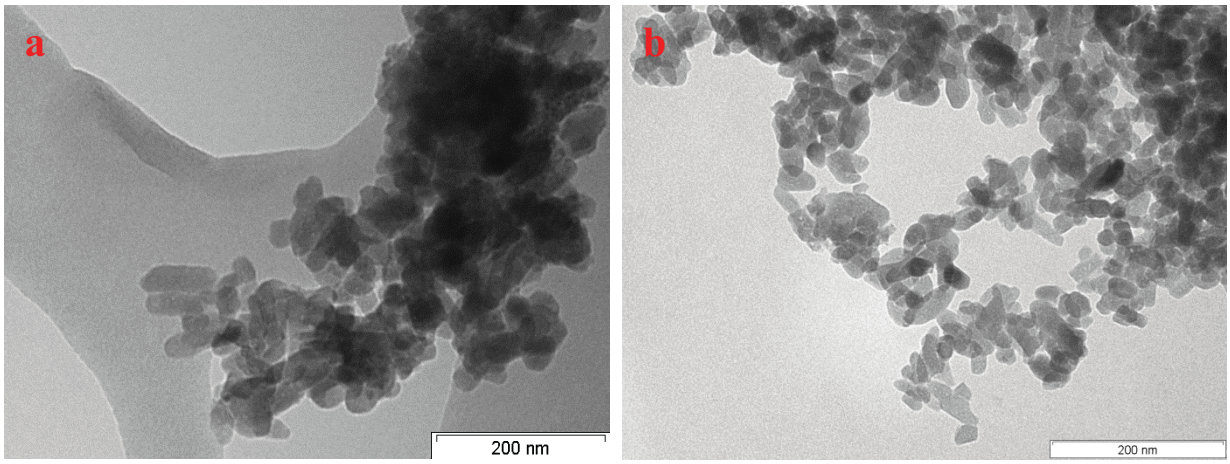

Figure 3.12: TEM micrographs of (a) the 3-WET catalyst and (b) the 9-WET catalyst

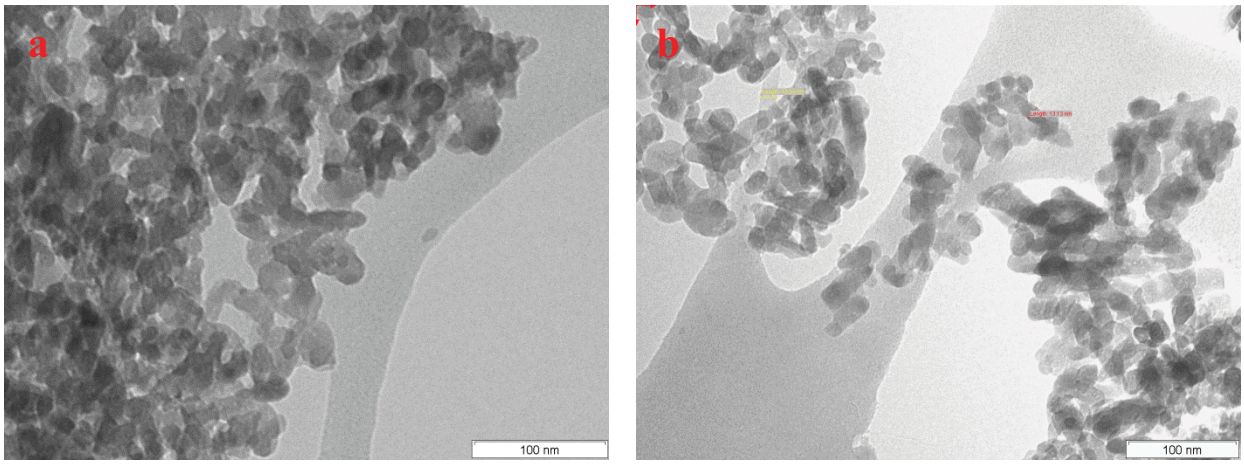

Figure 3.13: TEM micrographs of (a) the 3-COP catalyst and (b) the 9-COP catalyst

With the substitution of iron into the lattice of HAp, the rod like particles appeared to have contracted, forming clusters with particle sizes ranging between 60 – 90 nm for the 3-COP catalyst (Figure 3.13 a) and 90 – 150 nm for the 9-COP catalyst (Figure 3.13 b). The decrease in size and loss of hexagonal shape characteristics correlates well with the decreased crystallinity estimated from the PXRD patterns of these catalysts. The substitution of iron into the lattice of HAp seemed to have inhibited nucleation at low iron loading. At higher

loadings, iron promotes nucleation of the formed crystallites giving rise to particles with a lower degree of crystallinity but larger particle size when compared to that of HAp [26].

Scanning electron microscopy and energy dispersive X-ray spectroscopy

One of the primary roles of a support is to facilitate a uniform and homogeneous distribution of the catalytically active phase. The active phase should be well dispersed over the surface of the support to ensure uniform catalytic activity throughout the exposed surface of the material. SEM micrographs of HAp and the 9-WET catalyst (Figure 3.14) showed that these materials exist as polycrystalline particles composed of agglomerated nano-sized grains. The agglomeration of these grains was a result of the calcination of these materials at 550 °C [27].

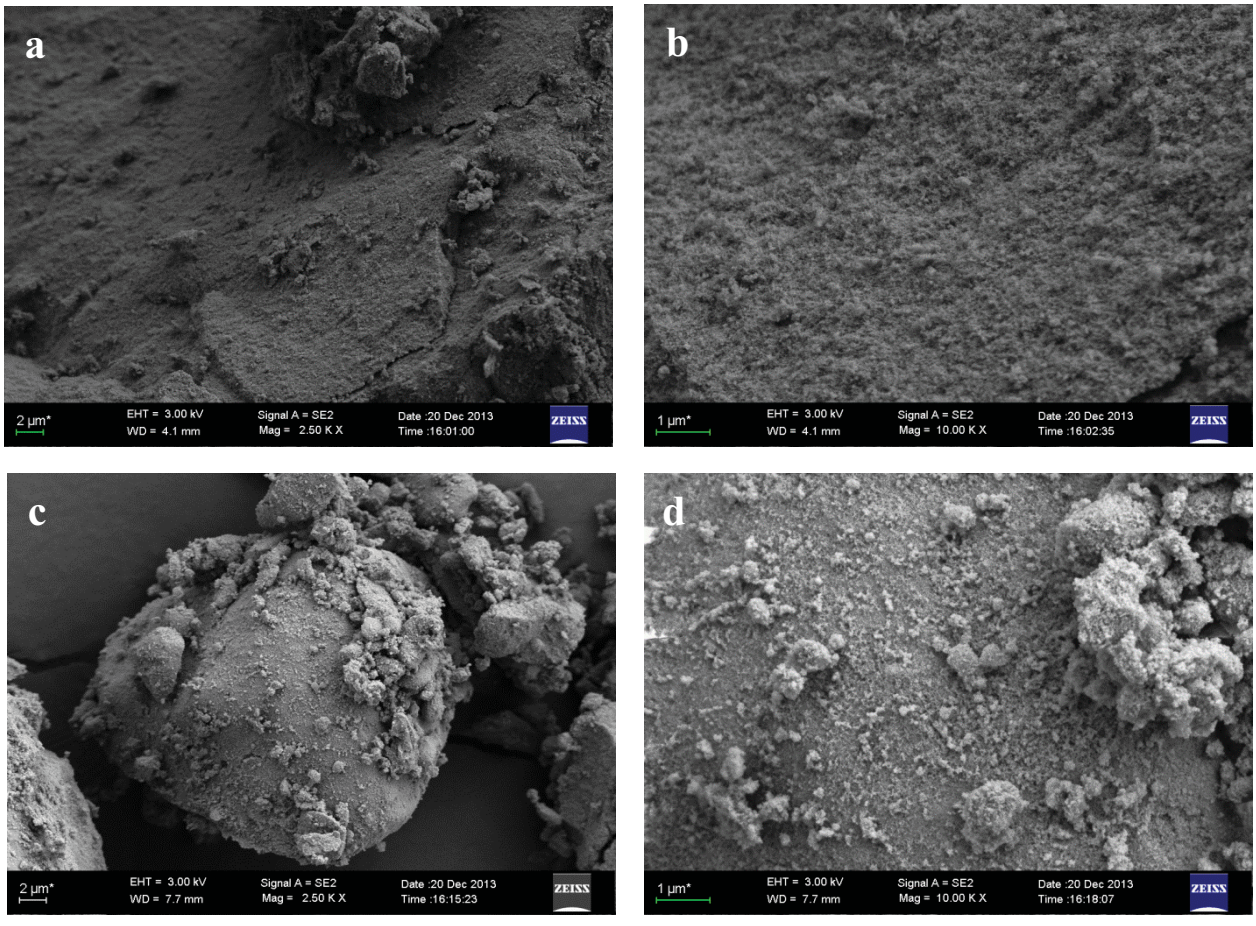

Figure 3.14: SEM micrographs of (a) HAp at 2.50 K ×, (b) HAp at 10.0 K ×, (c) the 9-WET catalyst at 2.50 K × and (d) the 9-WET catalyst at 10.0 K × magnification

Back scattered electron (BSE) imaging and energy dispersive X-ray spectroscopy (EDX) mapping of the support, HAp (Figure 3.15), showed an even distribution of calcium and phosphorus throughout the material.

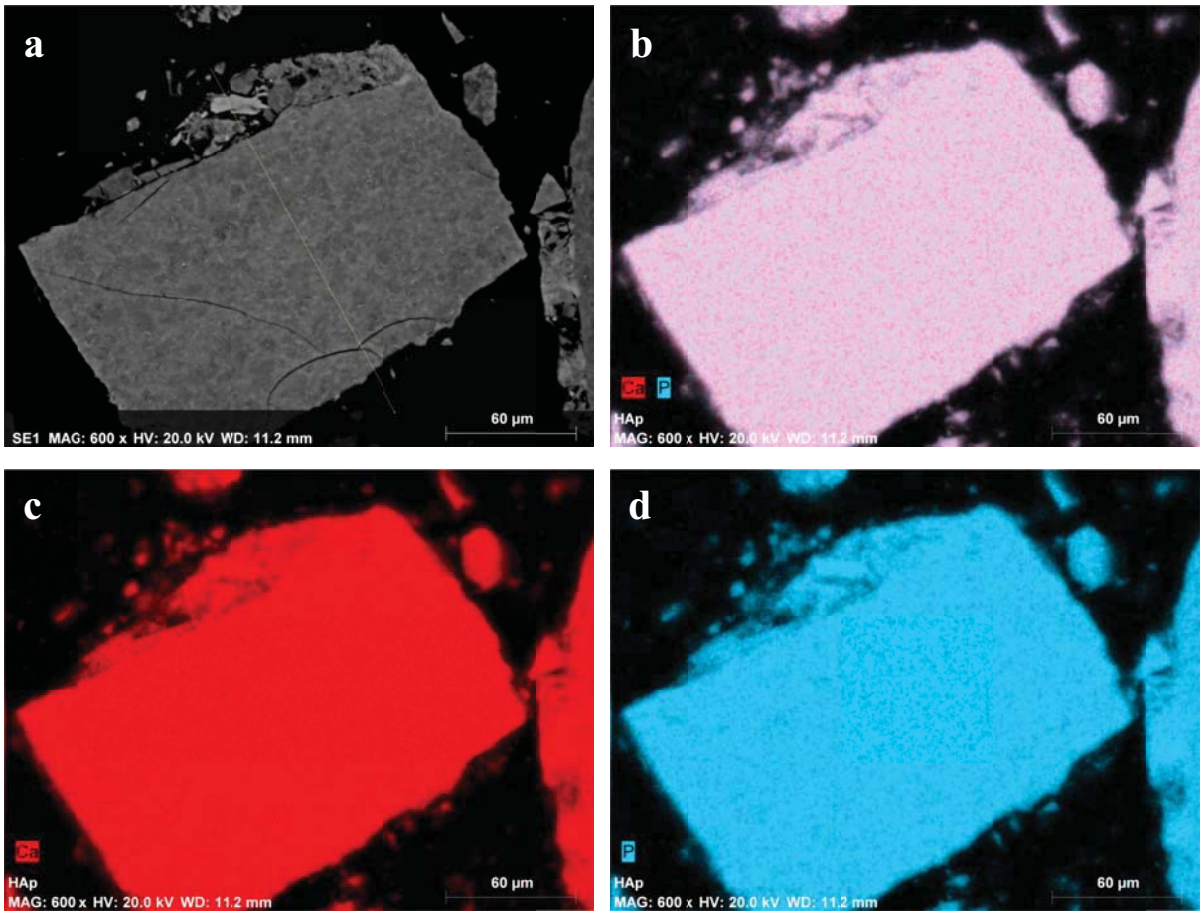

Figure 3.15: BSE SEM images of (a) HAp, (b) overlay of elemental maps of calcium and phosphorus distributed in HAp, (c) elemental map of calcium and (d) elemental map phosphorus

For the iron supported on HAp catalysts, there was an even distribution of iron along the surface of HAp. However, for the 9-WET catalyst, an aggregation of α-Fe_2O_3 clusters was observed (Figure 3.16 b). Line scans showed increased iron content at the positions of these clusters (Figure 3.17). The non-uniformity of the line representing the counts per second of iron demonstrated the aggregation of the dispersed α-Fe_2O_3 clusters possibly caused by the calcination temperatures employed during preparation. This result correlated well with the

well-known amorphous nature of iron oxide and the increase in surface area of the 9-WET catalyst when compared to the 3-WET catalyst. It can now be assumed that the highly dispersed α-Fe_2O_3 clusters led to greater pore blockage on the 3-WET catalyst, thus reducing the surface area (Table 3.5) further than the surface area of the 9-WET catalyst, which showed the presence of aggregated iron clusters leading to lower pore blockage. The wet impregnation technique appeared not to have influenced the elemental composition of the support (Figure 3.16 c and d), as inferred from the similarity of these maps to that of HAp (Figure 3.15 c and d). The α-Fe_2O_3 phase was distributed throughout the surface of the support (HAp) which would imply a greater exposure of the active iron phase to the gaseous reactant.

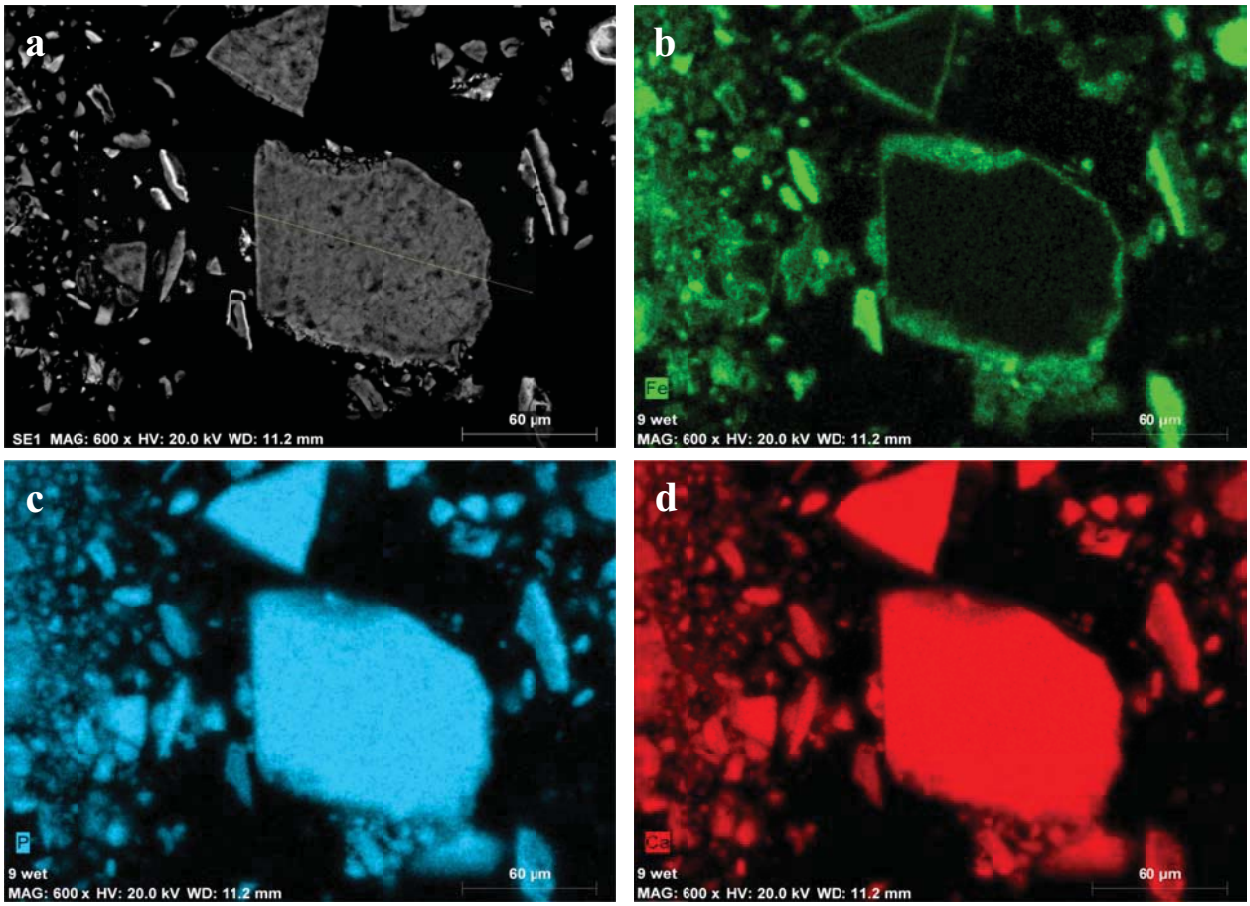

Figure 3.16: BSE SEM images of (a) the 9-WET catalyst and elemental mapping showing the distribution of (b) iron throughout the surface of the support (HAp). Included are the individual elemental maps of (c) calcium and (d) phosphorus

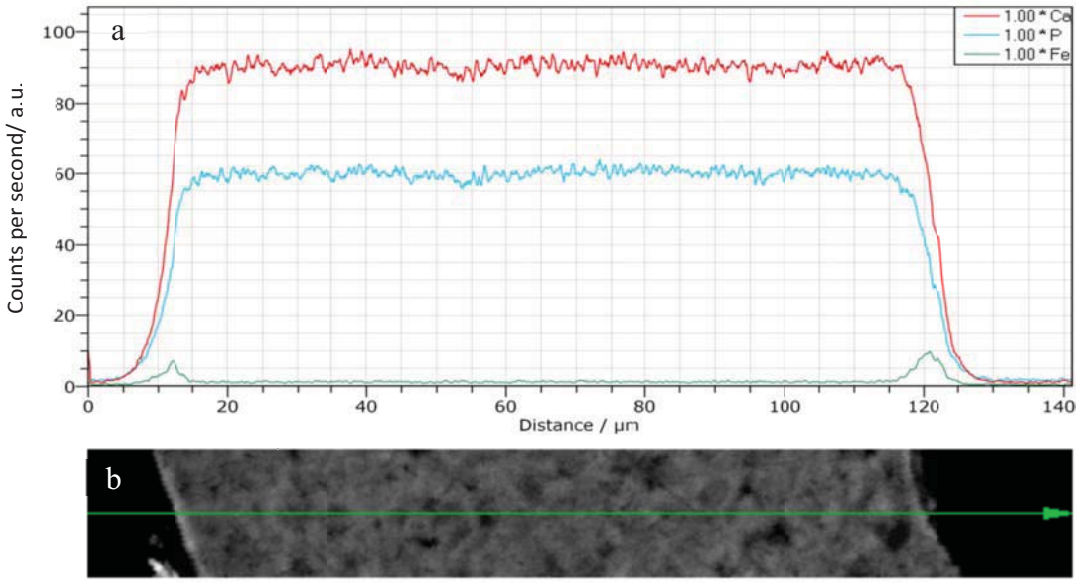

Figure 3.17: EDX line scan (a) illustrating the elemental content of calcium, phosphorus and iron of the 9-WET catalyst and (b) showing the area scanned of the BSE SEM image Figure: 3.16 a

SEM micrographs of the iron substituted HAp catalysts showed them as polycrystalline materials composed of an agglomeration of nano-sized grains (Figure 3.18 a and b) possibly formed during the calcination step of the synthetic procedure, similar to HAp (Figure 3.14 a and b).

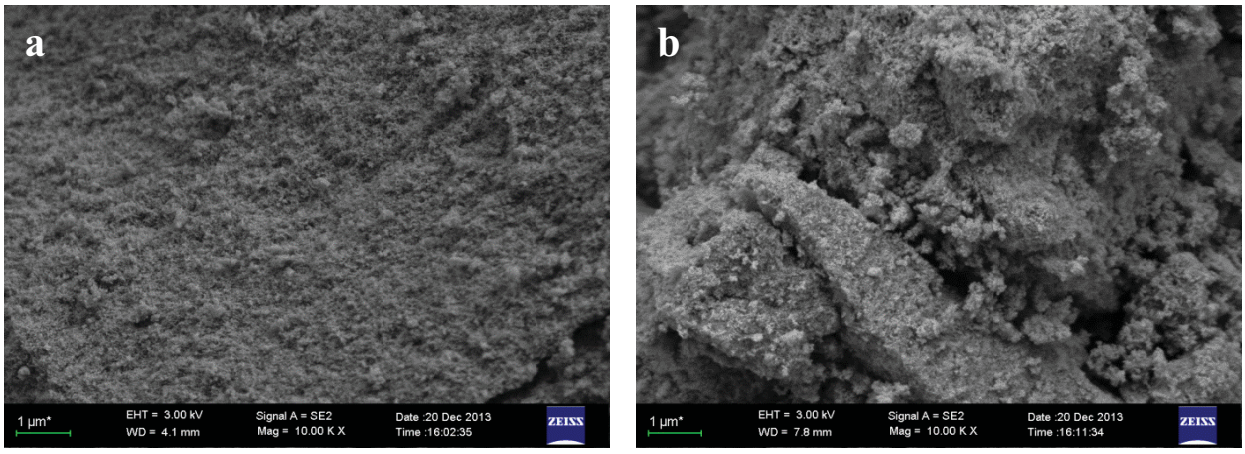

Figure 3.18: SEM micrographs (a) HAp at 2.50 K × and (b) the 9-COP catalyst at 10.0 K × magnification

BSE imaging and elemental mapping of the 9-COP catalyst (Figure 3.19) illustrated the distribution of iron throughout the surface and bulk of the materials. The aggregation of iron, without the layering of amorphous iron oxide on the surface of these materials at the microscopic level, further supported the formation of iron substituted HAp. Elemental mapping showed a fairly homogeneous distribution of calcium and phosphorus. Iron on the other hand was distributed throughout the material with clusters of iron species being observed. This suggested a higher probability of Fe^{3+}-O-Fe^{3+} species in these iron rich regions as suggested by Khachani *et al*. [13].

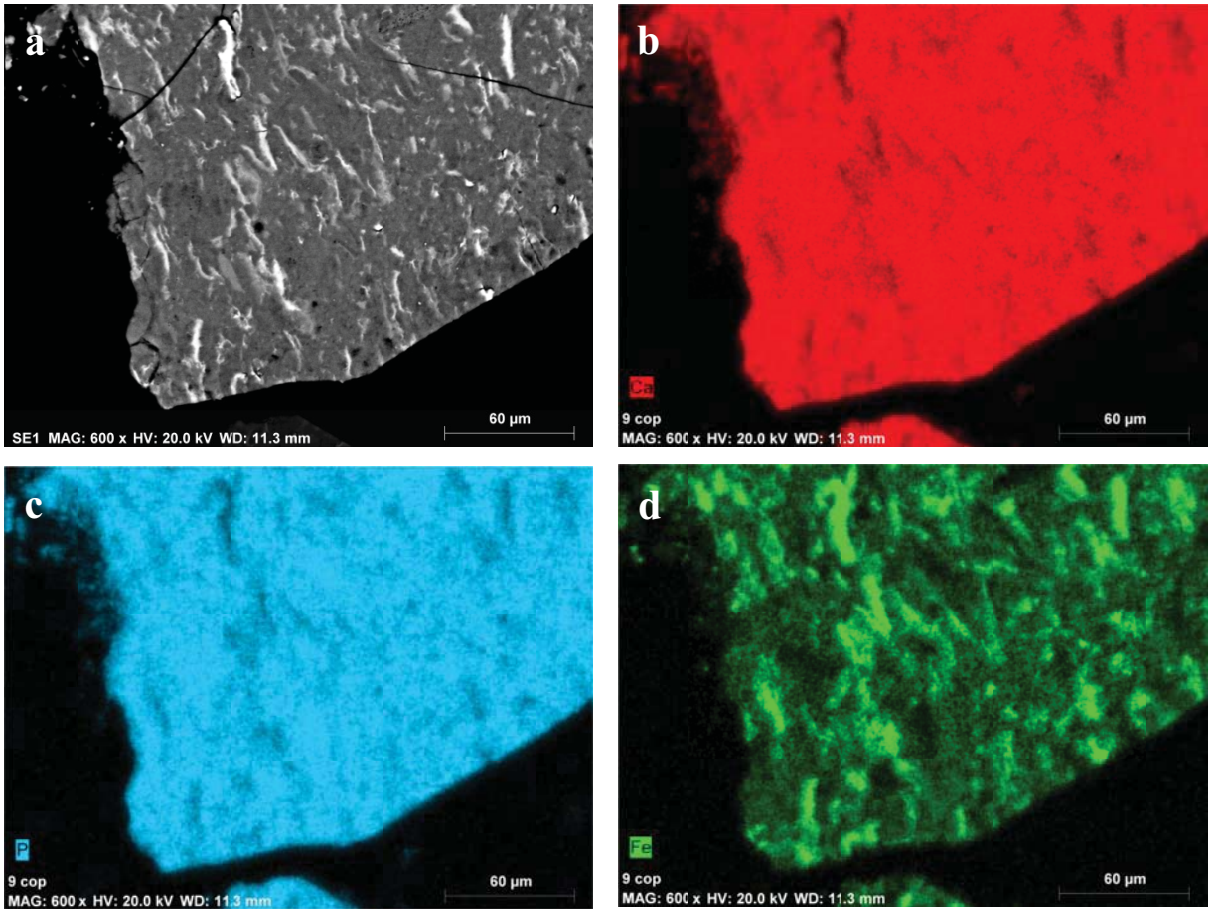

Figure 3.19: BSE SEM image of (a) the 9-COP catalyst and elemental mapping of (b) calcium, (c) phosphorus and (d) iron

EDX line scans of a flat particulate surface of the 9-COP catalyst (Figure 3.20) clearly illustrated the increase in iron content (measured as counts per second) along the bright

regions of the image. Iron rich regions appeared brighter in the backscattered electron image of the 9-COP catalyst (Figure 3.18 a) because iron has a larger atomic number than calcium and phosphorus, thus more electrons were backscattered in those regions.

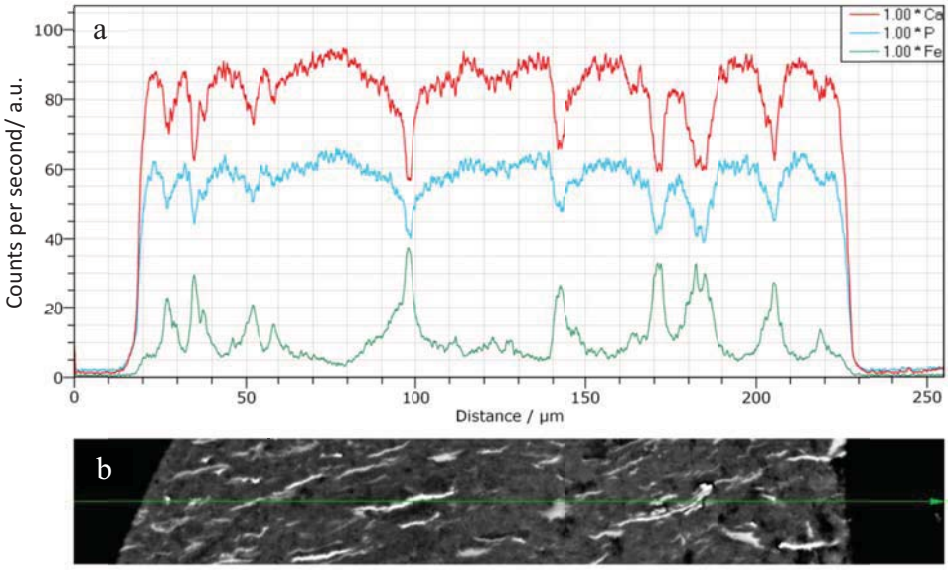

Figure 3.20: EDX line scan (a) illustrating the elemental content of calcium, phosphorus and iron of the 9-COP catalyst and (b) showing the area scanned of the BSE SEM image Figure: 3.19 a

3.8 Temperature programmed techniques

Temperature programmed reduction and oxidation

The reducibility of the iron supported on HAp catalysts were investigated by means of temperature programmed reduction (TPR) analyses. Hydrogen consumption was plotted as a function of temperature up to 950 °C. HAp was not reduced at the temperatures and conditions employed in this study, as was observed by Dasireddy *et al*. [28]. It is well known that the reduction of α-Fe_2O_3 takes place over three steps, viz. α-Fe_2O_3 → Fe_3O_4 → FeO → Fe [13, 29]. Thus, it can be assumed that changes in the TCD signal were due to the reduction of iron species present on the surface of HAp.

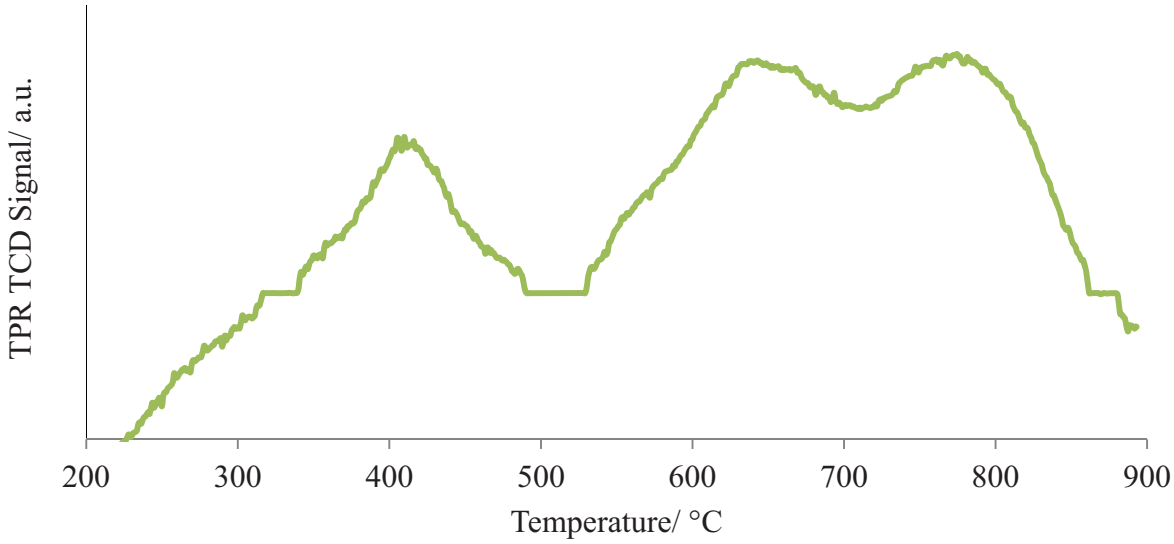

Figure 3.21: TPR profile of the 9-WET catalyst

The onset temperature of the reduction of α-Fe_2O_3 (Figure 3.21) was ± 350 °C, which corresponded to the H_2 uptake temperatures also observed by other researchers [29-32]. This peak could be assumed to represent the reduction of α-Fe_2O_3 → Fe_3O_4. The second stage reduction began at ± 510 °C and could be assigned to the complete reduction of Fe_3O_4 → FeO and the third reduction peak was observed from ± 690 °C due to the reduction of FeO → Fe. The H_2 consumed during the reduction steps became more prominent with increased iron loading on the surface of HAp. Kung and Kung [2] and Hossain *et al.* [30] have discussed the strong active metal-support interaction observed for α-Fe_2O_3 supported on SiO_2, TiO_2 and Al_2O_3 and the effect this interaction has on the reducibility of the active iron phase. The strong interaction that α-Fe_2O_3 forms with a support explains the poor sensitivity towards H_2 uptake over the iron supported on HAp catalysts with lower loadings, viz. the 1-WET and 3-WET catalysts (See Appendix B, Figure B3 and B4 respectively). The three distinct peaks observed for the 9-WET catalyst could have been caused by the agglomeration of the α-Fe_2O_3 clusters on the surface of HAp which led to an increase in the proportion of surface iron species interacting with internal iron layers. This increased the bond strength of the iron species bringing this closer to the bond strengths of pure or non-supported α-Fe_2O_3. The broader peaks associated with an increased iron loading were attributed to the increase in heterogeneity of the iron reduction centers.

Once a TPR analysis for the iron supported on HAp catalysts was conducted, the temperature was gradually reduced to 80 °C under a flow of argon. Thereafter a temperature programmed oxidation (TPO) experiment was conducted on the 9-WET catalyst. The TPO profile of the 9-WET catalyst (Figure 3.22) showed the onset temperature of oxidation to be ± 350 °C, the same as the onset temperature for reduction, which suggested that the oxidation of Fe → α-Fe_2O_3 was favourable.

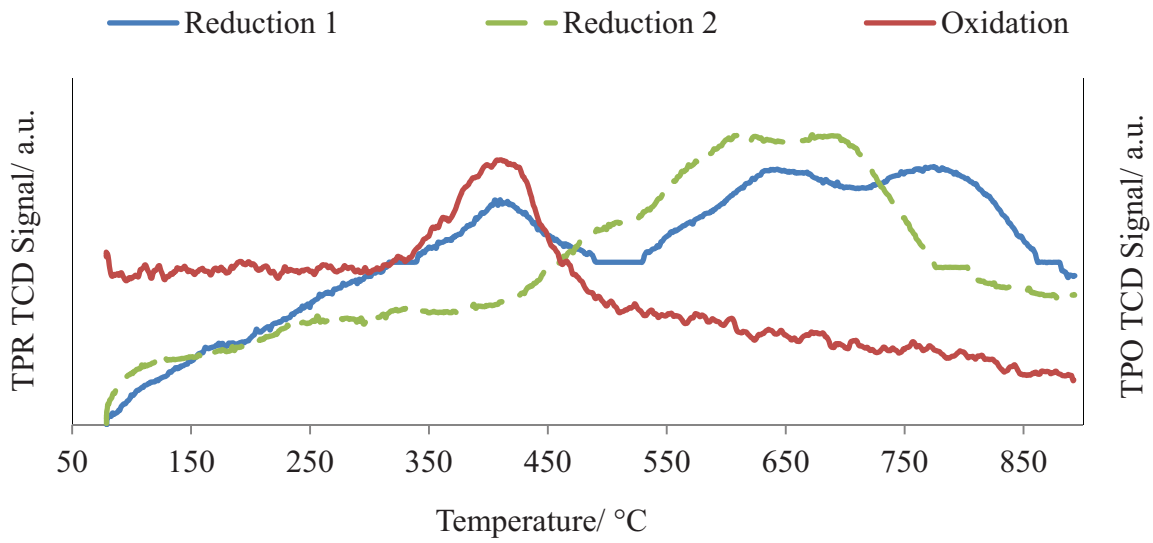

Figure 3.22: Temperature programmed reduction-oxidation-reduction profiles of the 9-WET catalyst

The second reduction profile obtained after cooling the oxidized material to 80 °C, once again under a flow of argon, showed an onset of reduction from ± 450 °C and a narrower peak which suggested behaviour similar to that of unsupported α-Fe_2O_3 as observed by Liang *et al.* [33] and Wimmers *et al.* [34]. They suggested that this could be due to the aggregation of re-oxidised α-Fe_2O_3 clusters after the first reduction. This assumption was plausible considering the amorphous nature of iron oxides. Further, after the aggregation of these clusters, a greater heterogeneity of iron reduction centers was affected throughout the surface of the catalyst resulting from a decreased metal-support interaction that increased the bond strength of the iron species bringing this strength closer to that of pure α-Fe_2O_3.

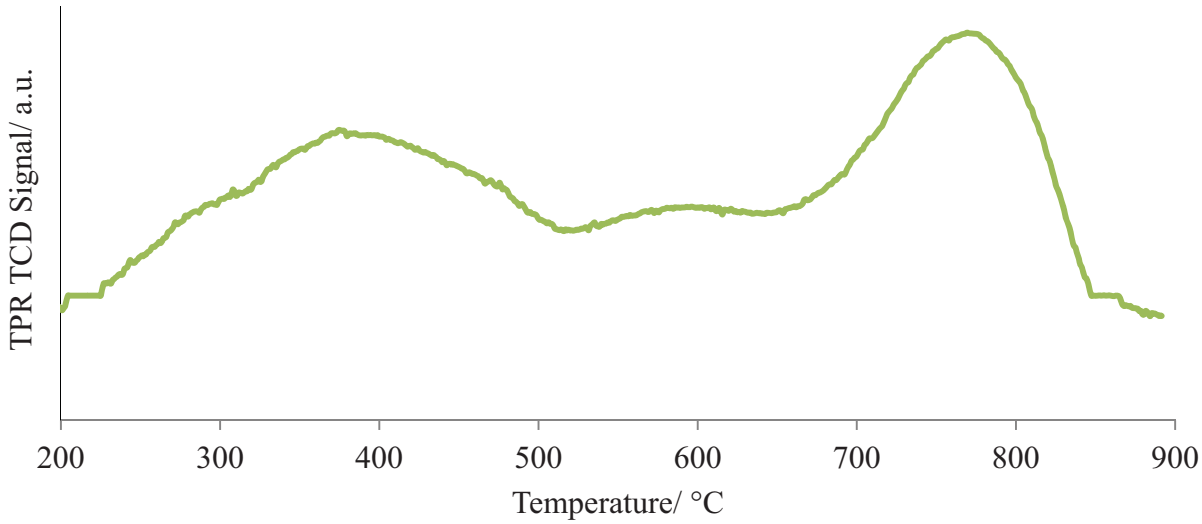

Figure 3.23: TPR profile of the 9-COP catalyst

As mentioned previously, calcium within the HAp lattice (Ca^{2+}) was not reduced under the conditions studied for TPR. Thus, any peaks observed were attributed to the reduction of iron. From the elemental mapping of the 9-COP catalyst (Figure 3.19), it can be assumed that iron was distributed throughout the apatite-like lattice of the materials as opposed to being dispersed on the surface of HAp. Wakamura *et al.* [35] showed this via XPS studies and elemental analyses and have indicated that iron species at or close to the surface of the material were reduced more easily than those distributed throughout the material. Khachani *et al.* [13] showed that the reduction of iron exchanged for calcium in the lattice of HAp did not exceed the (II) oxidation state. Similar results were observed for the catalysts used in this study. From Figure 3.23, the two reduction peaks observed with onset temperatures of 250 and 650 °C respectively were attributed to the reduction of $Fe^{3+} \rightarrow Fe^{2+}$. The first peak correlated to the reduction of surface Fe^{3+} and the second to the reduction of remnant iron distributed throughout the structural lattice of these materials but still accessible to gaseous H_2 through the porous apatite-like materials. The second reduction of Fe^{3+} occurred at a higher temperature probably due to thermal expansion of the HAp lattice associated with these high temperatures. The overall H_2 consumption was greater for these catalysts when compared to the iron supported on HAp catalysts. This was attributed to the greater stability afforded to the Fe^{3+} species substituted into the hexagonal lattice of HAp.

The 9-COP catalyst was studied under reduction-oxidation-reduction conditions (Figure 3.24). The reduced catalyst was cooled to 80 °C under a flow of argon. Thereafter, the catalyst was re-oxidized under a flow of air. The TPO together with the reduction profiles of the 9-COP catalyst are shown in Figure 3.23.

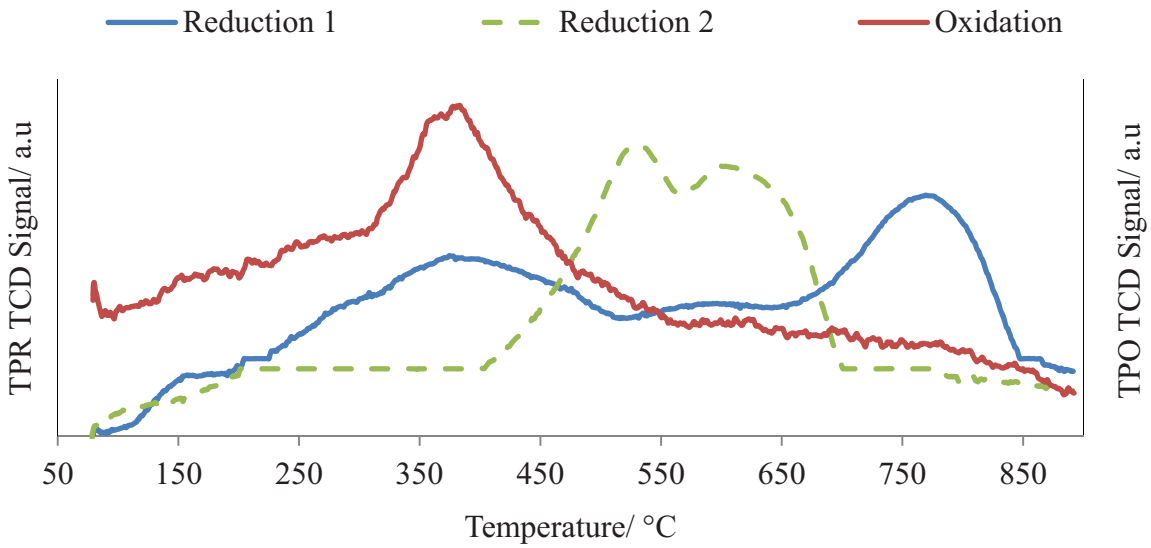

Figure 3.24: Temperature programmed reduction-oxidation-reduction profiles of the 9-COP catalyst

The onset temperature of oxidation was found to be equal to that of the first reduction temperature. The second TPR profile showed an onset temperature of 400 °C. Both peaks in this profile were presented as one peak. This suggested that the consecutive reduction of the catalyst occurs far more easily than the initial reduction. This is probably due to the increased heterogeneity of the iron reduction centers after the first two temperature programmed studies [28].

Temperature programmed desorption

With the exception of non-oxide catalysts, basic sites are believed to be surface oxygen species [36]. These species interact with protons and thus influence ODH reactions. Temperature programmed CO_2 desorption (CO_2-TPD) is commonly employed to measure the

strength of basic sites on solid heterogeneous catalysts. The basic strength of a catalyst material may be determined, qualitatively, by the area under the curve of a CO_2-TPD plot. Di Cosimo *et al*. [37] have shown that OH^- groups function as weakly basic sites and O^{2-} species as strong basic sites. The CO_2-TPD desorption profiles of HAp and the 9-WET catalyst (Figure 3.25) showed the lowest basicity. This was attributed to the structural OH^- groups of the hydroxyapatite lattice.

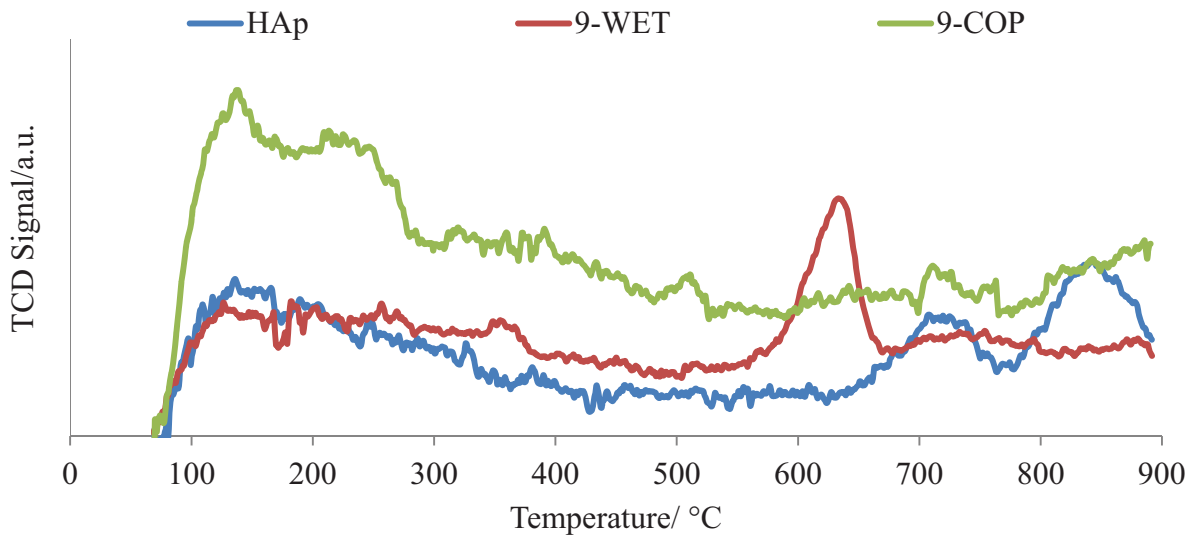

Figure 3.25: CO_2-TPD profile of HAp, the 9-WET catalyst and the 9-COP catalysts

The 9-COP catalyst demonstrated the highest basic strength. This was attributed to the stabilisation of O^{2-} species within the tunnels of the modified apatite framework [13]. Similar trends were observed for the 1 and 3 wt% iron modified HAp catalysts (See Appendix B, Figures B7 and B8).

References

[1] G. Bergeret, P. Gallezot, in: G. Ertl, H. Knozinger, J. Weitkamp (Eds.), Handbook of heterogeneous catalysis, 1st ed., VCH Verlagsgesellschaft mbH, Weinheim, Federal Republic of Germany, 1997, pp. 446 - 474.

[2] H.H. Kung, M.C. Kung, in: D.D. Eley, H. Pines, B.W. Paul (Eds.), Advances in Catalysis, Academic Press, 1985, pp. 159-198.

[3] R.X. Fuzeng Ren, Xiang Ge, Yang Leng, Acta Biomaterialia 5 (2009) 3141-3149.

[4] M. Rajkumar, N.M. Meenakshi Sundaram, V. Rajendran, Digest Journal of Nanomaterials and Biostructures 6 (2011) 169 - 179.

[5] R.A. Nyquist, R.O. Kagel, Infra Red Spectra of Inorganic Compounds, Academic Press, New York, 1991.

[6] H.-C. Wu, T. Wei, J.-S. Sun, W.-H. Wang, F.-H. Lin, Nanotechnology 18 (2007) 9.

[7] V.D.B.C. Dasireddy, S. Singh, H.B. Friedrich, Applied Catalysis A: General 421–422 (2012) 58-69.

[8] K. Elkabouss, M. Kacimi, M. Ziyaad, S. Ammar, F. Bozon-Verduraz, Journal of Catalysis 226 (2004) 16-24.

[9] A. Bigi, E. Boanini, C. Capuccini, M. Gazzano, Inorganic Chimica Acta 360 (2007) 1009-1016.

[10] B.O. Fowler, Inorganic Chemistry 13 (1974) 194-207.

[11] B.O. Fowler, Inorganic Chemistry 13 (1974) 207-214.

[12] D. Laurencin, N. Almora-Barrios, N.H. de Leeuw, C. Gervais, C. Bonhomme, F. Mauri, W. Chrzanowski, J.C. Knowles, R.J. Newport, A. Wong, Z. Gan, M.E. Smith, Biomaterials 32 (2011) 1826-1837.

[13] M. Khachani, M. Kacimi, A. Ensuque, J.-Y. Piquemal, C. Connan, F. Bozon-Verduraz, M. Ziyad, Applied Catalysis A: General 388 (2010) 113-123.

[14] J.C. Vedrine, J.M.M. Millet, J.-C. Volta, Catalysis Today 32 (1996) 115-123.

[15] E.V. Pecheva, L.D. Pramatarova, M.F. Maitz, M.T. Pham, A.V. Kondyuirin, Applied Surface Science 235 (2004) 176-181.

[16] C.G. Kontoyannis, N.C. Bouropoulos, P.G. Koutsoukos, Vibrational Spectroscopy 15 (1997) 53-60.

[17] M.D. O'Donnell, Y. Fredholm, A. de Rouffignac, R.G. Hill, Acta Biomaterialia 4 (2008) 1455-1464.

[18] M.R. Saeri, A. Afshar, M. Ghorbani, N. Ehsani, C.C. Sorrell, Materials Letters 57 (2003) 4064-4069.

[19] R. Cusco, F. Guitian, S. de Aza, L. Artus, Journal of the European Ceramic Society 18 (1998) 1301 - 1305.

[20] M. Khalid, M. Mujahid, S. Amin, R.S. Rawat, A. Nusair, G.R. Deen, Ceramics International 39 (2013) 39-50.

[21] S. Zhai, M. Kanzaki, T. Katsura, E. Ito, Materials Chemistry and Physics 120 (2010) 348-350.

[22] V.D.B.C. Dasireddy, S. Singh, H.B. Friedrich, Applied Catalysis A: General 456 (2013) 105-117.

[23] Y. Kamiya, E. Nishikawa, A. Satsuma, M. Yoshimune, T. Okuhara, Microporous and Mesoporous Materials 54 (2002) 277-283.

[24] K. Bhattacharyya, S. Varma, A.K. Tripathi, S.R. Bharadwaj, A.K. Tyagi, Journal of Physical Chemistry C 112 (2008) 19102-19112.

[25] R. Morrissey, L.M. Rodriguez-Lorenzo, K.A. Gross, Journal of Materials Science 16 (2005) 387-392.

[26] K.A. Gross, R. Jackson, J.D. Cashion, L.M. Rodriguez-Lorenzo, European Cells and Materials 3 (2002) 114-117.

[27] K. Agrawal, G. Singh, D. Puri, S. Prakash, Journal of Minerals and Materials Characterisation and Engineering 10 (2011) 727-734.

[28] V.D.B.C. Dasireddy, S. Singh, H.B. Friedrich, Applied Catalysis A: General 421-422 (2012) 58-69.

[29] J. Zieliński, I. Zglinicka, L. Znak, Z. Kaszkur, Applied Catalysis A: General 381 (2010) 191-196.

[30] M.M. Hossain, L. Atanda, N. Al-Yassir, S. Al-Khattaf, Chemical Engineering Journal 207-208 (2012) 308-321.

[31] X. Zhang, G. Dou, Z. Wang, L. Li, Y. Wang, H. Wang, Z. Hao, Journal of Hazardous Materials 260 (2013) 104-111.

[32] A. Basińska, W.K. Jóźwiak, J. Góralski, F. Domka, Applied Catalysis A: General 190 (2000) 107-115.

[33] M. Liang, W. Kang, K. Xie, Journal of Natural Gas Chemistry 18 (2009) 110-113.

[34] O.J. Wimmers, P. Arnoldy, J.A. Moulijn, Journal of Physical Chemistry 90 (1986) 1331-1337.

[35] M. Wakamura, K. Kandori, T. Ishikawa, Colloids and Surfaces A: Physiochemical and Engineering Aspects 164 (2000) 297-305.

[36] H. Hattori, Chemical Reviews 95 (1995) 537-558.

[37] J.I. Di Cosimo, V.K. Díez, M. Xu, E. Iglesia, C.R. Apesteguía, Journal of Catalysis 178 (1998) 499-510.

Chapter 4
Catalytic Testing

This chapter mainly focuses on the catalytic activity of the iron substituted and iron supported on hydroxyapatite (HAp) catalysts denoted #-COP and #-WET respectively, where # represents the nominal weight percentage of iron loading. Several investigations were carried out in an attempt to understand the stability, REDOX properties and overall performance of these catalysts. An investigation into the effects of gas hourly space velocity (GHSV) and carbon to oxygen (C:O) ratio was also carried out.

4.1 Non catalytic studies

Linear alkanes are relatively inert and require high activation temperatures. At higher temperatures the possible contribution from inherent homogeneous gas phase reactions cannot be ignored [1, 2]. The increase in reactivity concomitant with an increased chain length of linear alkanes is another factor to be considered. Thus, it became important to determine the contributions from homogeneous gas phase reactions to better understand the activity of catalysts tested using this reactor. Non catalytic testing was performed using a reactor tube packed with 24 gritt carborundum at GHSVs of 4000 and 6000 h^{-1} and C:O ratios of 8:0, 8:2, 8:4 and 8:6. The flow rates and oxygen content were some of the conditions generally employed in most of the studies in our laboratory [1, 3-7].

In the absence of air, i.e. under dehydrogenation conditions, no conversion was observed at GHSVs of 4000 and 6000 h^{-1}. When air was introduced into the feed mixture at such a rate that a GHSV of 4000 h^{-1} and a C:O ratio of 8:2 were attained, activity was only observed above 450 °C (Figure 4.1). This thermal activation of *n*-octane was attributed to the homogeneous gas phase reactions occurring within the spaces of the carborundum packed reactor tube. Conversion showed a linear increase with increasing temperature. Octenes,

predominantly 2-octene, showed the greatest selectivity at a temperature of 450 °C. Contributions from thermal cracking and combustion leading to the formation of CO_x also played a role. A decrease in the selectivity towards octenes was observed as the reaction temperature was increased from 450 to 500 °C, which corresponded to an increase in the selectivity of cracked products and CO_x. The formation of C8 aromatic compounds was only observed at 550 °C. Selectivity to these corresponded to a decrease in the selectivity towards CO_x, suggesting that the formation of C8 aromatics was more favourable than combustion.

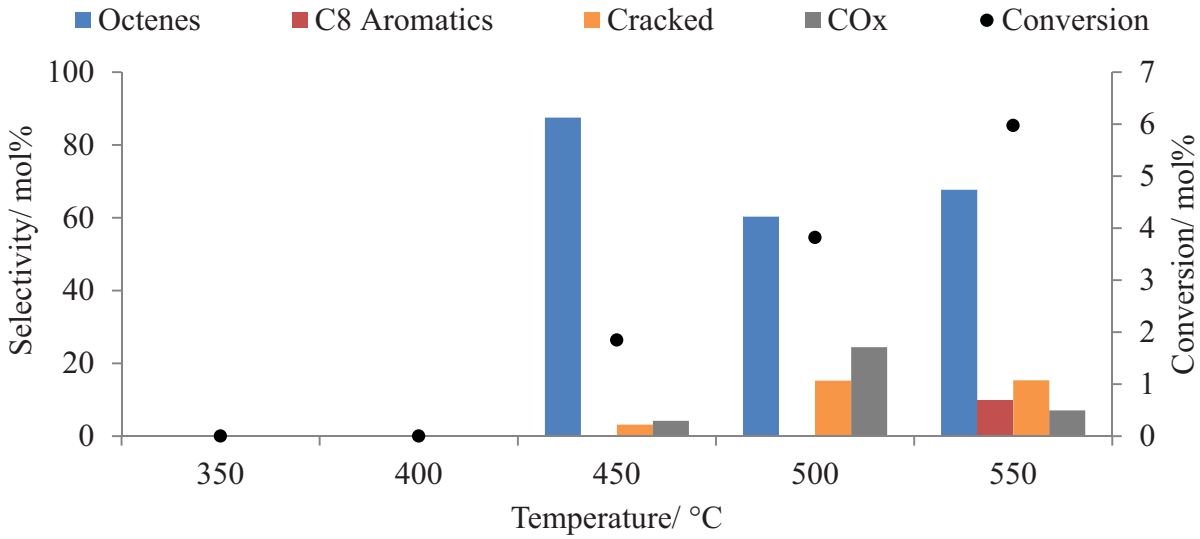

Figure 4.1: Conversion and selectivity profile of blank reactor contributions to the activation of *n*-octane as a function of increasing temperature at a GHSV of 4000 h^{-1} and C:O ratio of 8:2

When tested at a GHSV of 6000 h^{-1} and a C:O ratio of 8:2 (Figure 4.2), conversion was observed from 450 °C onwards. Octenes were the dominant product class observed, followed by CO_x and then cracked products. At a GHSV of 6000 h^{-1} and C:O ratios of 8:4 and 8:6 (Figures 4.3 and 4.4 respectively) similar product profiles were observed. Conversion increased with an increase in oxygen content in the feed. Also with respect to the testing of the carborundum packed reactor at a GHSV of 6000h^{-1} and a C:O ratio of 8:6, activity was observed above 400 °C.

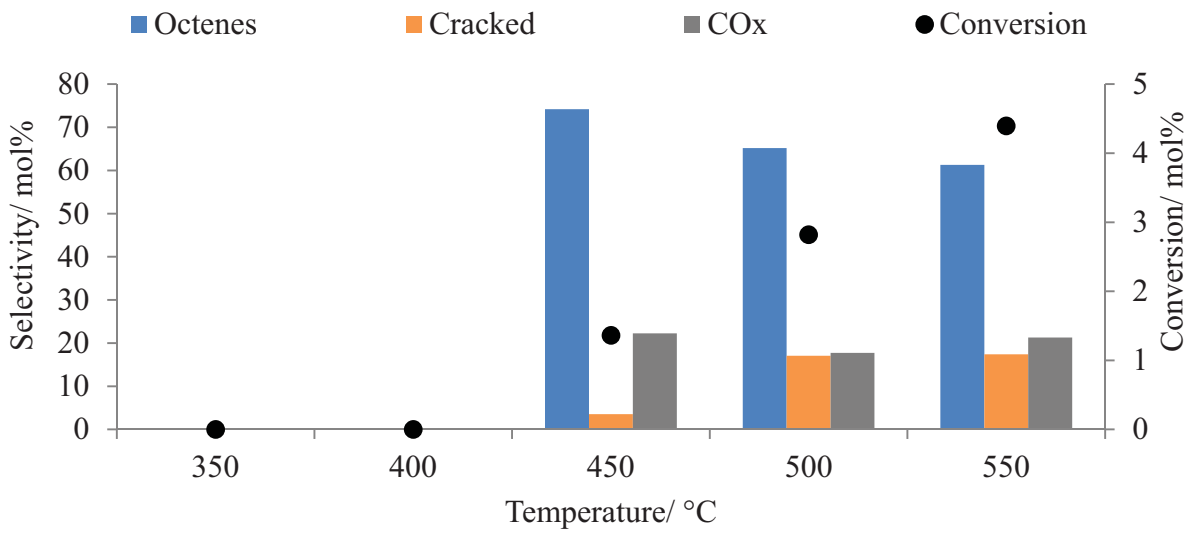

Figure 4.2: Conversion and selectivity profile of blank reactor contributions to the activation of *n*-octane as a function of increasing temperature at a GHSV of 6000 h^{-1} and C:O ratio of 8:2

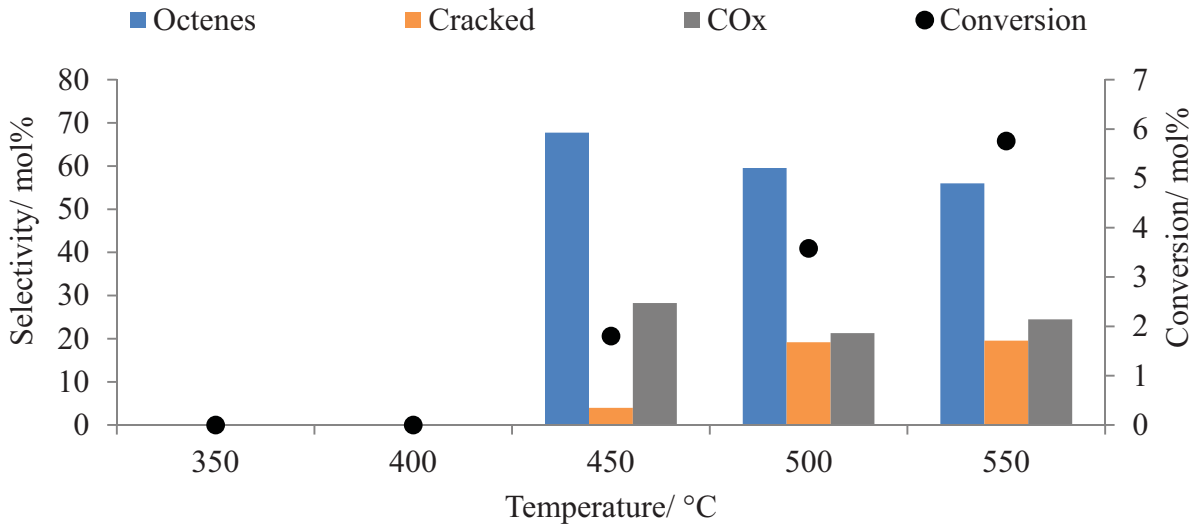

Figure 4.3: Conversion and selectivity profile of blank reactor contributions to the activation of *n*-octane as a function of increasing temperature at a GHSV of 6000 h^{-1} and C:O ratio of 8:4

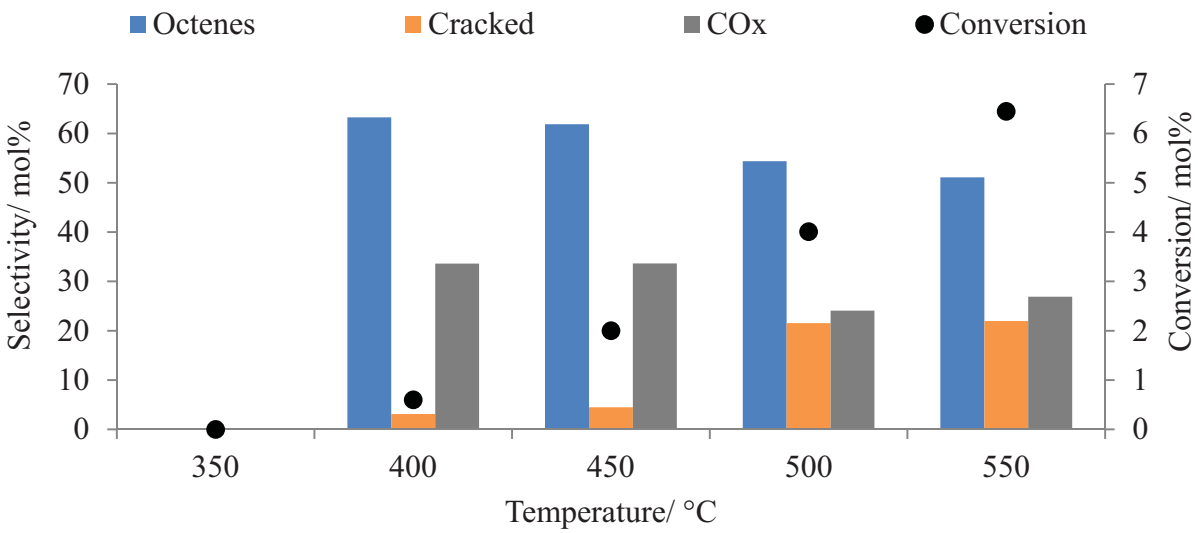

Figure 4.4: Conversion and selectivity profile of blank reactor contributions to the activation of *n*-octane as a function of increasing temperature at a GHSV of 6000 h^{-1} and C:O ratio of 8:6

4.2 An investigation into the role of hydroxyapatite in the activation of *n*-octane

Hydroxyapatite (HAp) tested under anaerobic (dehydrogenation) conditions, at a GHSV of 4000 h^{-1} (Figure 4.5), showed selective dehydrogenation of *n*-octane with a maximum in selectivity towards octenes over the temperature range tested and a minor contribution towards CO_x at 350 and 400 °C. The formation of CO_x was probably due to the participation of physisorbed oxygen atoms on the surface of HAp that were all activated at these temperatures. Conversion was also observed to have increased almost linearly. Under aerobic conditions (C:O ratio 8:2), an increase in conversion over the temperature range was observed (Figure 4.6). CO_x was the dominant product throughout the temperature range. Cracked product selectivity increased over the temperature range and corresponded to a decrease in the selectivity towards CO_x. Octenes were observed at 450 °C and decreased to trace amounts with an increase in temperature. The formation of octenes above 450 °C could have been due to the thermal energy supplied to the reaction at or above this temperature that appeared to have been greater than the energy of activation of these compounds. The decrease in both CO_x

and octenes selectivity corresponded to an increase in cracked product selectivity suggesting that a preference for thermal cracking existed.

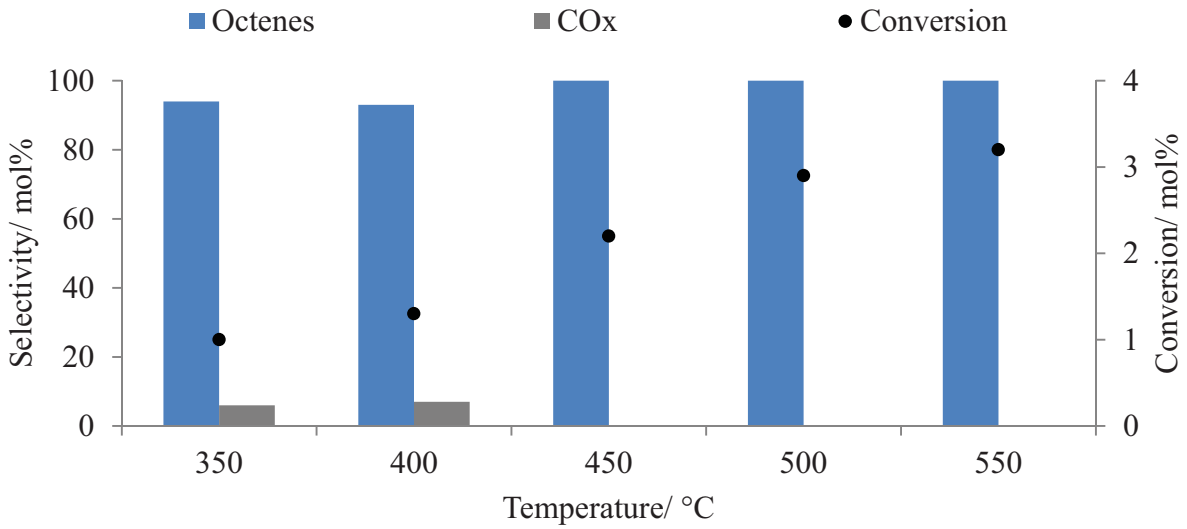

Figure 4.5: Conversion and selectivity profile over HAp as a function of increasing temperature at a GHSV of 4000 h^{-1} and a C:O ratio of 8:0

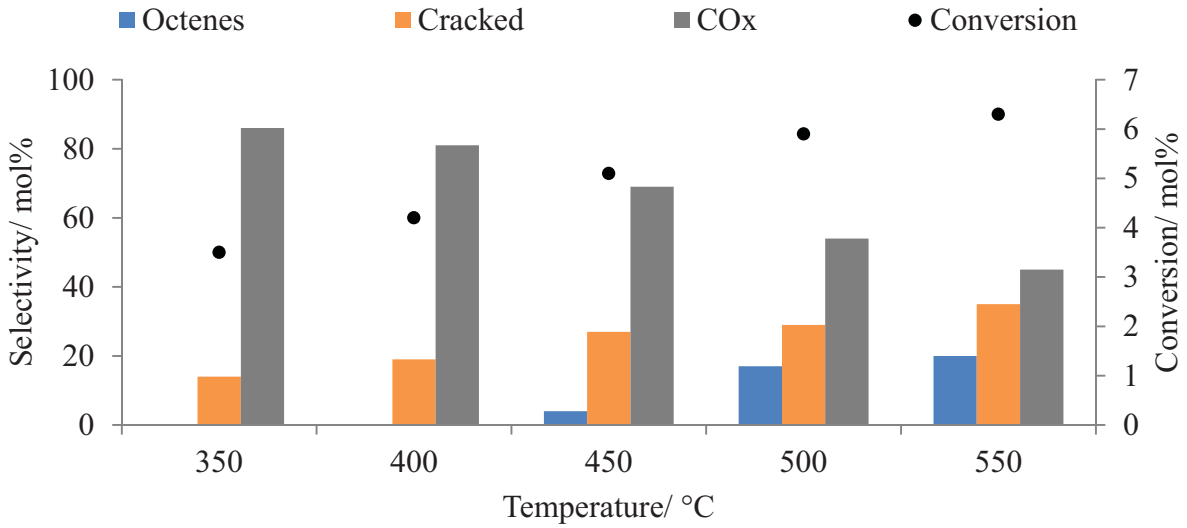

Figure 4.6: Conversion and selectivity profile over HAp as a function of increasing temperature at a GHSV of 4000 h^{-1} and a C:O ratio of 8:2

The ODH of *n*-octane over HAp has been investigated by Dasireddy *et al*. [3]. They have shown this catalyst to be stable under the conditions tested. An iron (1 % by weight) substituted HAp (1-COP) catalyst was investigated. This catalyst was tested isothermally (450 °C) at a GHSV of 4000 h^{-1} and a C:O ratio of 8:2 over a period of 48 hours in order to explore the stability of this catalytic system under oxidative dehydrogenation (ODH) conditions. The conversion of the 1-COP catalyst remained constant at 11 mol% (within experimental error of ± 2 mol%). In terms of C8 value added products, the selectivity towards octenes was 25 mol% ± 4 mol% and C8 aromatics 16 mol% ± 4 mol%.

4.3 The influence of GHSV on the activation of *n*-octane over the iron modified hydroxyapatite catalysts

An isothermal gas hourly space velocity (GHSV) variation was carried out over two of the iron modified hydroxyapatite (HAp) catalysts, where the rapid or delayed removal of the formed reaction intermediates was attempted. By controlling the gas flow rates while maintaining a constant catalyst bed volume of 1 cm^3, the GHSV of the reaction was altered.

The GHSV variation experiments were carried out using a 3 wt% iron supported on hydroxyapatite (3-WET) catalyst and a 3 wt% iron substituted (3-COP) catalyst.

4.3.1 Conversion as a function of GHSV

The 3-WET and the 3-COP catalysts were tested isothermally (450 °C) at three different GHSVs, i.e. 4000, 6000 and 8000 h^{-1}. The *n*-octane conversion over both catalysts showed an increase with a decrease in GHSV (Figure 4.7).

Lower GHSVs allow for greater residence time of the feed compound on the surface of a catalyst and this generally leads to an increase in conversion and a variation in the selectivity of a catalyst [1]. The increase in conversion was due to the low flow rates employed during the reaction that provided longer residence times of the feed on the catalyst's surface. Another observation was that the conversion of the 3-WET catalyst was greater than that obtained over

the 3-COP catalyst. The greater conversion achieved over the 3-WET catalyst can be related to the greater dispersion of iron on the surface of the catalyst and hence being more easily available to gaseous *n*-octane molecules. The active iron species would have been distributed throughout the structural lattice of the 3-COP catalyst and as a result not all of these would have been available to the reactant, despite the larger surface area of the 3-COP catalyst than the 3-WET catalyst. Thus, a greater conversion was observed over the 3-WET catalyst.

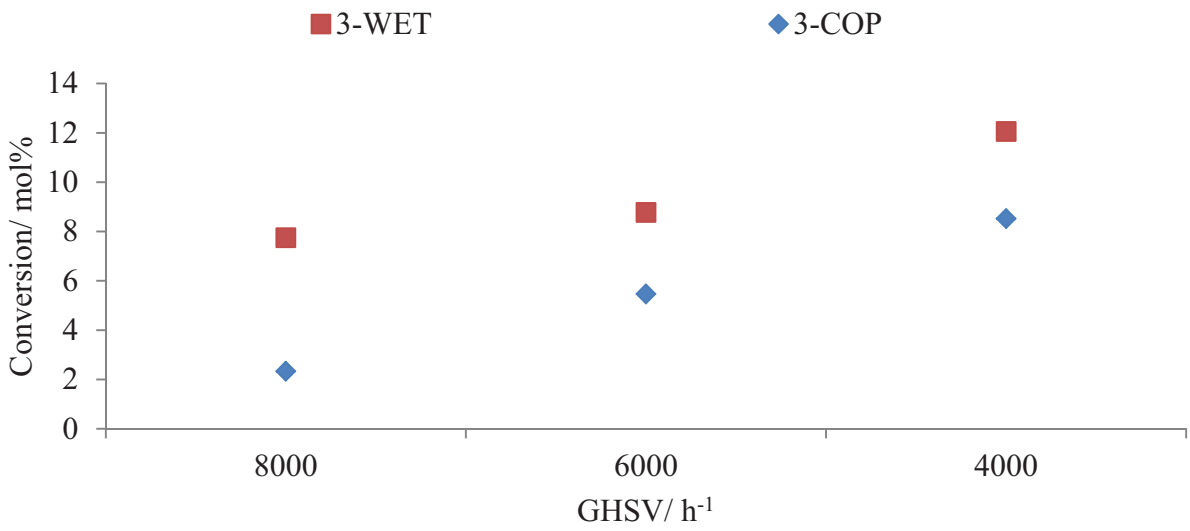

Figure 4.7: Conversion over the 3-WET and 3-COP catalysts as a function of decreasing GHSV under isothermal conditions (450 °C) at a C:O ratio of 8:2

4.3.2 Product profile with varied GHSV

One of the primary aims of an investigation into the ODH of *n*-alkanes is to prevent the total oxidation or rather combustion forming CO_x and H_2O [5, 8]. It is often observed that the desired products of a catalysed heterogeneous reaction serve as intermediates for other products and ultimately CO_x formation through complete oxidation [3, 4, 9]. The thermal stability of these undesirable products, viz. CO_x and H_2O, represent a driving force that pushes the reaction towards total oxidation thus lowering the selectivity towards desirable products. In the case of this investigation the desirable products included C8 aromatic compounds, octene isomers and C8 oxygenated compounds. It thus became clear that

designing and tuning a catalyst and the reaction conditions under which a catalyst is tested is very important. An attempt must be made to stop the reaction at the formation of these desired reaction intermediates. With respect to *n*-alkane activation, a product's selectivity is controlled or determined by the manner in which the formed alkyl species reacts with, and the time it spends on the catalyst surface [5].

The analysis of the product stream of the 3-WET catalyst (Figure 4.8) showed octenes, C8 aromatics, ≤ C7 aromatics, cracked products, cracked oxygenates as well as CO_x.

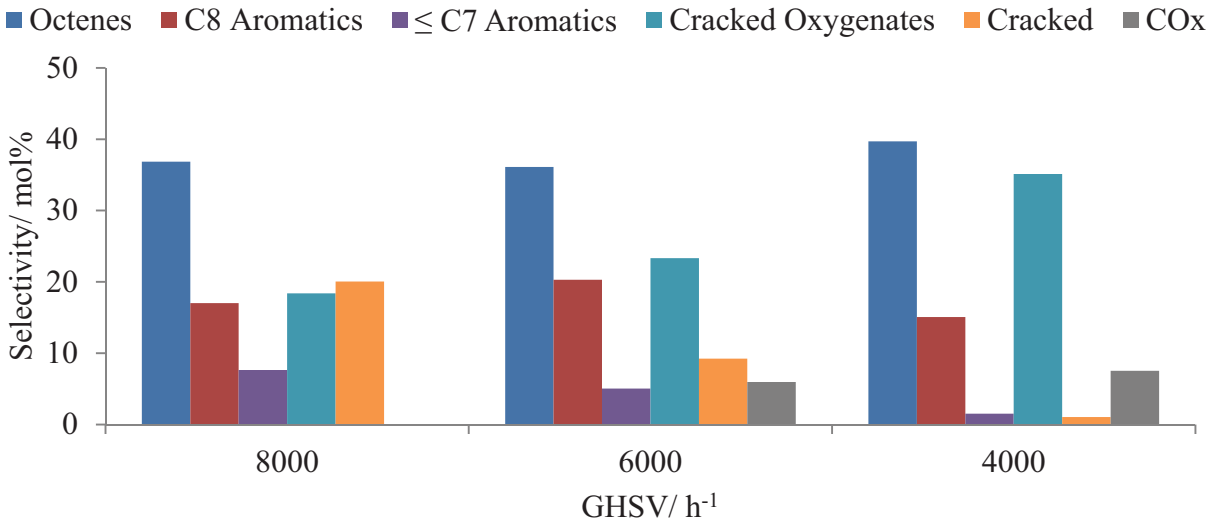

Figure 4.8: Selectivity profile over the 3-WET catalyst as a function of decreasing GHSV under isothermal conditions (450 °C) at a C:O of 8:2

The selectivity towards octenes varied within a 4 mol% range over the GHSV range. The selectivity towards octenes observed at a GHSV of 4000 h^{-1}, was marginally higher than that observed at GHSVs of 8000 and 6000 h^{-1}. This was probably due to the higher residence times of *n*-octane on the catalyst's surface allowing for greater conversion to octenes by reducing the rate of desorption of the feed. The selectivity towards octenes at 8000 and 6000 h^{-1} differed by ± 1 mol% which, due to an inherent associated experimental error, could be considered equal. The larger gas flow rates employed to attain these greater GHSV could have

led to the rapid desorption of *n*-octane from the catalyst's surface thus somewhat inhibiting the formation of these isomeric compounds.

An increase in the selectivity of C8 aromatics from a GHSV of 8000 to 6000 h^{-1} was observed. The lower gas flow rates associated with lower GHSV could have influenced the desorption rates of *n*-octane and octenes that could have affected the selectivity towards these compounds. The decrease in selectivity thereafter, with a decrease in GHSV from 6000 to 4000 h^{-1}, could have been due to the cracking or secondary combustion of these products. Literature has shown that iron catalysts favour combustion [10], thus it could be suggested that the decrease in selectivty towards C8 aromatics may have been due to the cracking or secondary combustion of octene isomers, which have been shown to function as precursors to C8 aromatic compound formation [3, 4, 6, 7, 9, 11].

Analysis of the product stream of the 3-WET catalyst showed no traces of C8 oxygenates. It seemed as though supporting iron oxide (α-Fe_2O_3) on the surface of HAp could have influenced the cracking of formed intermediates into shorter chain cracked oxygenates as inferred from the increased selectivity towards these over the decreasing GHSV range. The cracked oxygenates observed included mainly acetone, with minor contributions from ethanol and 2-propanol. CO_x was produced at a GHSV of 4000 h^{-1} and its selectivity decreased when the GHSV was increased to 6000 h^{-1}. CO_x was not observed at a GHSV of 8000 h^{-1}. The increase in selectivity towards cracked oxygenates and CO_x with the decreasing GHSV could have been due to the slow desorption rates of products from the catalyst surface. From the results observed it could be suggested that two competitive pathways existed. One being the oxidative cracking of formed reaction intermediates and the other being the combustion of the formed reaction intermediates. The increase in selectivity towards cracked oxygenates and CO_x corresponding to a decrease in selectivity towards $\leq$ C7 aromatics and cracked products supported this argument. It apeared as if the oxidative cracking pathway was favoured as inferred from the greater selectivity to these over the decreasing GHSV range. This oxidative cracking type reaction is commonly observed over iron oxide catalysts. Baldi *et al.* [8] suggested that iron oxide influenced the formation of propene as a reaction intermediate during the combustion of propane to form CO_2 and H_2O. Their study suggested that iron

oxide promoted secondary combustion. The fact that iron oxide led to the formation of a reaction intermediate in the combustion of propane suggested that the selectivity of the reaction intermediate could have been controlled through tuning of the catalyst employed and the reaction conditions it was tested under. The reaction intermediates formed via the ODH of *n*-octane over iron oxide supported on HAp seemed to have favoured an oxidative cracking pathway, which led to the formation of cracked oxygenated products.

An analysis of the product stream of the 3-COP catalyst tested under varying GHSV at a C:O ratio of 8:2 showed octenes to be the dominant products (Figure 4.9).

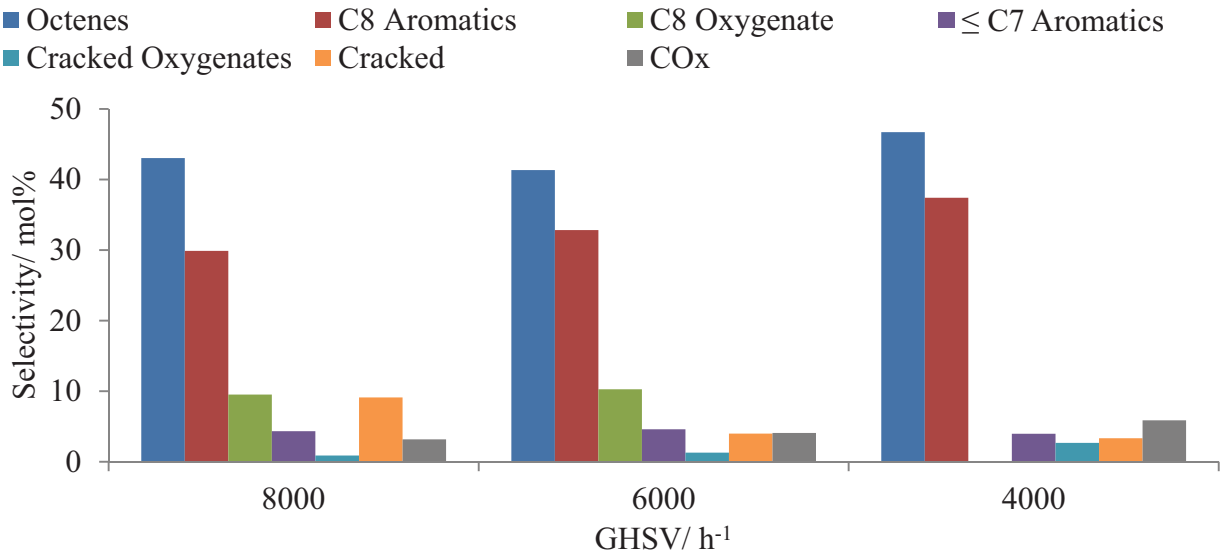

Figure 4.9: Selectivity profile over the 3-COP catalyst as a function of decreasing GHSV under isothermal conditions (450 °C) at a C:O of 8:2

C8 aromatics showed the second highest selectivity followed by C8 oxygenated products, viz. 1-octanol, at GHSVs of 8000 and 6000 h^{-1}. Other ODH products detected in the product stream were ≤ C7 aromatics (more specifically benzene), cracked oxygenates, cracked products and CO_x.

Over the GHSV range studied, the highest overall selectivity towards octenes was observed at 4000 h^{-1}, at which GHSV the slow desorption rate of *n*-octane from the surface of the 3-COP

catalyst associated with relatively low gas flow rates employed at this GHSV seemed to have favoured the formation of octenes. The second highest selectivity towards octenes was observed at 8000 h^{-1}. The rapid desorption rates of the formed reaction intermediates, viz. octenes, at this relatively high GHSV may have led to the greater selectivity. This observation suggested that at higher GHSV the residence time of *n*-octane on the surface of the 3-COP catalyst was reduced and thus consequently inhibited the expected ODH of *n*-octane to some extent. The selectivity towards octenes at a GHSV of 6000 h^{-1} was marginally lower than those obtained at 8000 and 4000 h^{-1}. This intermediate GHSV (6000 h^{-1}) seemed to have had a minor retardation effect on the formation of octenes over the 3-COP catalyst.

C8 aromatics showed the second highest selectivity. This class of compound consisted of ethylbenzene, styrene and *o*-xylene. A marginal increase was observed in the selectivity towards these compounds over the decreasing GHSV range. This suggested that the formation of these compounds was favoured at lower GHSV which could have been due to the greater residence times of *n*-octane on the surface of the 3-COP catalyst. The selectivity towards benzene remained fairly constant with decreasing GHSV. Benzene is a particularly stable compound due to the unusually large delocalisation energy associated with its six sp^2 carbon ring structure [12]. This may have been a contributing factor to the absence of change in the selectivity towards ≤ C7 aromatics with respect to varying GHSV.

Of the possible C8 oxygenates formed, only 1-octanol was detected in the product stream. Its formation was observed at GHSVs of 6000 and 8000 h^{-1} and the selectivity values were similar. The observation of 1-octanol at these GHSVs could have been due to its rapid desorption from the surface of the catalyst, preventing further oxidation or complete combustion. At a GHSV of 4000 h^{-1}, 1-octanol was not observed in the product stream. The absence of 1-octanol could have been due to it serving as a reaction intermediate that underwent thermal cracking or secondary combustion. An increased selectivity towards cracked oxygenates and CO_x supported this assumption.

The cracked oxygenates were dominated by acetone with minor contributions from ethanol, methanol and 2-propanol. The selectivity towards these cracked oxygenates demonstrated a

marginal increase over the decreasing GHSV range, which suggested that the increased residence time of the feed and reaction intermediates on the catalyst surface associated with the lower GHSV favoured oxidative cracking. Although these cracked oxygenates may be considered value added products, the key focus of this study was to optimize the reaction conditions to favour the formation of C8 value added products, viz. octenes, C8 aromatics and C8 oxygenates. A decrease in the selectivity towards CO_x was observed with an increase in GHSV. The low residence times associated with a high GHSV could have led to greater desorption rates of *n*-octane molecules and its corresponding reaction intermediates from the surface of the 3-COP catalyst, thus having an inhibitory effect on the partial or deep oxidation that led to the formation of CO_x and H_2O. The decrease in the selectivity of cracked products with decreasing GHSV corresponded to an increase in the selectivity of cracked oxygenated products and CO_x.

4.3.3 Varied GHSV over the iron supported on hydroxyapatite catalyst of smaller pellet sizes

This study aimed to investigate the influence of mass transfer effects and diffusion limitations associated with the ODH process. Conversion attained over the 3-WET catalyst with pellet sizes of 300 – 600 µm and 600 – 1000 µm (Figure 4.10) showed an increase with decreasing GHSV.

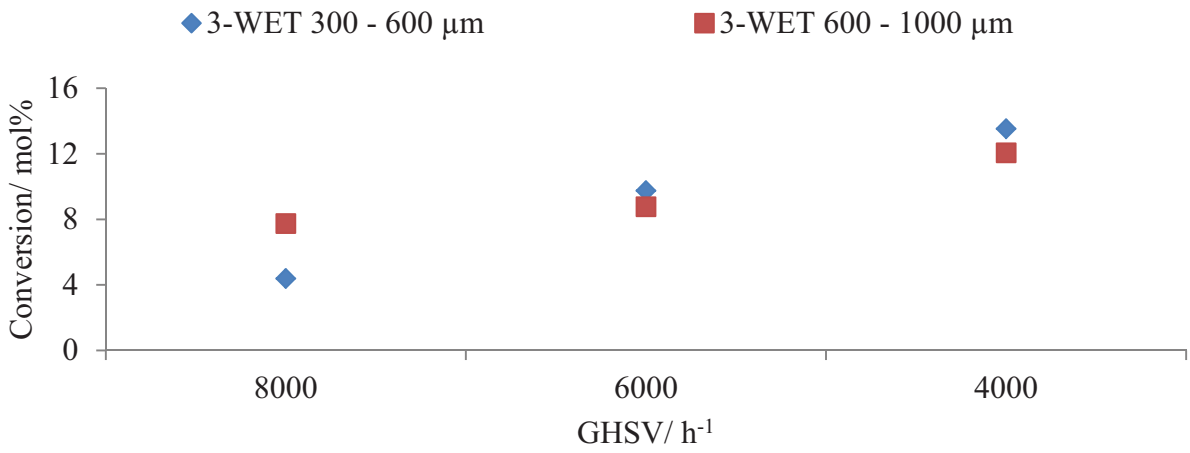

Figure 4.10: Isothermal conversion over the 3-WET catalyst with different pellet sizes as a function of decreasing GHSV, at 450 °C and a C:O of 8:2

At a GHSV of 8000 h^{-1}, the conversion achieved over the 3-WET catalyst with a smaller pellet size was lower than the conversion of the 3-WET catalyst with the larger pellet size. This implied the existence of diffusion limitations and mass transfer problems when operating at high gas and flow rates. At a GHSV of 4000 h^{-1}, a marginal difference in conversion between the larger and smaller pellet sizes was observed. This implied that minor diffusion limitations and mass transfer effects existed with respect to larger pellet sizes at lower GHSV, although the values may be within experimental error. At a GHSV of 6000 h^{-1} an approximate isothermal iso-converison of 9 mol% was attained over both pellet size ranges. This result suggested that at a GHSV of 6000 h^{-1} the activation of *n*-octane over the 3-WET catalyst was not governed by diffusion limitations or mass transfer effects.

The selectivity profile of the 3-WET catalyst with pellet sizes ranging between 600 – 1000 µm (larger pellet size) as a function of decreasing GHSV has been discussed previously (Figure 4.8). The selectivity towards the targeted value added C8 products showed a decrease over the decreasing GHSV range with respect to a smaller pellet size range (Figure 4.11).

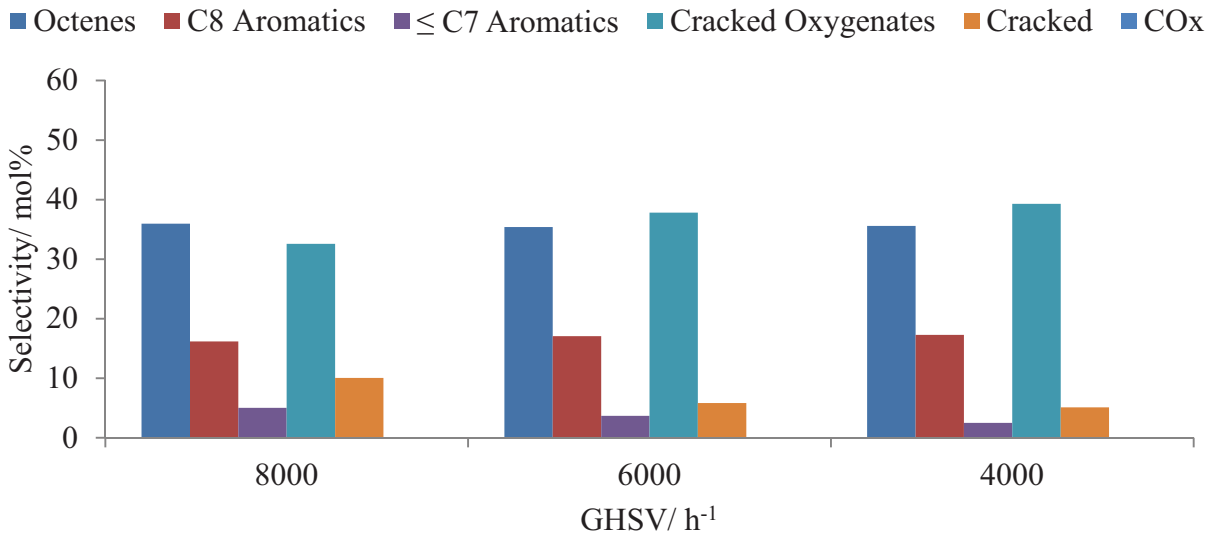

Figure 4.11: Selectivity profile over the 3-WET catalyst, with pellet size of 300 – 600 µm, as a function of decreasing GHSV under isothermal conditions (450 °C) at a C:O of 8:2

The selectivity towards other ODH products (viz. ≤ C7 aromatic compounds and cracked products) also showed a decrease over the decreasing GHSV range. The decrease in selectivity towards the value added and other ODH products corresponded to an increase in the selectivity of cracked oxygenates, predominantly acetone. Figure 4.8 shows that CO_x selectivity was greater for the 3-WET catalyst with a pellet size ranging between 600 – 1000 μm. The greater selectivity towards cracked oxygenates and the lower selectivity towards CO_x over the 3-WET catalyst with pellet sizes of 300 – 600 μm was due to smaller inter-particle voids. The smaller inter-particle voids resulted from packing the reactor with a catalyst of smaller pellet size. These smaller inter-particle voids result in a greater chance of radical quenching on the particle thus leading to a higher selectivity towards cracked oxygenates and a lower selectivity towards CO_x.

4.3.4 Summary of the effect of GHSV

In terms of value added products targeted by this study the three classes of compounds formed were octenes, C8 aromatics and C8 oxygenates. All three classes were observed in the product stream of the 3-COP catalyst at a GHSV of 6000 h^{-1} as opposed to only two at a GHSV of 4000 h^{-1}. The targeted value added products found in the product stream of the 3-WET catalyst were octenes and C8 aromatics. The cracked oxygenated products, predominantly acetone, which showed very high selectivity for the 3-WET catalyst were not considered as valorised products.

At a GHSV of 6000 h^{-1} an approximate isothermal iso-conversion was attained between the 3-WET catalysts with varying pellet sizes. This finding suggested that at this GHSV the reaction was not limited by diffusion constraints or mass transfer effects. Also with respect to pellet size, the larger sizes (600 – 1000 μm) were chosen for all catalytic testing as it appeared that there were no mass transfer or diffusion limitations associated with this pellet size range.

4.4 The effect of carbon to oxygen ratio

This investigation involved testing of the 3 wt% iron supported on HAp (3-WET) catalyst and the 3 wt% iron substituted HAp (3-COP) catalyst under different oxidation environments and at a constant GHSV of 6000 h^{-1}. These experiments determined the influence of these conditions on catalytic performance. The 3-COP catalyst was investigated under four different carbon to oxygen (C:O) ratios, viz. 8:0, 8:2, 8:4 and 8:6. The first of which, being non-oxidative, was aimed at investigating the reducible nature of the catalyst and its activity in terms of conversion and selectivity profile under dehydrogenation conditions. The 3-WET catalyst was investigated at C:O ratios of 8:0 and 8:2 to observe the behaviour of this catalyst, prepared by a different wet chemical technique, under dehydrogenation and oxidative dehydrogenation (ODH) conditions.

4.4.1 Conversion with varied carbon to oxygen ratio

When the 3-COP catalyst was tested under an anaerobic environment, activity was only observed at 550 °C at which temperature it showed the lowest conversion (Figure 4.12).

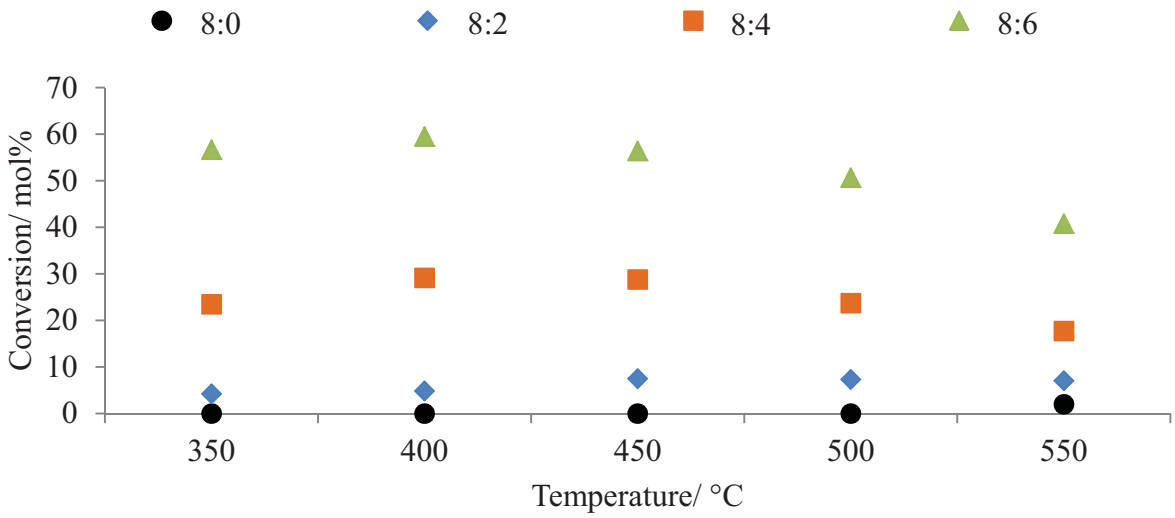

Figure 4.12: Conversion over the 3-COP catalyst under different oxidative environments as a function of increasing temperature at a GHSV of 6000 h^{-1}

At C:O ratios of 8:4 and 8:6 a decrease in conversion from 450 °C onwards was observed. Under the conditions tested the highest conversion over the 3-COP catalyst (Figure 4.12) was observed in an oxygen rich environment (corresponding to a relatively strong oxidative environment with a C:O ratio of 8:6) and the least conversion in an anaerobic environment (corresponding to dehydrogenation conditions with a C:O ratio of 8:0).

Literature has shown from work done on the ODH of *n*-octane that a decrease in the concentration of *n*-octane, and thus a corresponding increase in oxygen content (strengthening of the oxidative environment) is accompanied by an increase in conversion over the catalyst tested [1, 7, 13]. Elkhalifa and Friedrich [7] suggested that a strong oxidative environment influences the formation of thermodynamically stable CO_x pushing the equilibrium of reaction far to the right, thus higher conversion is attained. An observation made from this catalytic system was that CO_x formation was not favoured with an increase in the strength of the oxidative environment. What was favoured was the formation of cracked oxygenates and cracked products. From this result it was postulated that an increase in oxygen content during catalytic testing could have possibly favoured secondary cracking of the formed adsorbed reaction intermediates.

The decrease in conversion with an increase in temperature after 400 °C attained over the 3-COP catalyst in an oxygen rich environment (C:O ratio of 8:6) could have been due to an inhibition of the Mars and van Krevelen (MvK) mechanism. This statement can be further elaborated to suggest that an increase in oxygen richness in the feed possibly prevented the reduction of Fe^{3+} species substituted into the lattice of HAp. A similar result was observed by Khachani *et al*. [14] over an Fe^{3+} exchanged HAp. The presence of Fe^{3+} species could have favoured O_2 chemisorption and reduced the availability of active metal sites on the catalyst. This argument was supported by the increase in selectivity towards cracked oxygenated products under an oxygen rich environment, which could have formed through the postulated Eley-Rideal (ER) mechanism. By applying the assumptions made by this mechanism to this system one can argue that at higher temperatures the collisions between gas phase *n*-octane molecules and the chemisorbed O_2 species had a high probability of leading to a reaction in which the products escaped into the gas phase. According to the ER mechanism the products

of such a reaction should be highly energetic and retain a memory of the initial conditions of the gas phase reactant [15]. In the case of this system, the gas phase *n*-octane species having undergone a reaction with a chemisorbed O_2 species led to the formation of an oxygenated compound. This could have escaped into the gas phase and undergone further cracking due to interactions with gaseous oxygen species to lower cracked oxygenated products.

This argument provided a possible explanation for the increase in the selectivity towards cracked oxygenated compounds and the corresponding decrease in the conversion of *n*-octane. The decrease in this case would be attributable to the conversion of *n*-octane occurring predominantly via gas phase reactions and mostly occurring independently of the catalyst. Theoretical calculations that allowed an estimation of O_2 conversion showed that these values lay within a range of 20 – 80 % and varied with C:O ratio.

The conversion over the 3-WET catalyst (Figure 4.13) at a C:O ratio of 8:2 increased marginally from 350 – 400 °C suggesting a MvK mechanism [16] REDOX cycle of α-Fe_2O_3 $\leftrightarrow$ Fe_3O_4 at these temperatures.

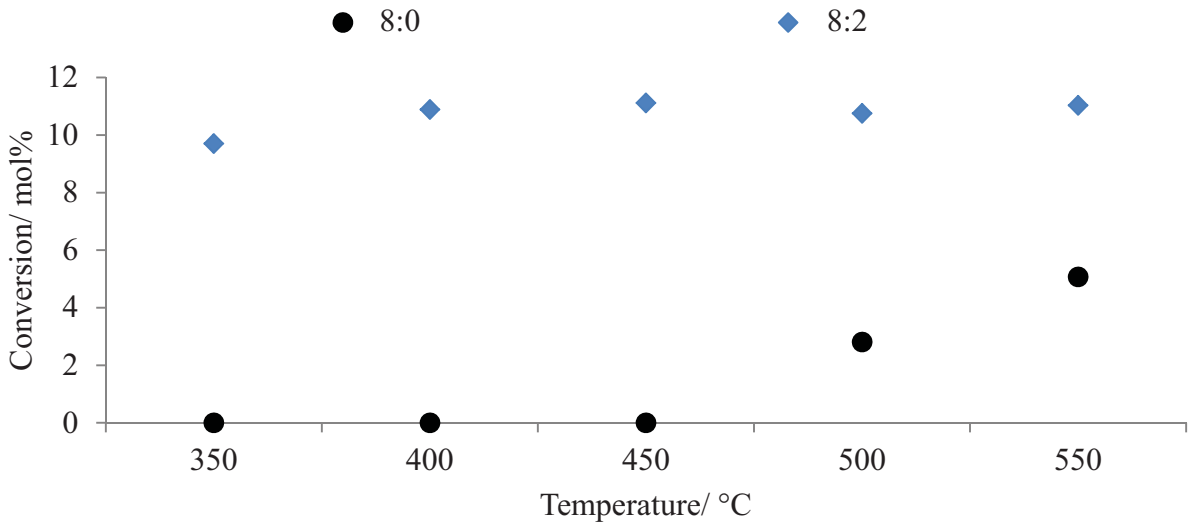

Figure 4.13: Conversion over the 3-WET catalyst in different oxidative environments as a function of increasing temperature at a GHSV of 6000 h^{-1}

However, above this temperature the activity levels off. This observation coupled with the changes in the selectivity patterns of ODH products above 400 °C suggested that the MvK mechanism was inhibited. This could have been due to the oxidation of $Fe_3O_4 \rightarrow \alpha\text{-}Fe_2O_3$ being more favourable at higher temperatures, thus preventing the REDOX couple mentioned above, common to iron oxide.

4.4.2 Selectivity profile of the iron substituted hydroxyapatite catalyst with varied carbon to oxygen ratio

From the breakdown of octenes selectivity under varying oxidative environments (Figure 4.14), it was evident that an increase in the strength of the oxidative environment (oxygen rich conditions corresponding to a C:O ratio of 8:6) consequently led to a decrease in the selectivity towards octenes except at 550 °C.

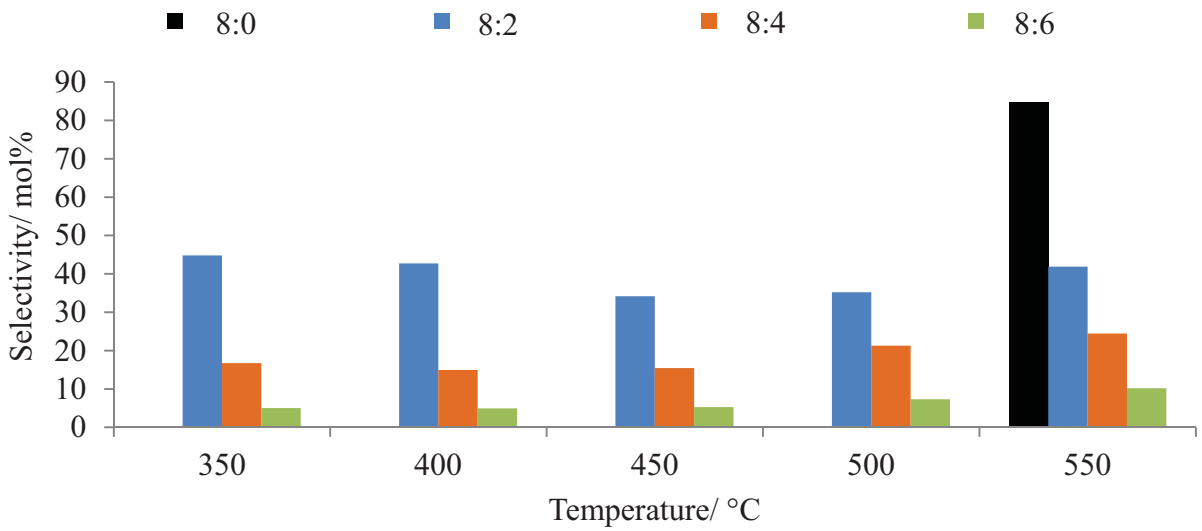

Figure 4.14: Summary of octenes selectivity over the 3-COP catalyst as a function of increasing temperature with varying C:O ratios at a GHSV of 6000 h^{-1}

The exception of the observed trend at higher temperatures was possibly due to the thermal stability of these predominantly trans-octene isomers [3]. A corresponding decrease in the selectivity towards C8 aromatic compounds with increased oxygen richness in the feed was

observed (Figure 4.15). Isothermally, the highest selectivity towards octene isomers was observed in an anaerobic environment (dehydrogenation conditions) at a temperature of 550 °C. Under dehydrogenation conditions both the 3-COP and 3-WET catalysts demonstrated catalytic activity at relatively high temperatures. This observation correlated well with the widely recognised thermodynamic limitations associated with the endothermic dehydrogenation of *n*-alkanes [3, 17].

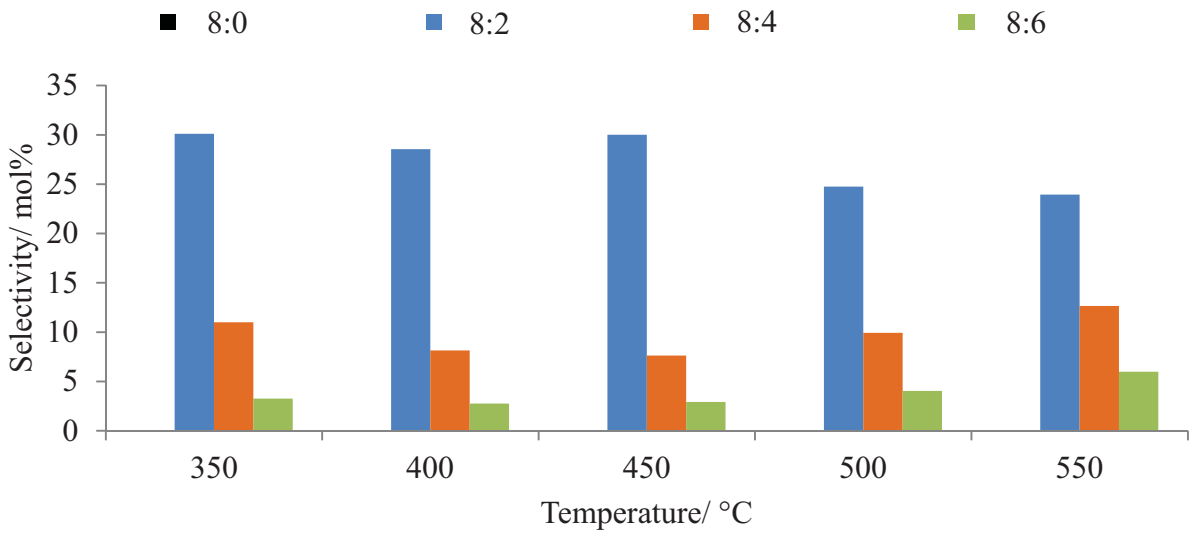

Figure 4.15: Summary of C8 aromatics selectivity over the 3-COP catalyst as a function of increasing temperature with varying C:O ratios at a GHSV of 6000 h^{-1}

The formation of the C8 oxygenated compound, viz. 1-octanol, was observed from 450 °C upwards (Figure 4.16). The selectivity of the C8 oxygenate (1-octanol) increased with temperature under both oxygen lean (C:O ratio of 8:2) and mildly oxidative conditions (C:O ratio of 8:4). The increase in selectivity of 1-octanol as a function of temperature was slightly more pronounced under a relatively mild oxidative environment, especially at higher temperatures. The formation of 1-octanol was not observed under oxygen rich conditions (C:O ratio of 8:6). The disappearance of this intermediate under an oxygen rich environment suggested that it underwent thermal cracking or secondary combustion to form cracked oxygenated products or CO_x respectively.

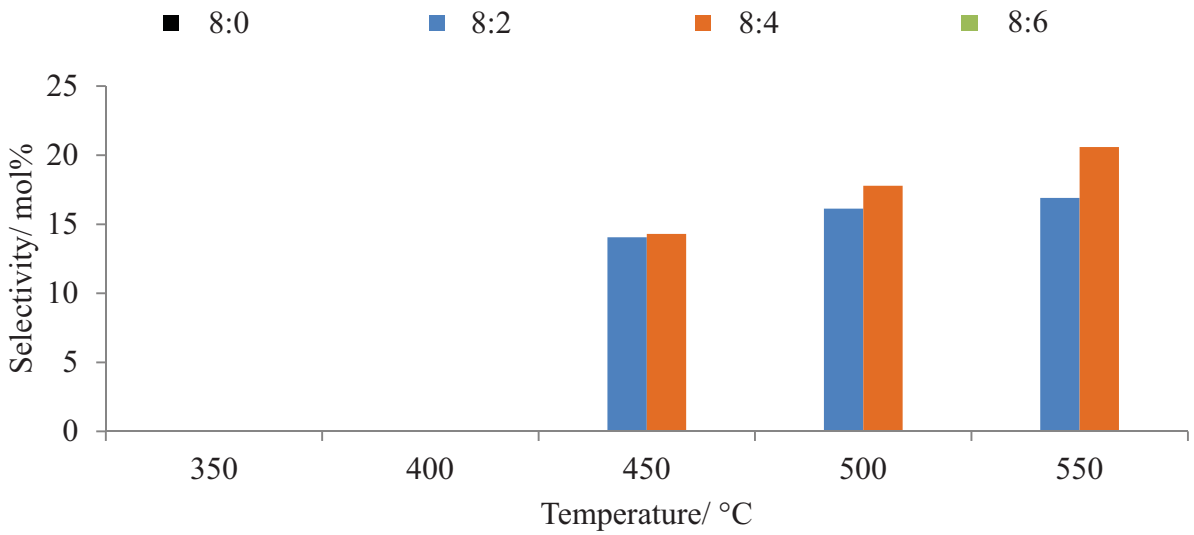

Figure 4.16: Summary of C8 oxygenate (1-octanol) selectivity over the 3-COP catalyst as a function of increasing temperature with varying C:O ratios at a GHSV of 6000 h^{-1}

A similar observation with respect to ≤ C7 aromatics, predominantly benzene with trace contributions from toluene, was made (Figure 4.17).

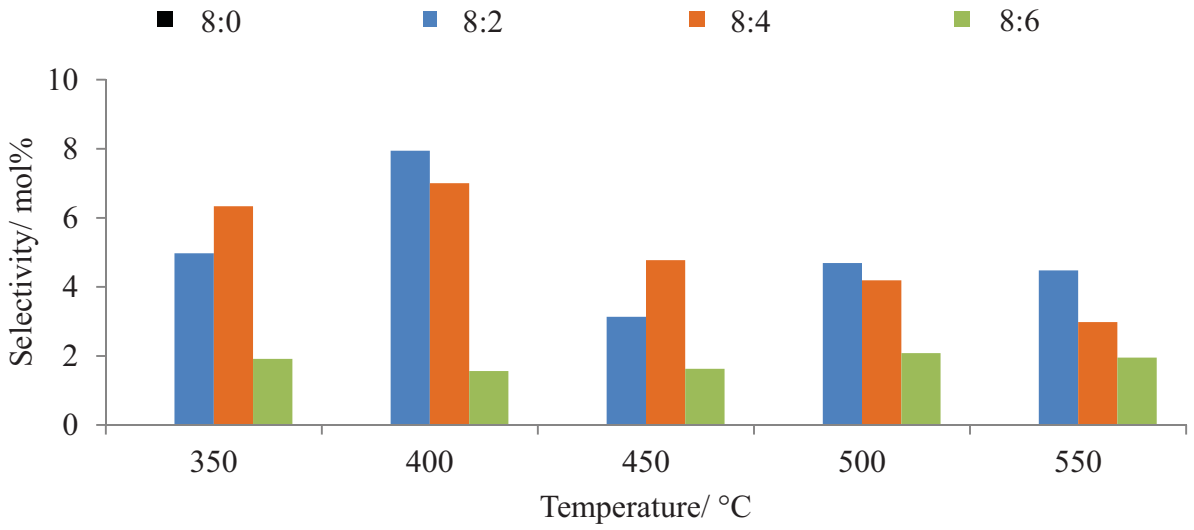

Figure 4.17: Summary of ≤ C7 aromatics selectivity over the 3-COP catalyst as a function of increasing temperature with varying C:O ratios at a GHSV of 6000 h^{-1}

Cracked products (lower alkanes and alkenes) showed the greatest selectivity under relatively mild oxidative conditions, i.e. C:O ratio of 8:4 (Figure 4.18). The selectivity towards cracked products under dehydrogenation conditions (anaerobic environment) only showed significant value at a temperature of 550 °C.

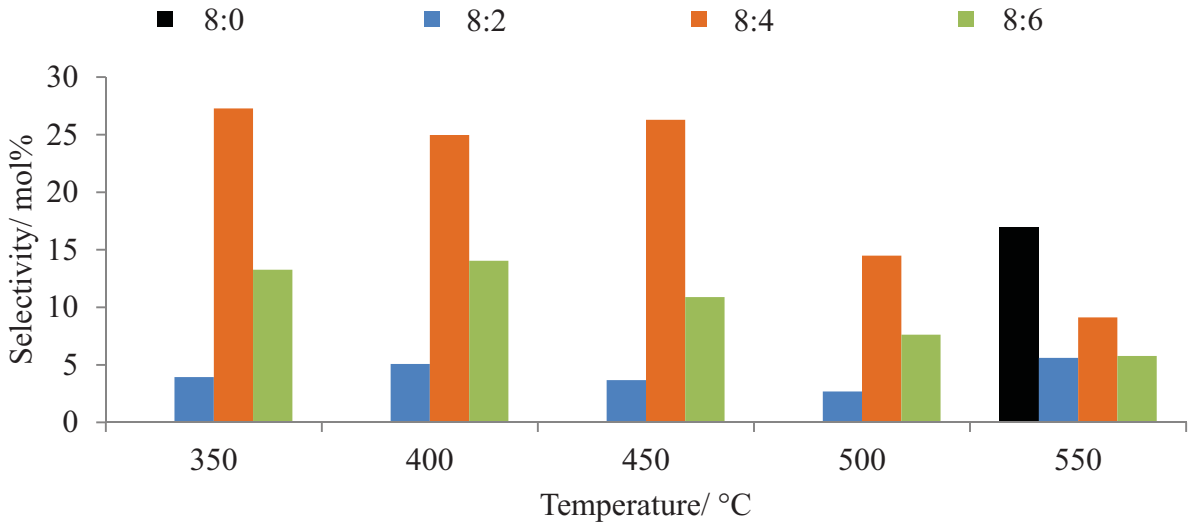

Figure 4.18: Summary of cracked product selectivity over the 3-COP catalyst as a function of increasing temperature with varying C:O ratios at a GHSV of 6000 h^{-1}

For C:O ratios of 8:2 and 8:4, CO_x selectivity (Figure 4.19) showed an increase from 350 °C to 400 °C, thereafter a decrease in CO_x selectivity was observed under these oxygen lean and mild conditions respectively. The decrease initially did not conform to results discussed in literature that have shown that CO_x was thermally favoured via the ODH process [7, 14]. The decrease in CO_x selectivity suggested that the formation of another group of compounds was thermally favoured over the 3-COP catalyst.

Under oxygen lean and an intermediate oxidative environment (C:O ratios of 8:2 and 8:4 respectively) an overall decrease in the selectivity towards cracked oxygenated products (Figure 4.20), predominantly acetone with contributions from methanol, ethanol and 2-propanol, was observed with increased temperature. The formation of these products under anaerobic conditions at 550 °C was probably caused by the interaction of adsorbed *n*-octane

molecules with O^{2-} species stabilised within the structural channels of this HAp-like catalyst material [14]. However, this only seemed to have made a minor contribution to the formation of cracked oxygenated products.

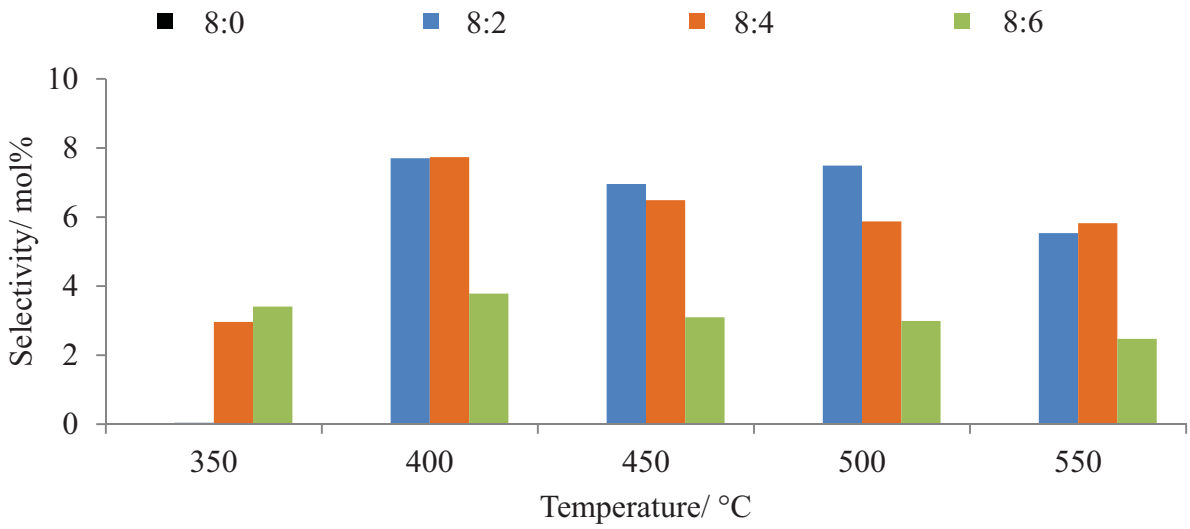

Figure 4.19: Summary of CO_x selectivity over the 3-COP catalyst as a function of increasing temperature with varying C:O ratios at a GHSV of 6000 h^{-1}

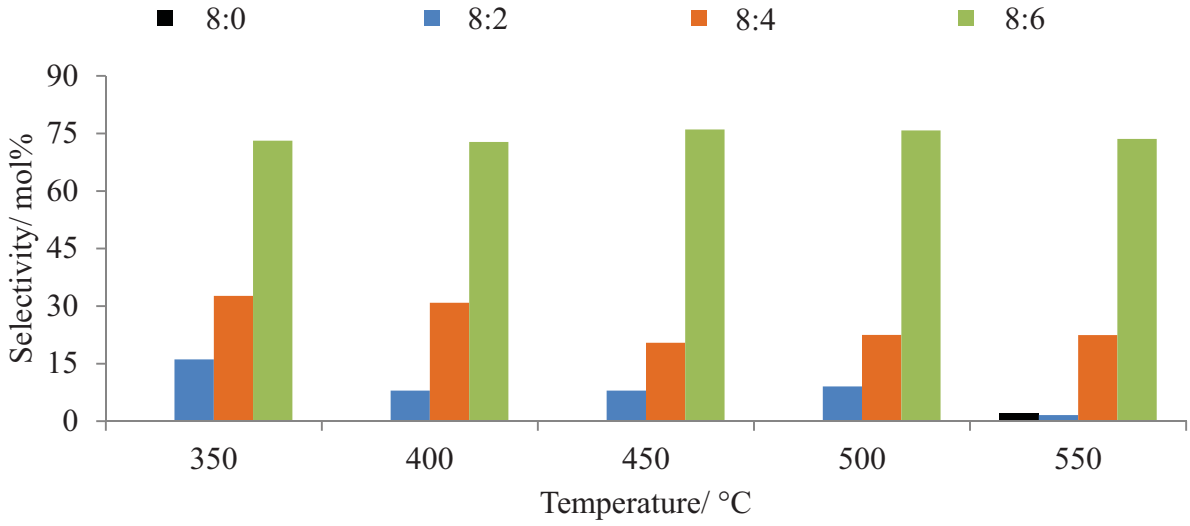

Figure 4.20: Summary of cracked oxygenates selectivity over the 3-COP catalyst as a function of increasing temperature with varying C:O ratios at a GHSV of 6000 h^{-1}

With respect to increased oxygen content in the feed mixture, the selectivity of cracked oxygenated products demonstrated significantly large increases. Over the C:O ratios tested the selectivity of these compounds was far higher than that of CO_x, which suggested that a preference for the cracking of *n*-octane or its formed reaction intermediates existed as opposed to partial or direct/secondary combustion. The formation of these products could have occurred through the postulated ER mechanism. As mentioned the increase in cracked oxygenates selectivity corresponded to an increase in the oxygen content in the feed mixture, further supporting the argument that cracked oxygenates were formed via the ER mechanism.

4.4.3 Selectivity profile of the iron supported on hydroxyapatite catalyst with varied carbon to oxygen ratio

Under dehydrogenation conditions (C:O ratio of 8:0), the 3-WET catalyst showed catalytic activity from 500 °C upwards with a high selectivity towards octenes (Figure 4.21) and increasing selectivity towards cracked products (Figure 4.25) as a function of temperature.

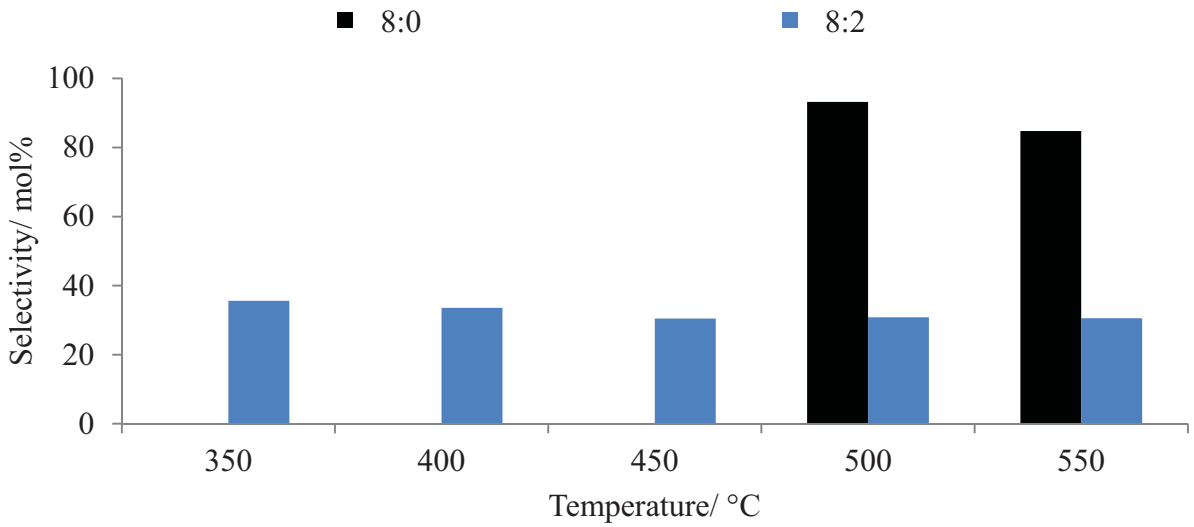

Figure 4.21: Summary of octenes selectivity over the 3-WET catalyst as a function of increasing temperature with varying C:O ratios at a GHSV of 6000 h^{-1}

The catalytic activity of the 3-WET catalyst in an anaerobic environment demonstrated the widely recognised thermodynamic limitations associated with these endothermic dehydrogenation reactions, as discussed earlier.

At a C:O ratio of 8:2 the selectivity towards octenes over the 3-WET catalyst (Figure 4.21) remained fairly constant within experimental error (± 5 mol%). A similar trend was observed for C8 aromatic compounds (Figure 4.22).

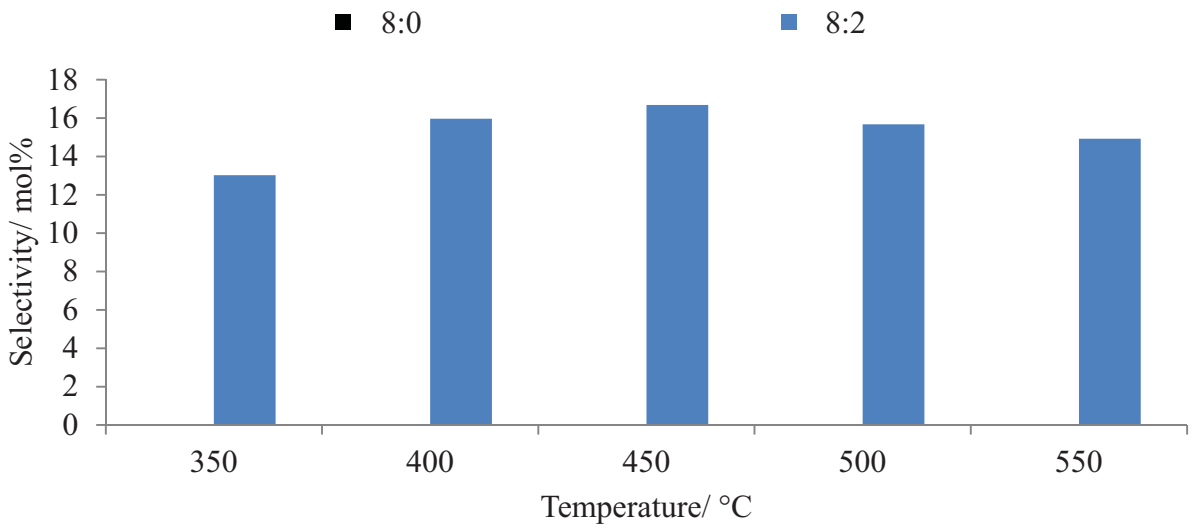

Figure 4.22: Summary of C8 aromatics selectivity over the 3-WET catalyst as a function of increasing temperature with varying C:O ratios at a GHSV of 6000 h^{-1}

The C8 oxygenate, viz. 1-octanol, (Figure 4.23) was only observed at a temperature of 350 °C. The cracking of this intermediate to cracked oxygenates could have been favoured at higher temperatures.

The selectivity towards ≤ C7 aromatic compounds (predominantly benzene) and lower cracked products remained constant (within an experimental error of ± 5 mol%) from 350 – 450 °C (Figures 4.24 and 4.25). Thereafter the selectivity demonstrated a marginal decrease as a function of temperature.

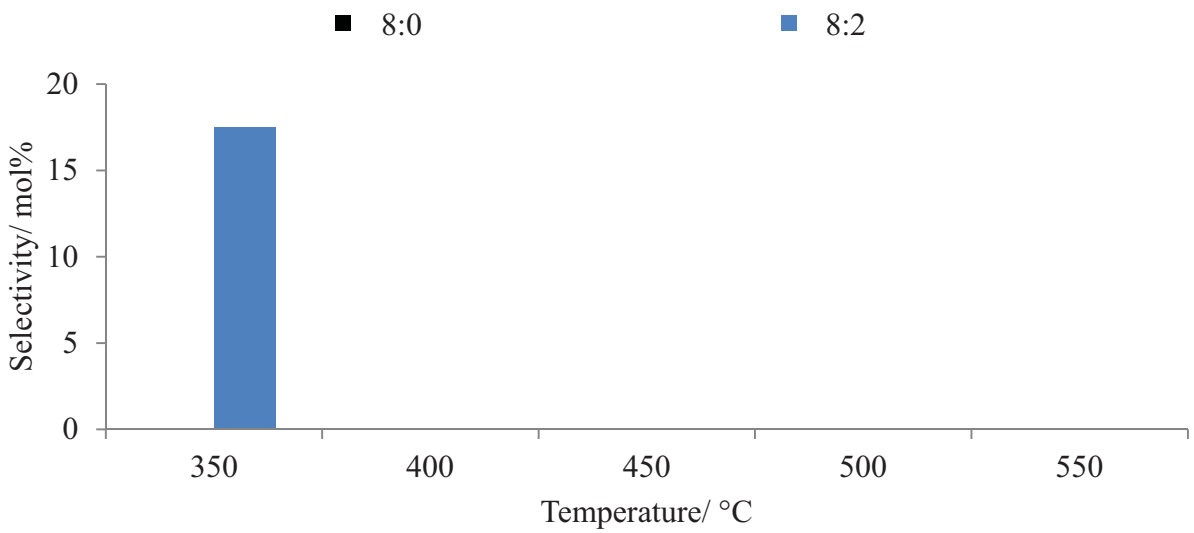

Figure 4.23: Summary of C8 oxygenate (1-octanol) selectivity over the 3-WET catalyst as a function of increasing temperature with varying C:O ratios at a GHSV of 6000 h^{-1}

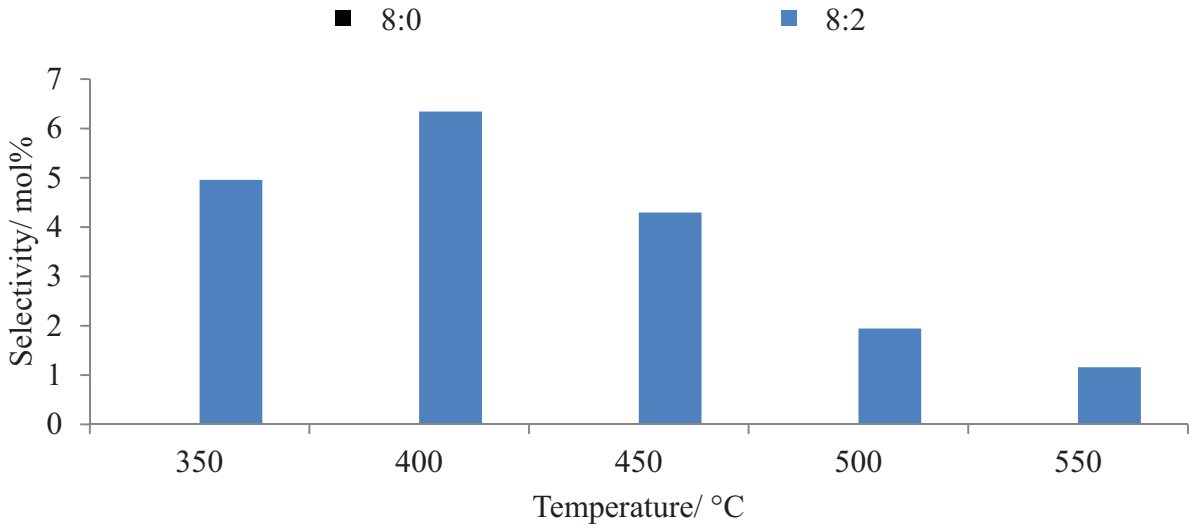

Figure 4.24: Summary of ≤ C7 aromatics selectivity over the 3-WET catalyst as a function of increasing temperature with varying C:O ratios at a GHSV of 6000 h^{-1}

The selectivity towards CO_x (Figure 4.26) also showed a decrease as a function of temperature at a C:O of 8:2. The selectivity towards cracked oxygenates (Figure 4.27) increased over the temperature range. The increase in the selectivity towards cracked oxygenates corresponded to a decrease in the selectivity towards other ODH products. This

suggested that the formation of cracked oxygenated products was favoured over the 3-WET catalyst in an ODH environment.

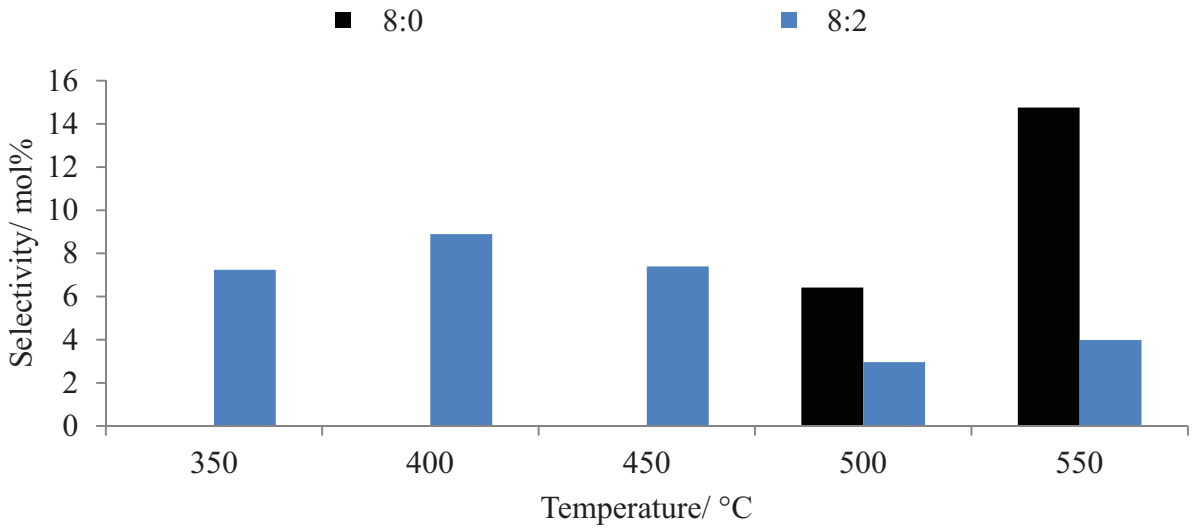

Figure 4.25: Summary of cracked products selectivity over the 3-WET catalyst as a function of increasing temperature with varying C:O ratios at a GHSV of 6000 h^{-1}

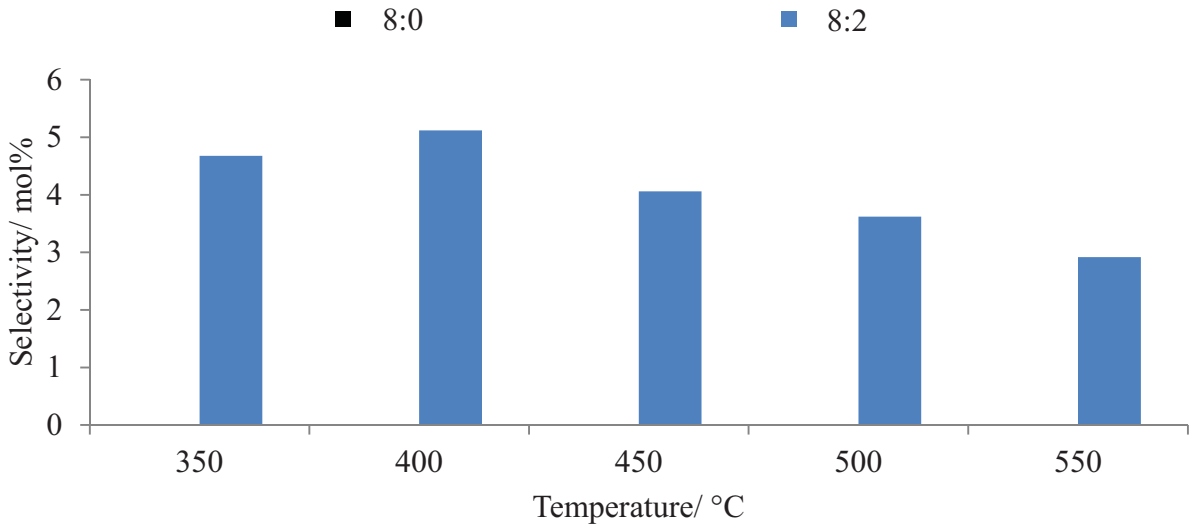

Figure 4.26: Summary of CO_x selectivity over the 3-WET catalyst as a function of increasing temperature with varying C:O ratios at a GHSV of 6000 h^{-1}

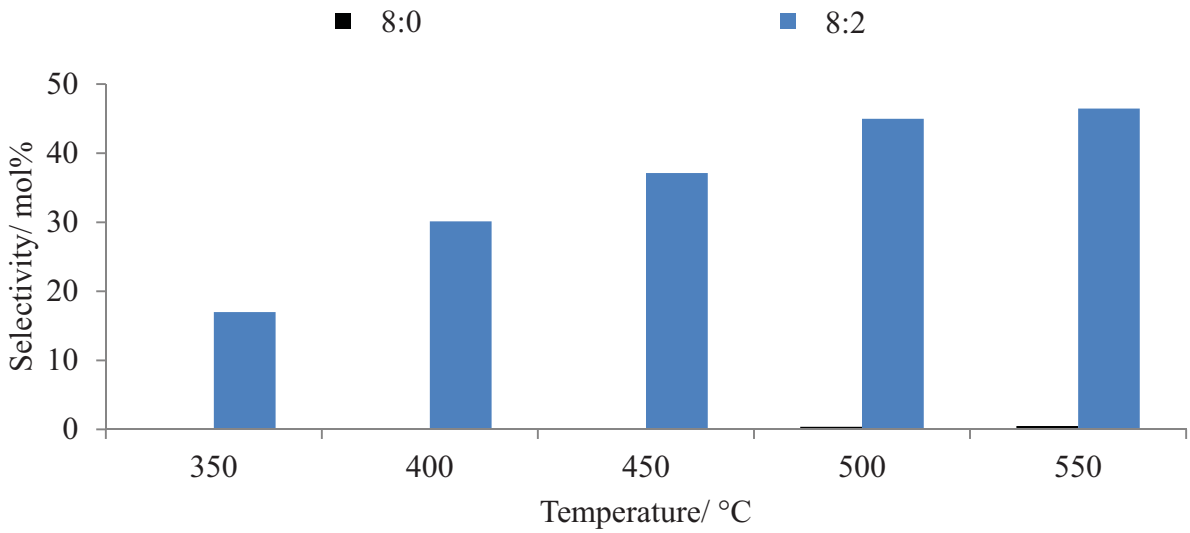

Figure 4.27: Summary of cracked oxygenates selectivity over the 3-WET catalyst as a function of increasing temperature with varying C:O ratios at a GHSV of 6000 h^{-1}

The increase in selectivity towards cracked oxygenated products with an increase in temperature suggested that gas phase cracking of *n*-octane via collisions with gaseous oxygen radicals could have occurred. Kung and Kung [18] showed that iron oxide was too basic and promoter metals had to be added to improve butene activation through manipulation of the catalyst's acid-base properties. The support (HAp) in this system contains both acidic and basic sites [3, 4, 9], and the influence of iron oxide species supported on the surface of HAp led to the increase in the basicity of the catalyst as suggested by the CO_2-TPD analysis (Figure 3.25). The increase in the area under the curve of the CO_2-TPD profile of the iron supported on HAp catalysts when compared to that of HAp confirmed this (Figure B7, Appendix B). The consideration of these factors suggested that iron oxide, with higher basicity, promotes the gas phase cracking at higher temperatures, which is observed in literature [18]. The same type of pattern was observed in this study. This could likely have also been a contributing factor to the decrease in ODH product selectivity above 400 °C and the corresponding increase in gas phase cracking.

4.4.4 Summary of the effect of carbon to oxygen ratio

Under an anaerobic environment the 3-COP and the 3-WET catalysts showed low activity at high temperatures giving low conversion. The introduction of oxygen increased the activity of these catalysed reactions by overcoming the thermodynamic limitations associated with these endothermic dehydrogenation reactions. The conversion over the 3-COP catalyst decreased above 400 °C when the oxygen content of the reaction was increased above levels that gave a C:O ratio of 8:2, most likely due to the phase change observed in the *in situ* PXRD of the 3-COP catalyst (Figures 3.3 and 3.4). The formation of value added C8 products was favoured in low oxygen environments, as proved by the greater selectivity towards octenes, C8 aromatics and C8 oxygenates at a C:O ratio of 8:2. The selectivity towards cracked oxygenates increased with an increase in oxygen content for the 3-COP catalyst. This increase in selectivity corresponded to a decrease in the selectivity towards value added C8 products.

Conversion over the 3-WET catalyst plateaued above 450 °C. An overall increase in selectivity towards cracked oxygenated compounds was observed for the 3-WET catalyst. This corresponded to a decrease in selectivity towards other ODH products.

4.5 The influence of iron loading on the activation of *n*-octane

An investigation was carried out to ascertain the effects of varying iron loading in the catalyst materials in an attempt to better understand the influence of iron on the activation of *n*-octane under ODH conditions. This study focused on the changes in the selectivity profiles and conversion of the iron supported on and iron substituted hydroxyapatite (HAp) catalysts, abbreviated as #-WET and #-COP respectively, where # denoted the weight percentage (wt%) of iron loading.

4.5.1 Iron supported on hydroxyapatite catalysts

The increase in conversion (Figure 4.28) observed with increased iron loading suggested that α-Fe_2O_3, identified by PXRD, was the active phase in the activation of *n*-octane. The greatest

conversion was attained at an iron loading of 9 wt%, however, this was at the expense of the selectivity towards octenes and C8 aromatics, whose formation was not thermally favorable at higher iron loadings as inferred from the decrease in selectivity, over the 9-WET catalyst, with increased temperature (Figure 4.32). Overall catalytic activity was altered, with an increase in iron loading as observed from the variation in conversion.

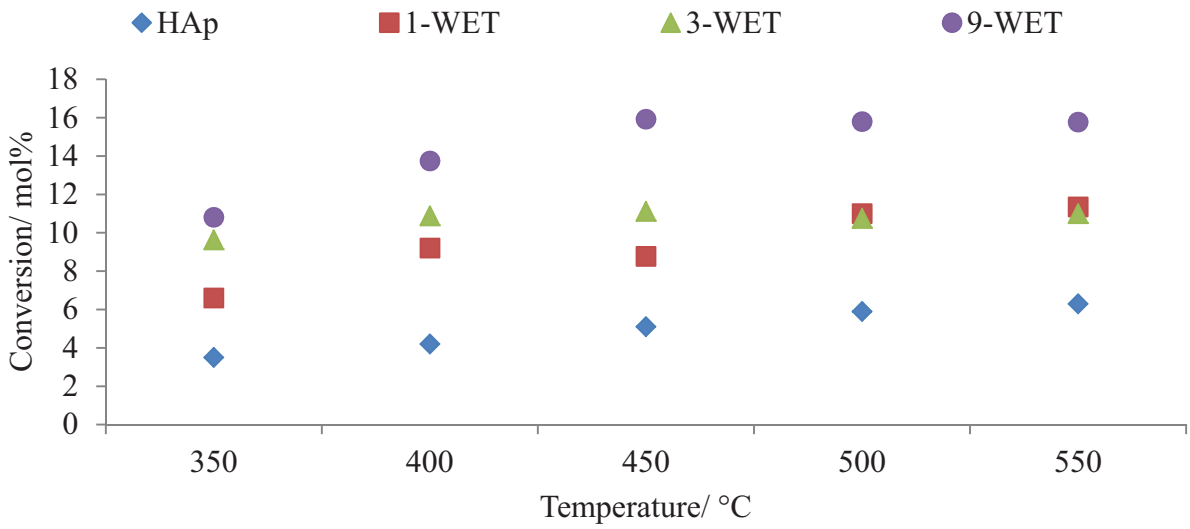

Figure 4.28: Conversion as a function of increasing temperature over the iron supported on HAp catalysts with varied iron loadings, tested at a C:O ratio of 8:2 and a GHSV of 6000 h^{-1}

Analyses of the product streams of the HAp, 1-WET, 3-WET and 9-WET catalysts identified a range of octenes, aromatics, cracked products and CO_x. Cracked products included lower alkanes and alkenes, methanol, ethanol, 2-propanol and acetone, the last four of which were classed as cracked oxygenates. Desirable C8 products included octene isomers, C8 oxygenates (or more specifically 1-octanol) and C8 aromatics, viz. ethylbenzene, styrene, and *o*-xylene. Other aromatic compounds detected were toluene and benzene and have been classed together as ≤ C7 aromatics.

Combustion leading to CO_x formation was favoured at all temperatures over HAp (Figure 4.29). Cracked products showed the second highest selectivity over the temperature range tested and increased with temperature. This suggested that thermal cracking was somewhat

favourable over this support [3]. Selectivity towards octenes was only seen from 450 °C onwards and also increased as a function of temperature. The increase in selectivity of the latter two products with temperature suggested that their formation was somewhat thermally favoured.

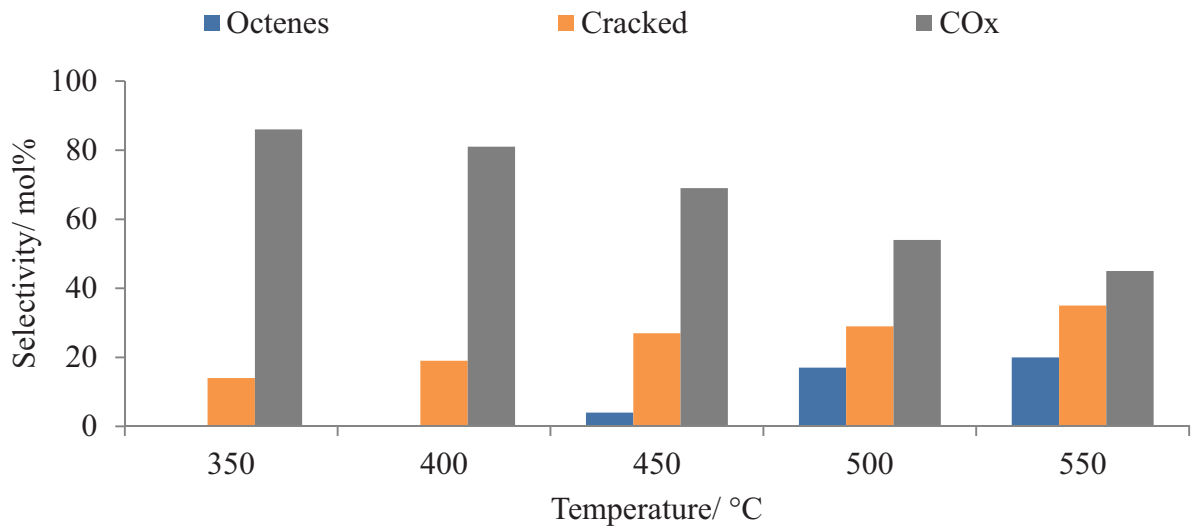

Figure 4.29: Selectivity profile over HAp tested at a GHSV of 6000 h^{-1} and a C:O ratio of 8:2

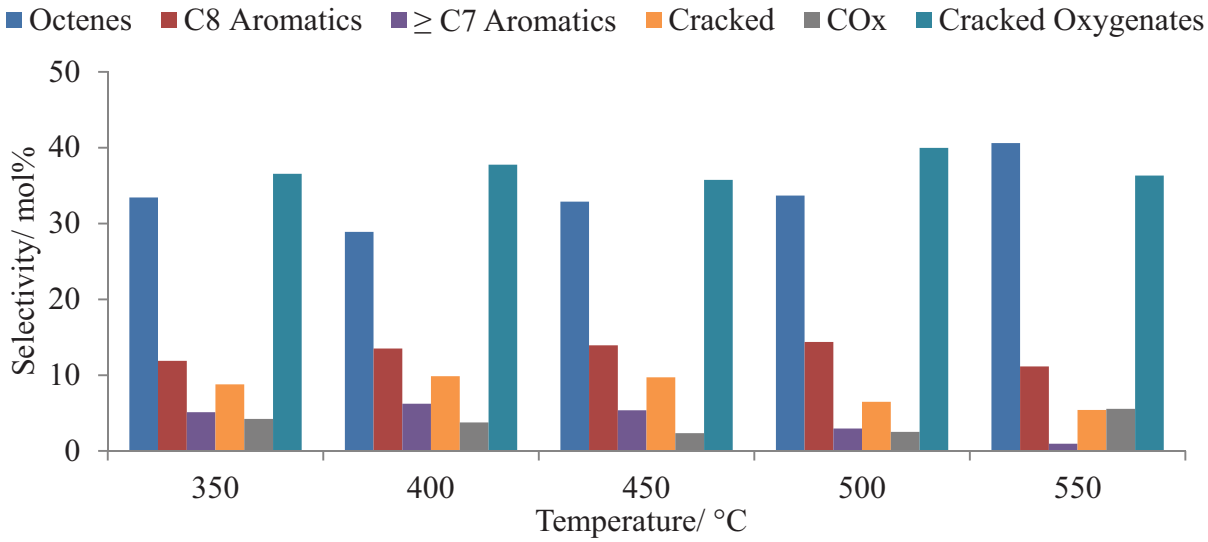

Figure 4.30: Selectivity profile over the 1-WET catalyst tested at a GHSV of 6000 h^{-1} and a C:O ratio of 8:2

What was immediately noticeable was the significant change in product profile of the iron supported on HAp catalysts when compared to HAp. An iron, 1 % by weight, supported on HAp (1-WET) catalyst showed no significant changes in selectivity towards octenes (Figure 4.30) as a function of increased temperature to warrant a discussion of any observed trend.

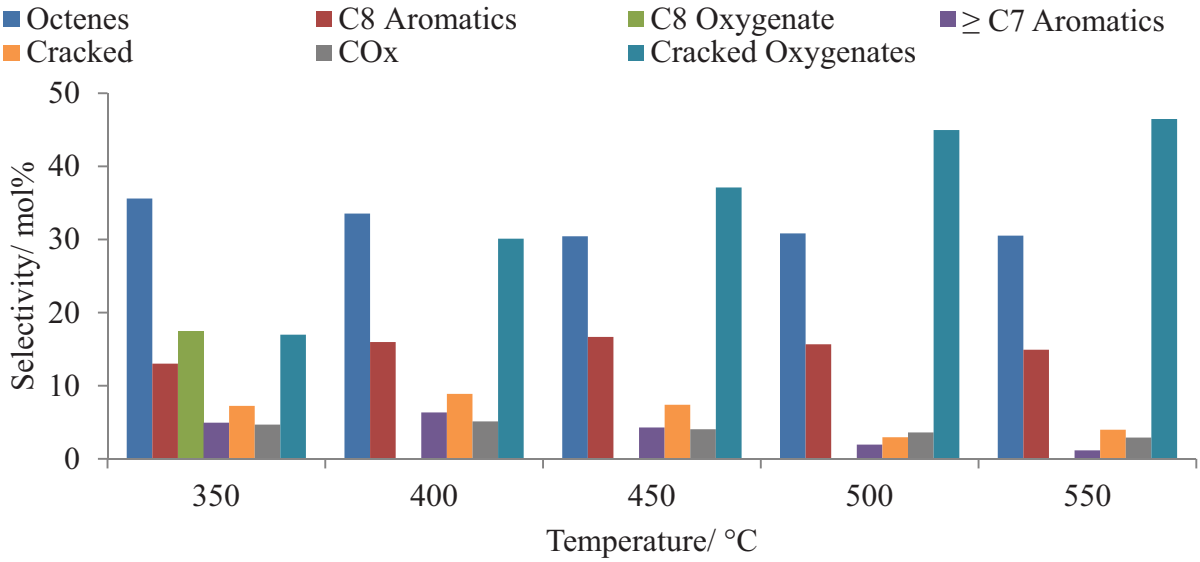

Figure 4.31: Selectivity profile over the 3-WET catalyst tested at a GHSV of 6000 h^{-1} and a C:O ratio of 8:2

However, at higher iron loadings, viz. 9 % (Figures 4.32), a decrease in selectivity towards octenes was observed with an increase in temperature. Once hydrogen abstraction from *n*-octane occurred [13], the resultant octenes could have either desorbed from the surface of the catalyst or served as reaction intermediates for other ODH product formation. Coincidentally, a decrease in selectivity towards C8 aromatics was observed with an increase in temperature for the 9-WET catalyst. This could have been due to the rapid desorption of octenes, which have been shown to serve as precursors for C8 aromatics formation [3, 4, 9, 11], from the catalyst surface. The basic nature of the catalyst could have influenced desorption of the formed octenes, thus inhibiting their selectivity and the formation of C8 aromatics.

1-Octanol was the only C8 oxygenate detected. This compound was only observed when the 3-WET catalyst was tested and showed a selectivity of 18 mol% at a temperature of 350 °C

(Figure 4.31). The absence of this product from the product streams of the other catalysts and at different temperatures could have been the result of it undergoing cracking to form cracked oxygenated compounds. It seemed plausible to suggest that 1-octanol formation resulted from an oxygen insertion reaction upon formation of an activated octene isomer, most likely 1-octene. The presence of 1-octanol in the product stream of the 3-WET catalyst was attributed to the α-Fe_2O_3 phase of the catalyst as no oxygenated compounds were observed in the product stream of the HAp catalyst (Figure 4.29). It could be suggested that iron influences the functionalisation of adsorbed octenes by reacting with chemisorbed oxygen species on the surface of the active metal phase (α-Fe_2O_3).

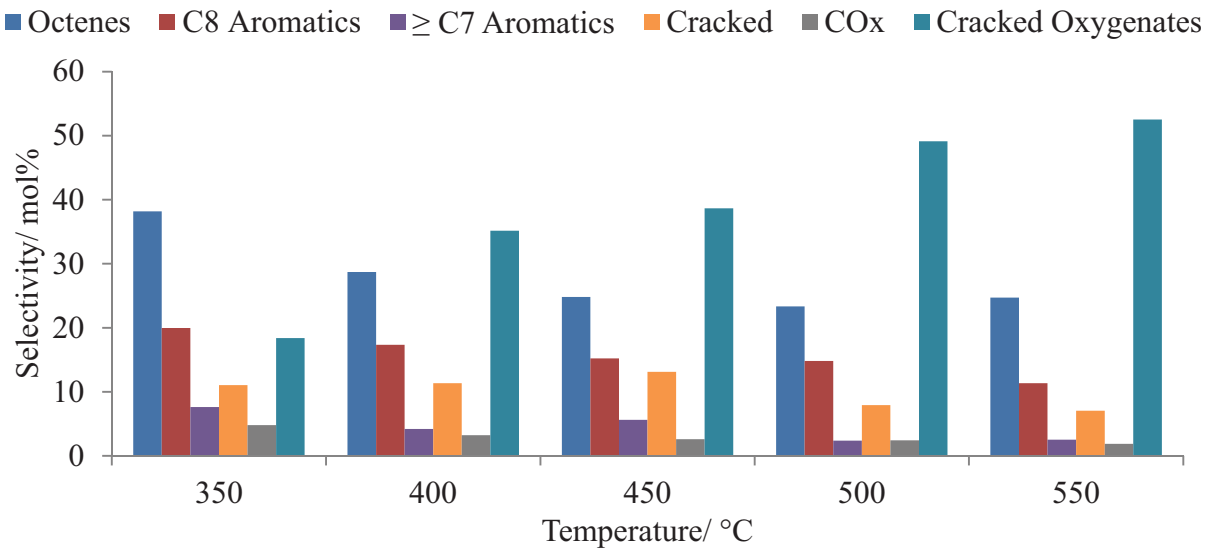

Figure 4.32: Selectivity profile over the 9-WET catalyst tested at a GHSV of 6000 h^{-1} and a C:O ratio of 8:2

Other aromatic compounds, viz. toluene and benzene (≤ C7 aromatics), showed a marginal decrease in selectivity with increased temperature for all catalysts. These aromatic compounds could have resulted from the cracking of the alkyl substituents of the C8 aromatics. If this was so, the decrease in both their selectivity with an increase in temperature suggested that the formation of C8 aromatics was favorable or a competitive pathway existed between cyclisation of formed octenes and the cracking of oxygen functionalised C8 products.

Cracked products and CO_x showed significant selectivity when HAp (Figure 4.29) was tested. Contributions from CO_x were far lower for the iron supported on HAp catalysts (Figures 4.30, 4.31 and 4.32). In all cases a decrease in CO_x selectivity was observed with an increase in temperature. This suggested that the formation of other ODH products were thermally favourable.

Iron seemed to have influenced an increase in the formation of cracked oxygenated products. An increase in the selectivity towards cracked oxygenates, as a function of temperature, was observed over all the iron supported on HAp catalysts. The selectivity towards cracked oxygenated compounds observed over the 1-WET catalyst remained constant within experimental error, ± 5 mol%. At higher temperatures (450 – 550 °C) cracked oxygenates were the dominant products formed over the 3-WET and 9-WET catalysts. The increase in selectivity and a corresponding decrease in selectivity towards other ODH products suggested a preference for cracked oxygenates formation. Cracked oxygenate formation could have occurred by the reaction of adsorbed octenes or gaseous *n*-octane radicals with chemisorbed oxygen species, thus forming oxygenated compounds that underwent thermal cracking on the surface of the catalyst influenced by the nature of the support HAp, which showed an increased selectivity towards cracked products with increasing temperature (Figure 4.29). The presence of chemisorbed oxygen species would have been a result of the active iron phase as no cracked oxygenated compounds were detected in the product stream of HAp. There was a pronounced decrease in the selectivity towards octenes observed over the 9-WET catalyst. Correspondingly the most pronounced increase in cracked oxygenates selectivity was observed over the 9-WET catalyst. This suggested that a competitive pathway existed between octene isomer formation and oxygenated compound formation.

4.5.2 Iron substituted hydroxyapatite catalysts

The substitution of iron into the lattice of hydroxyapatite (HAp) seemed to have improved the activity, with respect to conversion, of the catalysts (Figure 4.33). This finding suggested that the reducible iron species discussed in the temperature programmed reduction (TPR) analyses of these catalyst materials functioned as the active sites in these catalysed reactions. Overall

the lower conversion attained over the iron substituted HAp catalysts when compared to the iron supported on HAp catalysts was attributed to the lower amount of iron available at the surface of the catalyst materials as inferred from the energy dispersive X-ray spectroscopy mapping of the catalysts (Figure 3.19). Characterisation has proven that the substitution of iron throughout the HAp-like lattice of the material led to the distribution of iron within the crystallites of the formed particles.

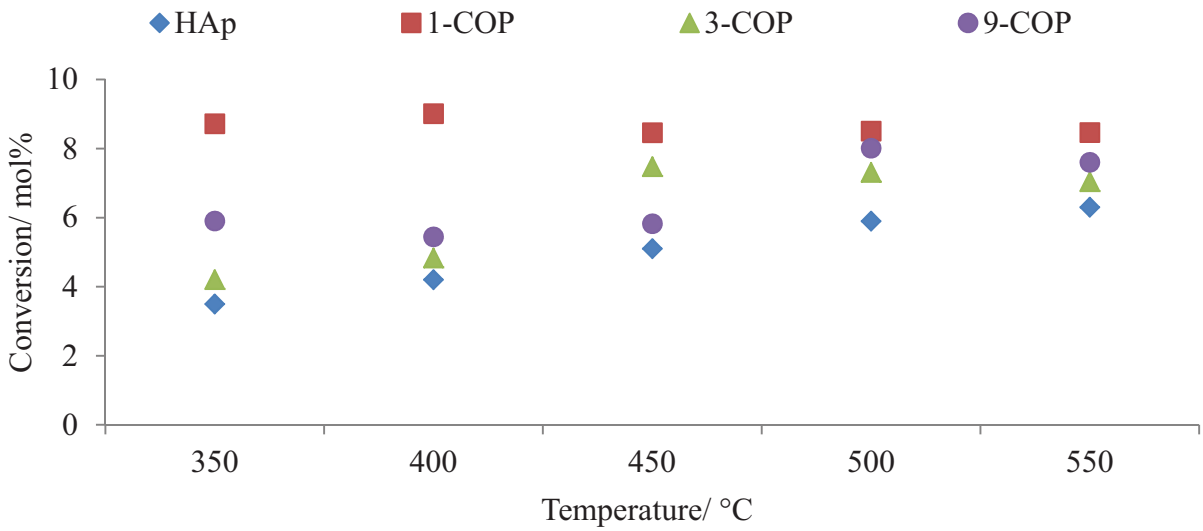

Figure 4.33: Conversion as a function of increasing temperature over the iron substituted HAp catalysts with different iron loadings, tested at a C:O ratio of 8:2 and a GHSV of 6000 h^{-1}

The analyses of the product streams of the iron substituted catalysts identified a range of octenes, C8 and ≤ C7 aromatics, a C8 oxygenate, cracked products, cracked oxygenates and CO_x.

A significant increase in selectivity towards octenes was observed for the iron substituted HAp (Figures 4.35, 4.36 and 4.37) catalysts when compared to HAp (Figure 4.34). This was attributed to the dehydrogenation ability of iron. The iron substituted HAp catalyst with low iron loading, viz. the 1-COP catalyst (Figure 4.35), showed a decrease in selectivity towards octenes with an increase in temperature. The 3-COP catalyst showed a lower selectivity towards octenes at temperatures of 450, 500 and 550 °C than when compared to 350 and 400

°C. Corresponding to the drop in octenes selectivity was the formation of 1-octanol. An increase in octenes selectivity at high iron loading, viz. the 9-COP catalyst (Figure 4.37) was observed. With increasing temperature, after hydrogen abstraction, formed octenes could have been desorbed rapidly thus inhibiting further catalysed pathways and consequently increasing octenes selectivity. The decrease in selectivity towards other ODH products detected for the 9-COP catalyst supported this argument. This result also related to the well cited ODH pathway of *n*-octane, where the activation of the linear alkane involves octene formation [3, 4, 6, 9, 11]. The rapid desorption of octenes would have been an influence of the strong basicity of the 9-COP catalyst. CO_2-TPD studies showed that the 9-COP catalyst demonstrated the strongest basicity in a comparison of HAp and the 9 wt% iron modified catalysts (Figure 3.25).

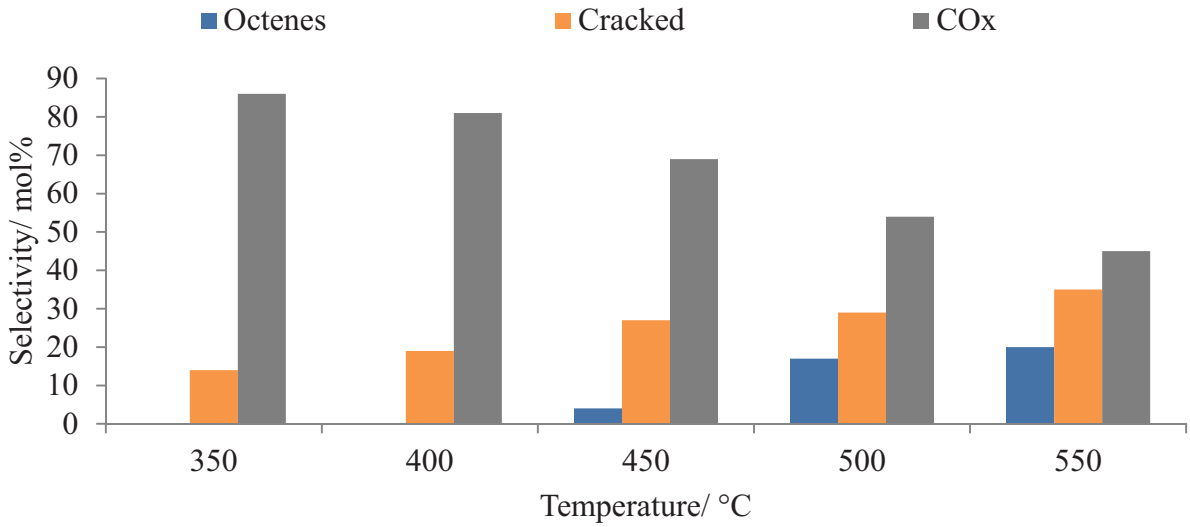

Figure 4.34: Selectivity profile over HAp tested at a GHSV of 6000 h^{-1} and a C:O ratio of 8:2

Iron substitution promoted the formation of C8 aromatics over all the catalysts in the temperature range investigated. At low iron loading (over the 1-COP catalyst), a marginal increase in the selectivity towards C8 aromatics was observed. The 3-COP and 9-COP catalysts both showed a decrease in selectivity towards C8 aromatics. A corresponding increase in octenes selectivity for the 9-COP catalyst was observed and suggested that the octenes were desorbing rapidly from the catalyst surface after hydrogen abstraction, thus an

increase in their selectivity was observed. The decrease in selectivity of C8 aromatics could have been caused by a slight inhibition of the dehydrocyclisation mechanism [11] brought on by the rapid desorption of octene isomers. The decrease in selectivity towards octenes and C8 aromatics for the 3-COP catalyst corresponded to an increase in the selectivity towards C8 oxygenates, more specifically 1-octanol. The iron substituted HAp catalysts selectivity towards C8 aromatics was higher for all the catalysts at all temperatures than the selectivity observed for the iron supported on HAp catalysts. This may have been due to the larger pore volumes of the iron substituted HAp catalysts (Table 3.5).

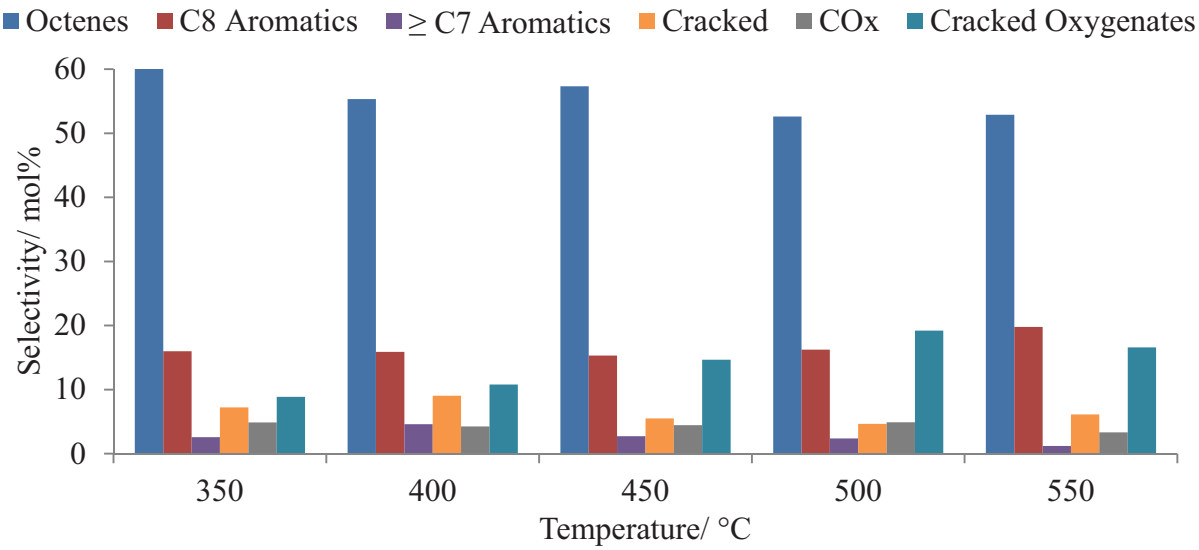

Figure 4.35: Selectivity profile over the 1-COP catalyst tested at a GHSV of 6000 h^{-1} and a C:O ratio of 8:2

The C8 oxygenate (1-octanol) may have been the result of an oxygen insertion reaction after octene formation, which could have formed through the postulated ER mechanism [15]. 1-Octanol was only detected in the product stream of the 3-COP catalyst above 450 °C. The selectivity of this compound increased with temperature. What was also worthy of noting, was the decrease in the selectivity towards octenes with respect to the 3-COP catalyst from 450 °C onwards. This suggested that octenes served as precursors to oxygenated compound formation. It seemed logical to suggest that 1-octanol could have been formed from an activated 1-octene radical that underwent a reaction with an activated O^{2-} molecule. This

further suggested that a competitive pathway existed between C8 aromatics and C8 oxygenate formation over this catalyst system.

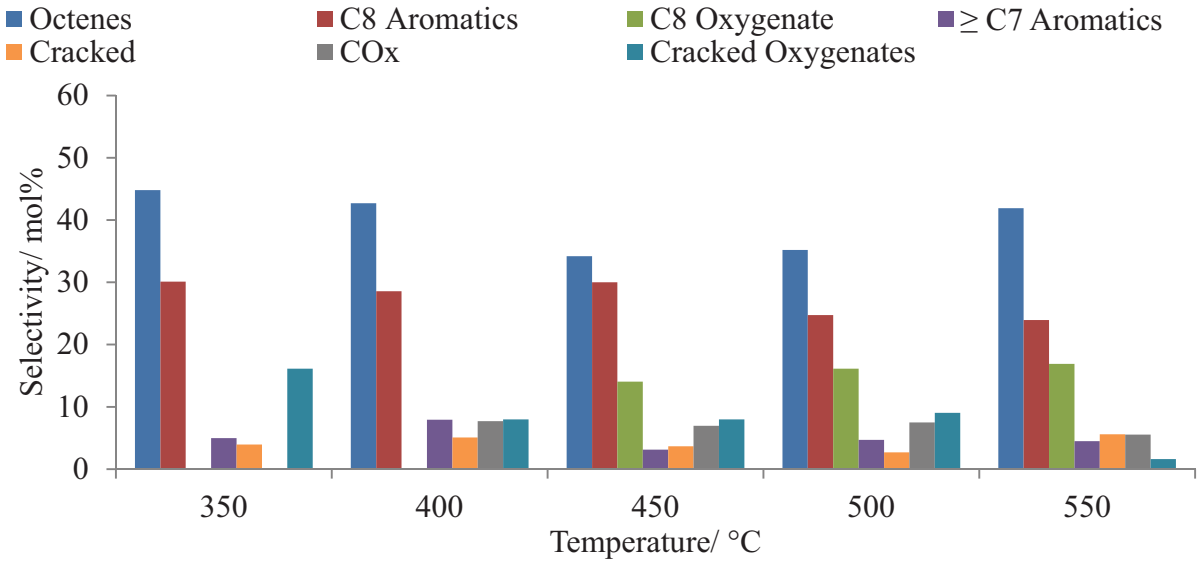

Figure 4.36: Selectivity profile over the 3-COP catalyst tested at a GHSV of 6000 h^{-1} and a C:O ratio of 8:2

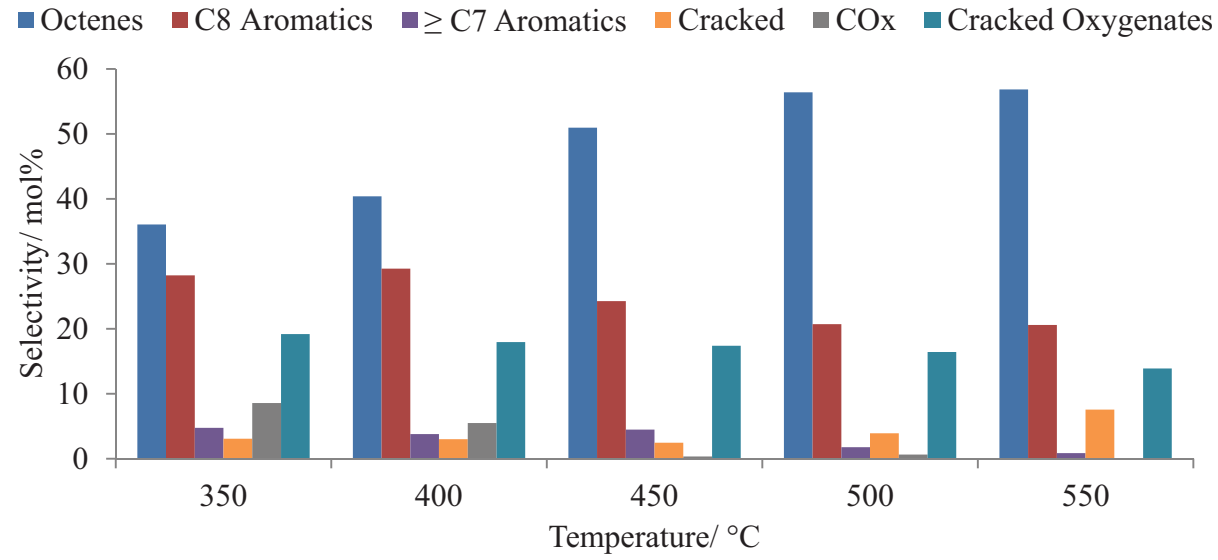

Figure 4.37: Selectivity profile over the 9-COP catalyst tested at a GHSV of 6000 h^{-1} and a C:O ratio of 8:2

The selectivity of ≤ C7 aromatics (benzene and toluene, with the dominant compound being benzene) remained constant, within an experimental error of ± 5 mol%, over the 1-COP and 3-COP catalysts. It is possible that these aromatic compounds formed from the cracking of the alkyl substituents of certain C8 aromatic compounds, viz. ethylbenzene and styrene.

HAp (Figure 4.34) showed a preference for cracked product formation throughout the temperature range tested, as depicted by the increased selectivity towards cracked products over the temperature range investigated. Upon substitution of iron into the lattice of HAp, minor contributions to cracked products were detected in the product streams of the catalysed reactions. This suggested an alternate pathway to the gas phase cracking observed over HAp.

Upon iron substitution there was an immediate decrease in the CO_x selectivity. This suggested that combustion was not favoured and a theoretical equilibrium lay further to the left of the overall reaction (equation 5):

$$C_8H_{18} + 12.5O_2 \rightarrow 8CO_2 + 9H_2O \qquad (5)$$

Another significant difference between the iron substituted HAp catalysts and HAp was that the iron substituted HAp catalysts favoured the formation of cracked oxygenated products as opposed to cracked alkane and alkene products. As both the iron supported on HAp and iron substituted HAp catalysts demonstrated this effect, it was assumed that iron led to significant cracking of oxygenated reaction intermediates and their subsequent desorption from the catalysts surface before combustion, as inferred from the low overall selectivity towards CO_x over the entire temperature range tested. CO_x formation represented the complete or partial combustion of *n*-octane.

At low iron loading, i.e. the 1-COP catalyst (Figure 4.35), cracked oxygenates selectivity increased with temperature. This increase in selectivity corresponded to a decrease in selectivity towards octenes, which suggested that these ODH products underwent oxygen functionalisation, possibly through an ER type mechanism, and then cracking, thus forming cracked oxygenates. There was no observable variation in the selectivity towards C8

aromatics. This could have been due to the stable aromatic nucleus of these compounds which represented a driving force for their formation [6], thus inhibiting further reaction to form cracked oxygenates or combustion to form CO_x. The 3-COP catalyst showed a minor decrease in selectivity towards cracked oxygenates with an increase in temperature. A corresponding increase in C8 oxygenates selectivity was observed from 450 °C. This suggested a preference for an oxygen insertion reaction at higher temperatures possibly caused by a reaction with a chemisorbed oxygen species through an ER type mechanism. This would have represented an alternate or competitive pathway to the dehydrocyclisation mechanism leading to the formation of C8 aromatics [11] and explained the decrease in selectivity towards these compounds above 450 °C. No C8 oxygenates were detected in the product stream of the 9-COP catalyst (Figure 4.37). The decrease in selectivity towards all other products observed as a function of increased temperature, corresponded to an increase in octenes selectivity (Figure 4.37), of which the trans-2-octene isomer dominated. This could have been due to a combination of the rapid desorption of these octenes as discussed previously and the relatively high thermodynamic stability of geometric trans alkene isomers when compared to their cis-isomer counterparts [12, 19]. In terms of octene isomers, 2-octenes showed the highest selectivity, followed by 3-octene, 1-octene and lastly 4-octene. This trend was observed for all the iron modified HAp catalysts.

4.5.3 Yields of value added products

Octenes, C8 aromatics and C8 oxygenates were the targeted value added products in this project. The results obtained from catalytic testing are summarised in Table 4.1. These results suggested that the formation of C8 value added products was favoured at lower temperatures (350 and 400 °C) and at 500 °C over the 9-COP catalyst. The iron supported on HAp catalysts showed the highest value added product yield when the 9-WET catalyst was tested at temperatures of 350, 400 and 450 °C. From the results of the iron substituted HAp catalysts tested it was evident that the 1-COP catalysts yielded the most C8 value added products at a temperature of 350 °C.

Out of the iron supported on HAp catalysts, the 9-WET catalyst showed the highest yield of value added products over the entire temperature range tested. The yield of valued added products observed for the 3-WET catalyst was also higher than that of the 1-WET catalyst. These results suggested that higher iron loadings in the iron supported on HAp catalysts favoured the formation of value added products. This may be due to the higher accessibility of the α-Fe_2O_3 active sites distributed on the surface of HAp, which would have been an inherent property of an increased iron loading. The 1-COP catalyst showed a slightly higher value added product yield at a temperature of 350 °C than the 3-COP and 9-COP catalysts.

Table 4.1: Summary of the yields of value added C8 products with varied temperature

Catalyst	**Temperature/ °C**				
	350	**400**	**450**	**500**	**550**
HAp	0.0	0.0	0.2	1.0	1.3
1-WET	3.0	3.9	4.1	5.4	5.9
3-WET	6.4	5.4	5.2	5.0	5.0
9-WET	6.3	6.3	6.4	6.0	5.7
1-COP	6.7	6.4	6.1	5.9	6.2
3-COP	3.2	3.4	5.9	5.6	5.8
9-COP	3.8	3.8	4.4	6.2	5.9

4.6 Isothermal iso-conversion of the iron (3 % by weight) modified hydroxyapatite catalysts

The 3 wt% iron supported on hydroxyapatite (HAp) and 3 wt% iron substituted HAp catalysts were investigated at iso-conversion to compare selectivity differences of the catalyst materials prepared by different wet chemical techniques. The catalysts discussed were abbreviated as the 3-WET catalyst, which represented the iron supported on HAp catalyst prepared by wet-impregnation, and the 3-COP catalyst, which represented the iron substituted HAp catalyst prepared by co-precipitation. In order to achieve an isothermal iso-conversion, the GHSV of the catalysed reactions were varied until conversions lay within a 1 mol% range of each other.

The 3-WET catalyst was studied at a GHSV of ± 6000 h^{-1} and the 3-COP catalyst at a GHSV of ± 4000 h^{-1}, both at a C:O ratio of 8:2 and a temperature of 450 °C. Variations in selectivity as a function of temperature have already been discussed and the different product classes have been elaborated on. This investigation focused on the selectivity differences between the iron modified HAp catalysts.

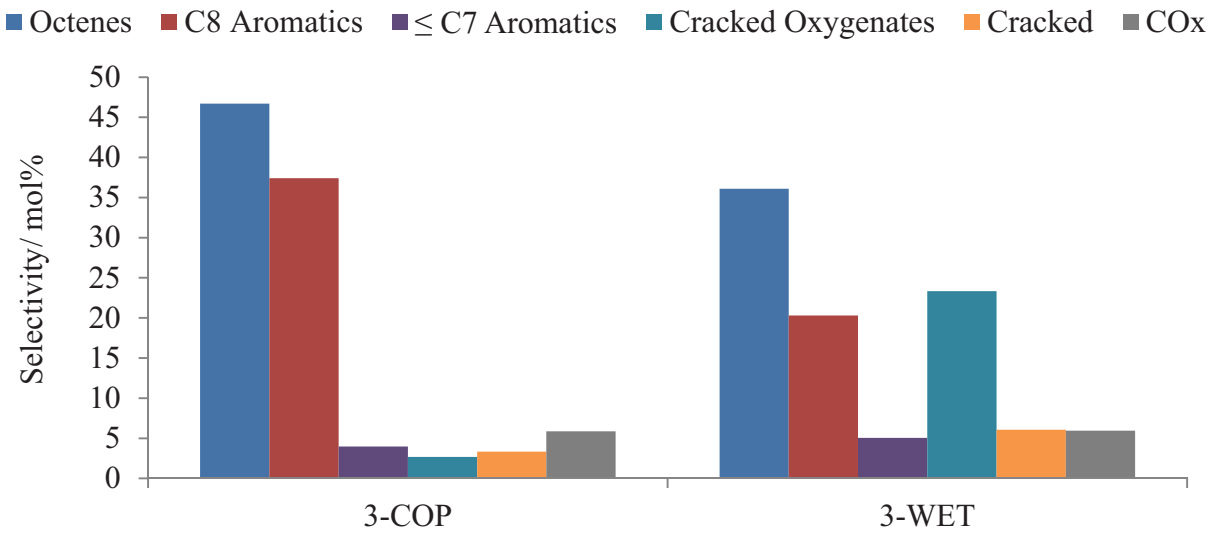

Figure 4.38: Selectivity profile at isothermal (450 °C) iso-conversion of 9 mol% over the 3-WET and the 3-COP catalysts

Octene isomers and C8 aromatics were the dominant products detected in the product streams of the 3-COP catalyst (Figure 4.38) with minor contributions from ≤ C7 aromatics, cracked products, cracked oxygenates and CO_x. The selectivity profile of the 3-WET catalyst reflected octenes, C8 aromatics and cracked oxygenates as the dominant product classes with minor contributions from ≤ C7 aromatics, cracked products and CO_x. The selectivities towards octenes and C8 aromatics observed over the 3-WET catalyst were lower than those observed for the 3-COP catalyst. This difference corresponded to an increase in the selectivity towards cracked oxygenates. This result once again suggested that octenes were the precursors for aromatics formation and the presence of reducible iron centers supported on (3-WET) or substituted into the catalyst materials (3-COP) produced an alternate reaction pathway that led to the conversion of octenes to cracked oxygenated products, which, as discussed, probably

proceeded via the formation of C8 oxygenated compounds. Another contributing factor to the greater selectivity towards C8 aromatic compounds observed over the 3-COP catalyst may be the larger pore volume of this catalyst (Table 3.5). The increase in pore volume of the HAp-like catalyst material (3-COP) seemed to enhance aromatisation of the activated octene isomers, probably through a dehydrocyclisation mechanism [11].

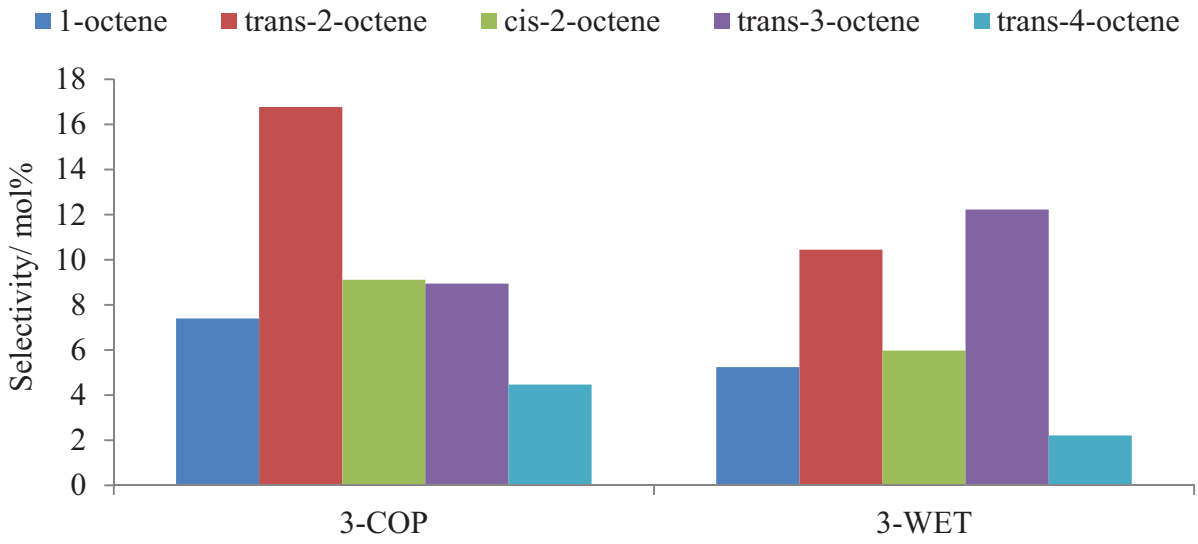

Figure 4.39: Selectivity breakdown of octenes at isothermal (450 °C) iso-converison of 9 mol% over the 3-WET and the 3-COP catalysts

The selectivity breakdown of the octene isomers (Figure 4.39) showed 2-octene to be dominant. Of the geometric isomers of 2-octene, a greater selectivity towards trans-2-octene was observed. This is most likely due to the relatively greater thermodynamic stability of trans geometric isomers when compared to their cis-isomer counterparts [12, 19]. It could be postulated that the greater thermal stability of the trans-2-octene isomer provided a driving force that pushed for its formation. Trans-3-octene selectivity showed the second highest selectivity, followed by 1-octene and lastly trans-4-octene.

Shi and Davis [11] put forward a dehydrocyclization mechanism of *n*-octane that occurred when the C_1 and C_6 or C_2 and C_7 positions were activated respectively to produce ethylbenzene or *o*-xylene. Elkhalifa *et al.* [6] proposed that the activation of *n*-octane at the C_2

and C_3 positions occurred to a greater extent than at the C_1 and C_4 positions as also observed by this system. One would not expect there to be a minimum in selectivity towards 4-octene as the energies of the C-H bonds at C_2, C_3 and C_4 are equal [19]. However a mechanism suggested by Hodnett [13] proposed that the rate determining step of *n*-alkane activation involves the homolytic cleavage of C-H bonds from the surface alkyl species with the catalyst, followed by the rapid elimination of a second hydrogen atom from a neighbouring carbon atom to form the double bond. Other mechanistic studies into the activation of *n*-octane have suggested that steric restraints may have an inhibitory effect on the accessibility of large molecules to the active sites of a catalyst's surface, thus making steric constraints a limiting factor [3, 4, 9]. Thus it may be suggested that the minimum in selectivity towards trans-4-octene, despite the greater thermodynamic stability of trans geometric isomers, could have been due to steric constraints involved with the activation of *n*-octane at the C_4 position.

The 3-COP catalyst demonstrated the highest selectivity towards octene isomers and C8 aromatics. The minimum in selectivity towards cracked oxygenates over the 3-COP catalyst suggests that activated octenes formed on the surface of this catalyst favoured the dehydrocyclisation mechanism put forward by Shi and Davis [11] as opposed to the oxygen insertion reaction which would have led to the formation of cracked oxygenated compounds. An opposite trend was observed for the 3-WET catalyst which showed a preference for an oxidative cracking type reaction pathway.

In terms of desirable value added products, C8 aromatic compounds showed the second highest selectivity. Further breakdown of the selectivity profile of C8 aromatic compounds showed ethylbenzene and styrene to be dominant (Figure 4.40). Upon closer inspection it was noted that the selectivity toward these compounds increased upon the substitution of iron into the lattice of HAp as opposed to supporting it on the surface of HAp, in the form of α-Fe_2O_3. The selectivity towards *o*-xylene over the 3-WET catalyst was slightly lower than that over the 3-COP catalyst and overall it was significantly lower than the selectivity towards ethylbenzene and styrene. It thus became apparent that the formation of ethylbenzene and styrene was comparatively favourable.

Shi and Davis [11] suggested that ethylbenzene was formed via a $C_1 \rightarrow C_6$ cyclisation mechanism and *o*-xylene via a $C_2 \rightarrow C_7$ cyclization mechanism. Further to this, Dasireddy *et al.* [3, 4] suggested that the $C_1 \rightarrow C_6$ cyclization mode consumed 1-octene to form ethylbenzene and styrene and the $C_2 \rightarrow C_7$ cyclisation mode preferentially consumed 2-octene and 3-octene to form *o*-xylene.

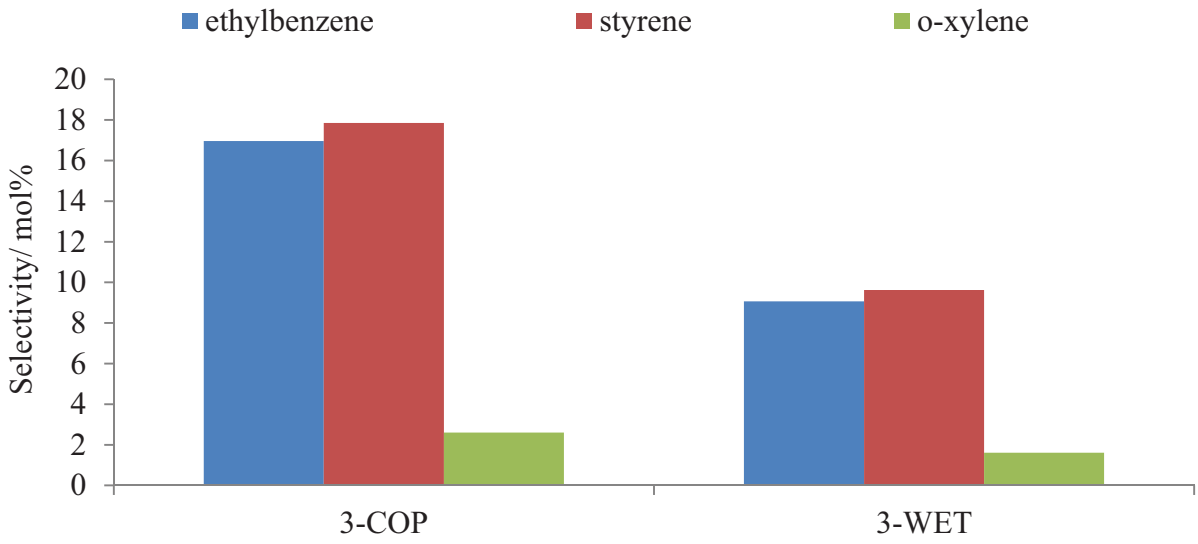

Figure 4.40: Selectivity breakdown of C8 aromatics at isothermal (450 °C) iso-converison of 9 mol% over the 3-WET and the 3-COP catalysts

This proposed mechanism supported the findings made from the results obtained in this study. The relatively low selectivity towards 1-octene corresponded to a relatively high selectivity towards ethylbenzene and styrene. This suggested that if terminal activation of *n*-octane was favored, the formed, highly reactive, 1-octene intermediate may have been consumed via the $C_1 \rightarrow C_6$ cyclisation mechanism. Also worthy of mention was the relatively high selectivity towards 2-octene and 3-octene, which as suggested, would serve as intermediates for the $C_2 \rightarrow C_7$ cyclization mode forming *o*-xylene, and the correspondingly low selectivity towards this C8 aromatic compound. From the mechanistic suggestions proposed in literature it was possible that a $C_1 \rightarrow C_6$ cyclisation mode of *n*-octane over the catalysts was favoured. Toluene was detected in trace amounts and made only a minor contribution to the $\leq$ C7 aromatic compounds group. Benzene is a particularly stable compound because of the

unusually large delocalization energy associated with its six sp^2 carbon ring structure [12]. This may have been a contributing factor to the relatively high selectivity towards benzene when compared to that of toluene. The formation of benzene and toluene could have formed through cracking of alkyl substituents of the C8 aromatic compounds formed, more specifically, the alkyl substituent of ethylbenzene or more likely styrene, which contained an activated alkenyl functional group. This process could have been influenced by geometric constraints brought on by the pore channels of the catalyst [20].

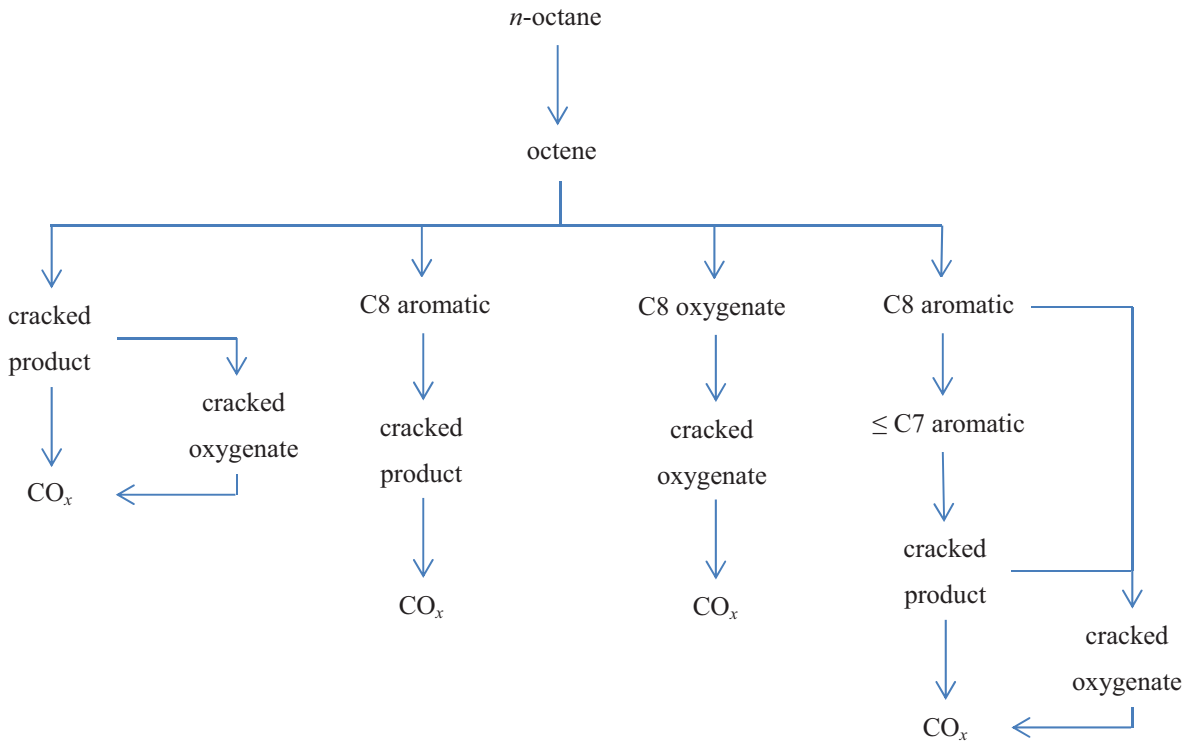

Figure 4.41: Overview of the transformation of *n*-octane over HAp and the iron modified HAps showing four possible pathways

Figures 4.41 and 4.42 represent proposed reaction pathways for the ODH of *n*-octane over the iron modified HAp catalysts. These reaction pathways are theoretical assumptions based on the selectivity profiles of all the catalysts tested. At any point the formed reaction intermediates (desired products included) may have desorbed from the catalyst surface, thus increasing their selectivity. The pathways illustrated in Figure 4.42 depict the transformation

of *n*-octane into value added C8 products. At any point in this scheme the products formed may have followed any of the pathways depicted in Figure 4.41.

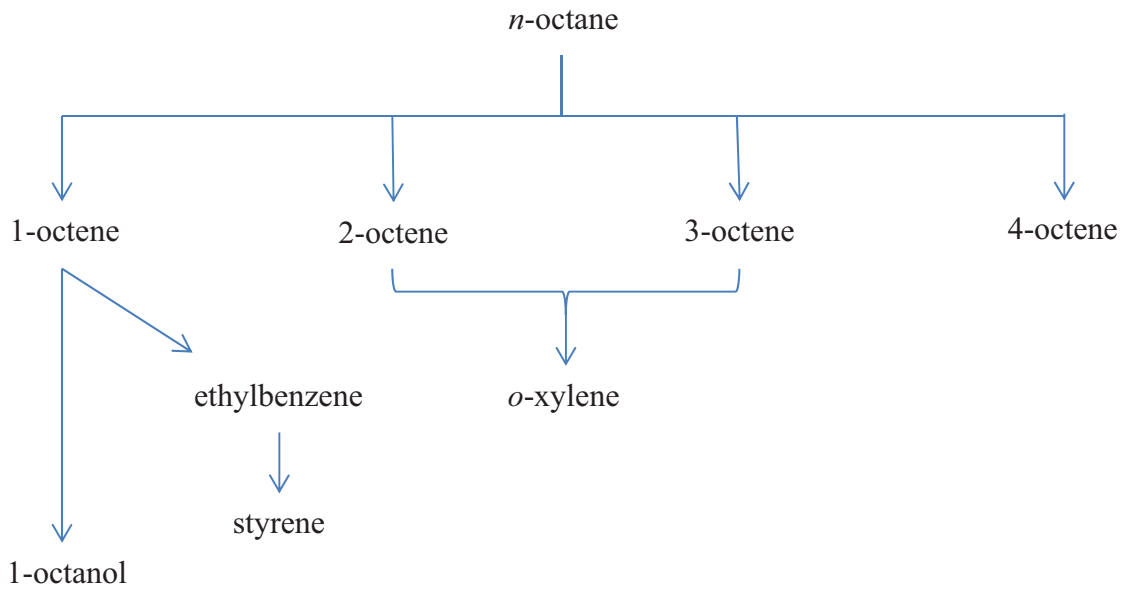

Figure 4.42: Overview of the transformation of *n*-octane into valorised C8 products over the iron modified HAp catalysts

4.7 Used catalyst characterisation

4.7.1 Powder X-ray diffraction studies

PXRD patterns of the used iron substituted and iron supported on hydroxyapatite (HAp) catalysts both showed no additional phases, thus implying that their structures remained intact and the active phases remained unchanged (Figures 4.43 and 4.44). What was observed was a decrease in the sharpness and definition of the reflections thus implying a loss in crystallinity of the powders as inferred from the broader peaks. Peak widening is an indication of an increase in the amorphous nature of a sample.

The PXRD patterns of the 3-COP and 3-WET catalysts after being subjected to reaction under a purely reducing environment (Figure 4.44), specifically, under dehydrogenation conditions, also showed no phase changes.

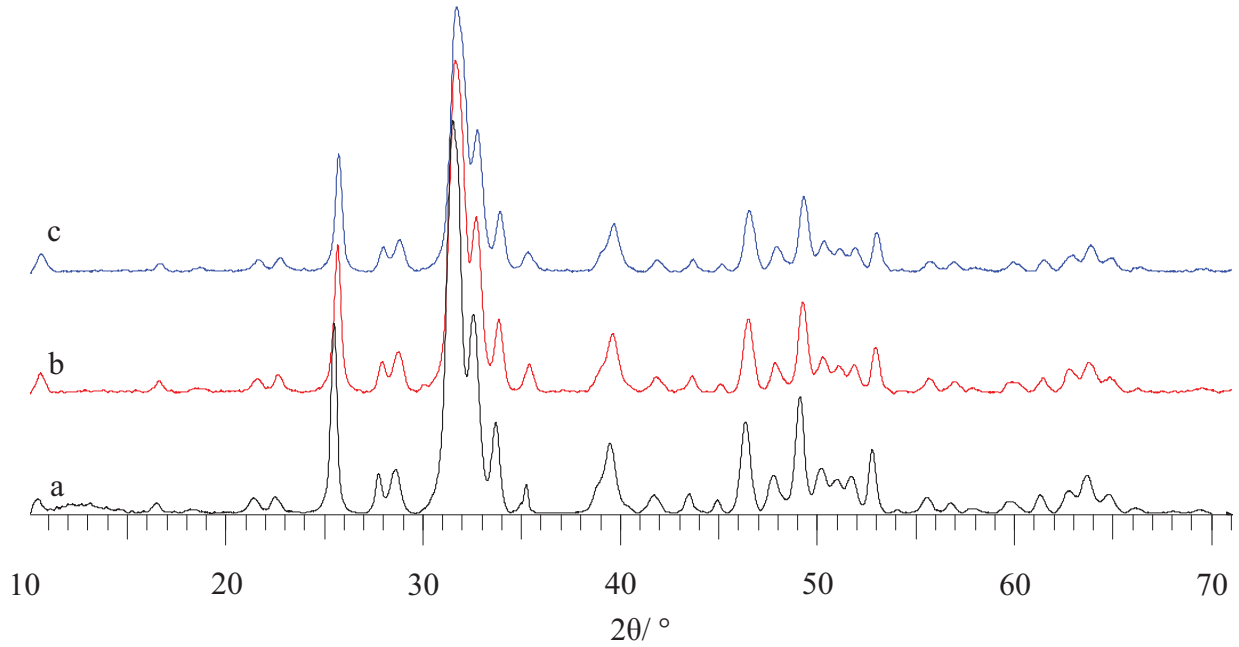

Figure 4.43: PXRD patterns of (a) HAp, (b) the 3-COP and (c) the 3-WET catalysts tested under oxidative dehydrogenation conditions

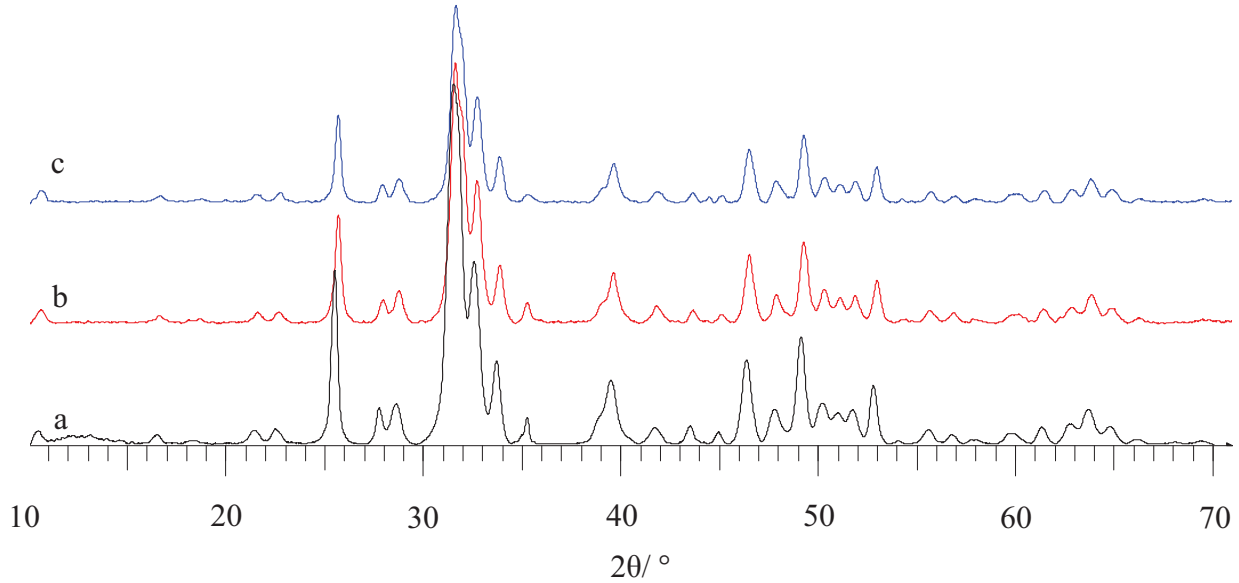

Figure 4.44: PXRD patterns of (a) HAp, (b) the 3-COP and (c) the 3-WET catalysts tested under dehydrogenation conditions

4.7.2 Nitrogen physisorption analysis

The decrease in pore volume and surface area observed in the used catalysts (Table 4.2) when compared to the fresh catalysts (Table 3.5) could have been due to the deposition of carbonaceous materials in the pores of the materials or as a result of the incessant surface changes accompanying the continuous REDOX cycle of the active phases present. Catalysts tested at C:O ratios of 8:0 (under dehydrogenation conditions) showed a greater decrease in surface area and pore volume. This could have been due to the formation of 'coke' which could be further elaborated to explain that under dehydrogenation conditions a greater amount of carbonaceous deposits remained adsorbed to the catalyst surface, thus causing blockage of the narrow pores along the surface of these materials, making them less accessible to N_2 molecules, thus having resulted in the decreased BET measurements. These results suggested that oxidative dehydrogenation (ODH) conditions reduce the tendency of coke formation, possibly due to the reaction of these carbonaceous deposits with gaseous or chemisorbed oxygen and their subsequent desorption.

Table 4.2: BET surface area, pore volume and pore size of used catalysts tested at a GHSV of 6000 h^{-1} and varying carbon to oxygen (C:O) ratios

Catalyst	**C:O ratio tested**	**Surface Area/ m^2 g^{-1}**	**Pore volume/ cm^3 g^{-1}**
HAp	8:0	65	0.27
HAp	8:2	67	0.29
1-COP	8:2	72	0.31
3-COP	8:0	58	0.29
3-COP	8:2	58	0.36
9-COP	8:2	71	0.38
1-WET	8:2	59	0.26
3-WET	8:0	55	0.24
3-WET	8:2	57	0.22
9-WET	8:2	48	0.23

4.7.3 Fourier transform infrared spectroscopy

No additional bands corresponding to carbonaceous deposits were detected on the catalyst materials post reaction after cooling to room temperature. This could have been due to a relatively low amount of these deposited throughout the surface of the materials, thus being below the instruments limit of detection. Correspondingly there were no observed changes in the characteristic functional groups of the catalysts. This suggested that they were stable under the conditions tested and retained their structure.

4.7.4 Electron microscopy

Transmission electron microscopy

Transmission electron microscopy (TEM) images of the used catalysts showed no significant changes to the catalyst materials (Figures 4.45 and 4.46)

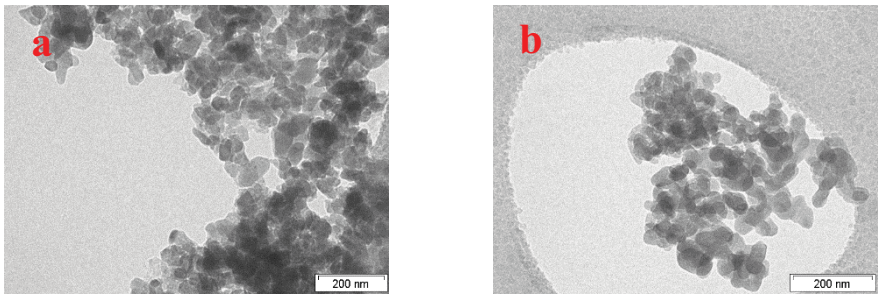

Figure 4.45: TEM images of the used (a) 3-COP catalyst tested under dehydrogenation conditions and (b) 3-COP catalyst tested under oxidative dehydrogenation conditions

A slight deformation of the hexagonally rod shaped particles was observed and related to the loss in crystallinity observed from the PXRD patterns of these powdered catalysts. The loss in crystallinity was observed to have occurred to a greater extent in the catalyst materials tested under dehydrogenation conditions. This could have been due to the continuous reduction of the active metal species.

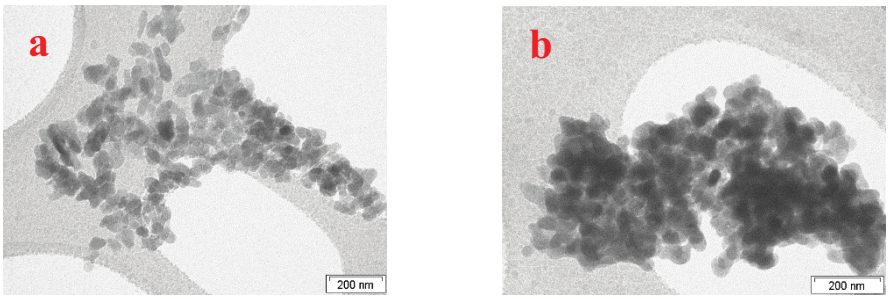

Figure 4.46: TEM images of the used (a) 3-WET catalyst tested under dehydrogenation conditions and (b) 3-WET catalyst tested under oxidative dehydrogenation conditions

Scanning electron microscopy

Scanning electron microscopy (SEM) images illustrated changes in the surface morphology of the catalysts after catalytic testing.

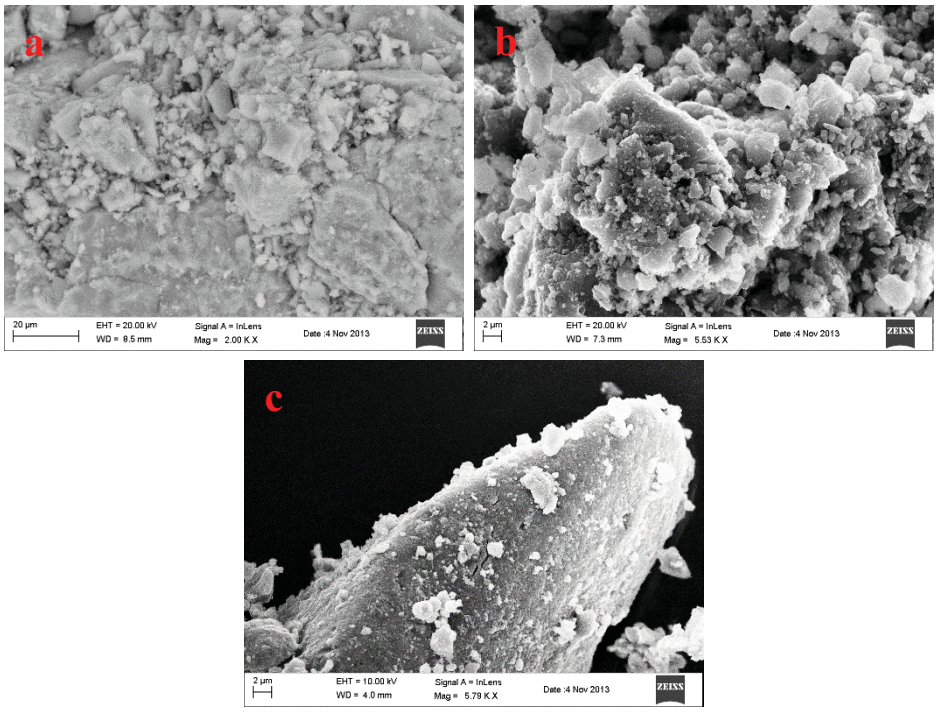

Figure 4.47: SEM images of the used (a) HAp, (b) 9-COP catalyst and (c) 9-WET catalysts tested under oxidative dehydrogenation conditions

The images discussed were captured after reaction and cooling down of the pelletized powders to room temperature. The morphological changes in the catalyst surface may have been due to the REDOX cycle of the active metals, or the presence of vaporized water (H_2O) in the reactor tube as a result of combustion, or the exothermic nature of the reactions.

References

[1] H.B. Friedrich, A.S. Mahomed, Applied Catalysis A: General 347 (2008) 11-22.

[2] N. Govender, Compartive study of mixed metal oxide catalysts for the oxidation of C4, C6 and C8 linear alkanes, PhD Thesis, College of Agriculture, Engineering and Science, University of KwaZulu-Natal, Durban, 2007, p. 325.

[3] V.D.B.C. Dasireddy, S. Singh, H.B. Friedrich, Applied Catalysis A: General 421–422 (2012) 58-69.

[4] V.D.B.C. Dasireddy, S. Singh, H.B. Friedrich, Applied Catalysis A: General 456 (2013) 105-117.

[5] E.A. Elkhalifa, On the activation of *n*-octane using vanadium-magnesium oxide catalysts, PhD Thesis, College of Agriculture, Engineering and Science, University of KwaZulu-Natal, Durban, 2010, p. 198.

[6] E.A. Elkhalifa, H.B. Friedrich, Applied Catalysis A: General 373 (2010) 122-131.

[7] E.A. Elkhalifa, H.B. Friedrich, Catalysis Letters 141 (2011) 554-564.

[8] M. Baldi, V.S. Escribano, J.M.G. Amores, F. Milella, G. Busca, Applied Catalysis B: Environmental 17 (1998) L175-L182.

[9] V.D.B.C. Dasireddy, H.B. Friedrich, S. Singh, Applied Catalysis A: General 467 (2013) 142-153.

[10] F.G.E. Nogueira, J.H. Lopes, A.C. Silva, R.M. Lago, J.D. Fabris, L.C.A. Oliveira, Applied Clay Science 51 (2011) 385-389.

[11] B. Shi, B.H. Davis, Journal of Catalysis 157 (1995) 626-630.

[12] P.Y. Bruice, Organic Chemistry, fifth ed., Pearson Prentice Hall, New Jersey, 2007.

[13] B.K. Hodnett, Heterogeneous Catalysis Oxidation: Fundamental and Technological Aspects of the Selective and Total Oxidation of Organic Compounds, Wiley-VCH, 2000.

[14] M. Khachani, M. Kacimi, A. Ensuque, J.-Y. Piquemal, C. Connan, F. Bozon-Verduraz, M. Ziyad, Applied Catalysis A: General 388 (2010) 113-123.

[15] D.D. Eley, E.K. Rideal, Nature 146 (1946) 401.

[16] P. Mars, D.W. van Krevelen, Chemical Engineering Science 3, Supplement 1 (1954) 41-59.

[17] N. Mimura, M. Saito, Catalysis Today 55 (2000) 173-178.

[18] H.H. Kung, M.C. Kung, in: D.D. Eley, H. Pines, B.W. Paul (Eds.), Advances in Catalysis, Academic Press, 1985, pp. 159-198.

[19] R.T. Morrison, R.N. Boyd, Organic Chemistry, Sixth ed., Prentice Hall, New Jersey, 1992.

[20] S. Jongpatiwut, P. Sackamduang, T. Rirksomboon, S. Osuwan, D.E. Resasco, Journal of Catalysis 218 (2003) 1-11.

Chapter 5
Summary and Conclusions

With over 1 million tons of medium chain length linear alkanes being produced per annum, much of this as by-products from coal-to-liquid and gas-to-liquid plants in South Africa alone, the activation of these relatively unreactive alkanes has gained increasing attention over recent years, especially with respect to medium chain alkanes like *n*-octane. Hydroxyapatite (HAp), as a support, has been investigated in the oxidative activation of *n*-octane and has been shown to produce carbon oxides and cracked products, with minor contributions from octene isomers [1]. The low price, ease of acquirement and environmentally benign nature of iron metal has made it an excellent alternative to precious metals used in catalysis [2]. There has been an increase in the number of iron catalysed reactions reported. Khachani *et al*. [3] have investigated the applications of iron exchanged HAp catalysts in the oxidative dehydrogenation (ODH) of propane showing good conversion with high selectivity towards propylene. It is for these reasons, amongst others, that it was decided to synthesise and test iron supported on HAp and iron substituted HAp catalysts in the oxidative activation of *n*-octane.

HAp and the iron substituted HAp (COP) catalysts were prepared by a co-precipitation technique. The iron supported on HAp (WET) catalysts were prepared by a single step wet impregnation synthesis. Elemental analysis of HAp and the iron modified HAp (prepared with varied weight percentages, wt%, of iron) catalysts showed a calcium deficiency. The COP catalysts showed a greater variation in Ca/P molar ratio. This was attributed to distortions induced into the structural lattice of these HAp-like materials caused by the substitution of calcium with iron cations. Powder X-ray diffraction (PXRD) analysis of the 9 wt% iron (9-WET) catalyst showed an additional phase corresponding to hematite, α-Fe_2O_3. The absence of this phase or any iron containing phase in the PXRD patterns of the COP catalysts suggested that calcium was substituted with iron cations, thus forming a HAp-like material. Fourier transform infrared spectroscopy (FTIR) and Raman spectroscopy were used to

confirm the presence of the characteristic functional groups of HAp. Further support of the substitution of calcium with iron cations in the catalysts prepared by the co-precipitation method (COP catalysts) was provided by the Raman spectra of these catalyst materials. A shift in the phosphate bands was observed concomitant with changes in the intratetrahedral bond distances of the tetrahedral PO_4^{3-} present in the crystalline lattice of the HAp-like materials. Nitrogen physisorption analysis showed a decrease in the surface area and pore volume of the WET catalysts with an increase in iron wt%, caused by the presence of α-Fe_2O_3 distributed on the surface of the support which led to pore blockage. The COP catalysts showed an increase in surface area and pore volume with an increase in iron wt%. This was due to changes in the pore structure of the HAp-like materials caused by distortions in the crystalline lattice upon substitution of calcium cations with iron cations.

Transmission electron microscopy (TEM) images showed that the hexagonal structure of HAp was retained after supporting iron on the surface of HAp and slightly distorted when substitution of calcium cations with iron cations was carried out. The latter was in accordance with the loss in crystallinity of the COP catalysts with an increase in iron weight percentage observed from the PXRD patterns and the Raman spectra of the iron substituted HAp catalysts

Scanning electron microscopy and energy dispersive X-ray spectroscopy (SEM and EDX respectively) analysis of HAp and the 9 wt% iron modified catalysts showed iron distributed throughout the surface of HAp for the WET catalyst and iron distributed throughout the particles of the COP catalyst. Temperature programmed reduction (TPR) and oxidation were used to investigate the REDOX nature of the iron species present in the catalysts. TPR analysis of the iron supported on HAp catalysts showed reduction properties similar to that of α-Fe_2O_3 observed in literature [4-7]. TPR analysis of the iron substituted HAp catalysts showed reduction patterns of the Fe^{3+} species substituted throughout the lattice of the HAp-like catalyst material. An increase in iron loading for the WET catalysts demonstrated a greater degree of reducibility, thus having led to greater conversions when compared to the COP catalysts of the same iron weight percentage. The highest conversion was observed over the 9 wt% iron supported on HAp (9-WET) catalyst. Temperature programmed CO_2

desorption (CO_2-TPD) analysis showed that the iron substituted HAp catalysts had the strongest basicity, followed by the iron supported on HAp catalysts and then HAp.

The partial oxidation of *n*-octane over HAp showed carbon oxides (CO_x) to be the dominant products produced over the temperature range tested (350 – 550 °C). The second highest selectivity observed was that of cracked products, which showed an increase in selectivity as a function of temperature. A minor contribution from octenes, which were considered one of the classes of value added C8 products, was observed from 450 °C onwards. The partial oxidation of *n*-octane over the iron modified HAp catalysts showed an increase in conversion and selectivity towards value added C8 products (octenes, C8 aromatics and C8 oxygenates) at all the temperatures tested. Other products formed from the ODH reactions included cracked products, cracked oxygenates, ≤ C7 aromatics and CO_x. The main products produced included octenes, C8 aromatics and cracked oxygenates. 2-Octenes were the dominant isomers with 4-octene having showed the lowest selectivity. Of the geometric isomers of octene, the trans configurations were favoured. Ethylbenzene and styrene were the dominant C8 aromatics formed. Albeit by an almost insignificant difference, styrene selectivity was slightly higher than ethylbenzene in accordance with the unique dehydrogenation ability of iron which has led to the implementation of potassium promoted iron oxides in the commercial dehydrogenation of ethylbenzene to styrene [8, 9].

The performance of these catalysts was found to be sensitive to reaction conditions. As observed, lower gas hourly space velocity (GHSV) favoured oxygen functionalisation and cracking, producing high yields of cracked oxygenated products. At higher GHSV, a greater selectivity towards valorised C8 products, viz. octenes and C8 aromatics was observed. However this was at the expense of conversion. The carbon to oxygen molar ratios played a significant role in catalyst performance. These catalysts performed better under oxygen deficient conditions which minimised oxidative cracking and also led to an increase in conversion at higher temperature.

An increase in iron wt% of the iron supported on HAp catalysts seemed to have favoured the formation of cracked oxygenated products. The tendency towards cracked oxygenates

formation was lower for the iron substituted HAps, possibly because of an increased basicity at the surface of the material due to the stabilisation of O^{2-} species within the structuaral channels of the HAp-like materials. This could have influenced the rapid desorption of formed octenes, thus increasing their selectivity and consequently reducing the selectivity towards cracked oxygenates. It was assumed that the reaction pathways occurred via a Mars and van Krevelen (MvK) mechanism which was responsible for the formation of octenes and C8 aromatics (value added products) and an Eley-Rideal (ER) mechanism responsible for the formation of oxygenated products (value added C8 oxygenates included).

References

[1] V.D.B.C. Dasireddy, S. Singh, H.B. Friedrich, Applied Catalysis A: General 421–422 (2012) 58-69.

[2] S.-F. Zhu, Y. Cai, H.-X. Mao, J.-H. Xie, Q.-L. Zhou, Nature Chemistry 2 (2010) 546-551.

[3] M. Khachani, M. Kacimi, A. Ensuque, J.-Y. Piquemal, C. Connan, F. Bozon-Verduraz, M. Ziyad, Applied Catalysis A: General 388 (2010) 113-123.

[4] J. Zieliński, I. Zglinicka, L. Znak, Z. Kaszkur, Applied Catalysis A: General 381 (2010) 191-196.

[5] M.M. Hossain, L. Atanda, N. Al-Yassir, S. Al-Khattaf, Chemical Engineering Journal 207-208 (2012) 308-321.

[6] X. Zhang, G. Dou, Z. Wang, L. Li, Y. Wang, H. Wang, Z. Hao, Journal of Hazardous Materials 260 (2013) 104-111.

[7] A. Basińska, W.K. Jóźwiak, J. Góralski, F. Domka, Applied Catalysis A: General 190 (2000) 107-115.

[8] N. Mimura, M. Saito, Catalysis Today 55 (2000) 173-178.

[9] R. Iezzi, D. Sanfilippo, Process for the dehydrogenation of ethylbenzene to styrene, Google Patents, 2005.

Chapter 6

Motivation and Plan for Future Work

With the number of coal-to-liquid and gas-to-liquid plants increasing world-wide, the world production of linear alkanes (produced as by-products from these plants) is expected to rise enormously [1]. These cheap and easily available alkanes seem like suitable substitutes for alkene and aromatic feed-stock and valuable oxygenated compounds [2, 3]. The dehydrogenation of alkanes for the production of alkenes and, if desired, their functionalisation is of great importance in the petrochemical industry. Until recently the commercial production of alkenes occurred to a large extent through the dehydrogenation of alkanes in the absence of oxygen. The oxidative dehydrogenation (ODH) of alkanes using oxygen as an oxidant reduces the limitations brought on by the thermodynamic restraints of these endothermic dehydrogenation reactions, in addition to lowering carbon deposition on the active sites of the catalysts. This in turn eliminates decoking shutdowns. Furthermore, the use of alkanes as feed-stock allows for the development of new processes with lower environmental impact and more economic viability [4].

The use of a support or carrier with adjustable acid-base properties is advantageous in an ODH process, as the selectivity may be varied by altering the acid-base characteristics of the catalyst. Calcium hydroxyapatite (HAp) is a mineral found in the form of calcium apatite. It is a bi-functional material with acidic or basic properties that depend on its composition. The adjustable acid-base properties together with its high stability and the various substitutions allowed by the apatite structure make HAp an ideal active metal carrier or support for the ODH process.

The powder X-ray diffraction (PXRD) pattern and the Fourier transform infrared (FTIR) spectrum of the 9 wt% iron supported on and substituted HAp (9-WET and 9-COP respectively) catalysts suggested that the HAp structure of the materials were retained. An additional phase corresponding to iron oxide (hematite, α-Fe_2O_3) was observed for the 9-WET catalyst. The shift in the position of the characteristic PO_4^{3-} bands of HAp in the Raman spectrum of the 9-COP catalyst confirmed that calcium cations were substituted with iron cations in the HAp lattice [5,

6]. The shift in the position of the Raman bands also suggested that distortions in the HAp lattice were induced as a result of iron substitution. From the Raman spectrum of the 9-WET catalyst, there was no observable shift in the position of the characteristic PO_4^{3-} bands. The 9-COP catalyst showed a higher surface area (86 m^2 g^{-1}) than HAp (69 m^2 g^{-1}), while the 9-WET catalyst showed a lower surface area (56 m^2 g^{-1}). The increase in the surface area of the 9-COP catalyst was attributed to a change in the pore structure, and thus pore volume, influenced by the lattice distortion. The decrease in surface area for the 9-WET catalyst was an effect of pore blockage, influenced by supporting α-Fe_2O_3 on the surface of HAp. Both catalysts displayed a hysteresis loop characteristic of a type IV (IUPAC) isotherm, demonstrating its mesoporous nature [7]. Transmission electron microscopy (TEM) images showed the particles existing as deformed hexagonal rods, between 90 – 150 nm in length for the 9-COP catalyst, and 70 – 100 nm in length for the 9-WET catalyst. Scanning electron microscopy and energy dispersive X-ray spectroscopy (SEM and EDX) mapping of the 9-COP catalyst illustrated the distribution of calcium, phosphorus and iron throughout the particles investigated. The 9-WET catalyst showed an even distribution of calcium and phosphorus throughout the particles investigated with iron distributed on the surface. Two distinct peaks were observed in the temperature programmed reduction (TPR) profile of the 9-COP catalyst. Calcium(II) ions were not reduced under the conditions investigated, thus the peaks were attributed to the iron species present. The TPR profile of the 9-WET catalyst showed three peaks, attributed to the reduction of the α-Fe_2O_3 phase. The reducible nature of the catalyst suggested that it could function as an ODH catalyst. Subsequent reduction, oxidation and reduction studies suggested that the iron species present in the catalysts could undergo a reduction and oxidation (REDOX) cycle, thus confirming that they could be used as ODH catalysts. To gain insight on the oxidation state of the iron modified HAp catalysts and their behaviour under REDOX conditions, the catalysts are currently being studied using Mössbauer and *in situ* Mössbauer spectroscopy.

The ODH reactions were carried out in a continuous flow fixed-bed reactor, operated in a down-flow mode. Carbon oxides (CO_x) were the dominant product formed in the ODH of *n*-octane over HAp. Octene isomers, aromatics and oxygenates were the dominant products formed in the ODH of *n*-octane using the 9-COP and 9-WET catalysts. At a temperature of 500 °C, HAp showed an octene isomer selectivity of 17 mol% with a conversion of 6 mol %. The CO_x

selectivity of the HAp catalyst was 54 mol% at this temperature. At 500 °C, the 9-WET catalyst demonstrated a 23 mol% selectivity towards octene isomers at a conversion of 16 mol%. The dominant product class observed at this temperature was cracked oxygenated products with a selectivity of 49 mol%. The 9-COP catalyst showed an octene isomer selectivity of 56 mol% and conversion of 8 mol% at a temperature of 500 °C. The selectivity towards CO_x observed for both the 9-WET and 9-COP catalysts at this temperature was less than 5 mol%.

This research effort showed that both the 9-COP and 9-WET catalysts demonstrated improved oxidative dehydrogenation ability and reduced CO_x formation when tested in the ODH of *n*-octane when compared to the performance of HAp under the same conditions. The 9-COP catalyst, however, showed a greater yield of octene isomers (4.5 %) than the 9-WET catalyst (3.7 %). Thus the 9-COP catalyst was chosen to investigate the iron modified catalyst systems further.

The use of iron exchanged HAp catalysts in the ODH of propane has been discussed by Khachani *et al*. [8]. Their research effort has been discussed in detail in Chapter 1. There are several more articles that discuss the activation of light alkanes using metal ion substituted and modified HAp catalysts. Sugiyama *et al*. [9] investigated the effects of gas and solid phase additives on the ODH of propane on strontium hydroxyapatite (Sr-HAp) and barium hydroxyapatite (Ba-HAp) catalysts. They found that the activity of the Sr-HAp catalysts was higher than the Ba-HAp. Treatment of the Sr-HAp and Ba-HAp catalysts with lead, led to a decrease in propylene yield. The treatment of the catalysts with copper, led to improved activity. In particular the treatment of the Sr-HAp catalyst with Cu^{2+} gave a conversion of 16 mol% with a propylene selectivity of 80 mol%. Elkabouss *et al*. [10] used cobalt exchanged HAp catalysts in the ODH of ethane. They found that the yield of ethylene reached a maximum of 22 mol% for a 0.96 wt% Co exchanged HAp catalyst at 550 °C. This result was attributed to two reasons, one being the partial compensation of the intrinsic dehydrogenation ability of Co and a decrease in the basicity of HAp induced by the exchange of Ca^{2+} with Co^{2+}. The other being the involvement of the two types of sites. Singh and Jonnalagadda [11] experimented with the selective oxidation of *n*-pentane and *n*-hexane on HAp and a series of HAp-like materials containing Co, Fe or Sr, synthesised using a co-precipitation technique. Conversion and selectivity were largely

influenced by changes in the temperature and gas flow rates. The selective oxidation of *n*-pentane produced a range of products including cracked products, oxygenated compounds, carbon oxides, 1,3-pentadiene, furan and furfural. The selective oxidation of *n*-hexane yielded hexene isomers and aromatic compounds. These research efforts have shown that metal substituted HAp and HAp-like materials behave as selective catalysts with good activity in the activation of light alkanes. With the results of these investigations and of the iron substituted HAp catalysts investigated in this study considered, it was decided that a series of iron substituted magnesium hydroxyapatite (Mg-HAp), Sr-HAp and Ba-HAp catalysts, with varied iron wt%, are going to be prepared using the co-precipitation technique discussed in Chapter 2. The activation of *n*-octane and *n*-decane are going to be investigated using these catalyst materials. In addition to the characterisation techniques used in this study, temperature programmed NH_3 desorption (NH_3-TPD) investigations are to be conducted using each of the catalysts to determine the variation of the acid-base nature of the catalysts and its influence on catalytic performance. Mechanistic and kinetic studies are also going to be carried out to fully understand the activity of these catalysts in the ODH of heavier alkanes.

The future work of this study aims to investigate the catalytic performance of iron modified Mg-HAp, Sr-HAp and Ba-HAp catalysts with different iron loadings in the ODH of *n*-octane and *n*-decane. The use of these iron modified catalyst materials has not been reported to date.

The study of vanadium catalysts is by far one of the most extensively researched topics in heterogeneous catalysis, following their application in the oxidation of *n*-butane to maleic anhydride on an industrial scale. In literature, many papers discuss the results of vanadium catalyst systems and the application of these in the oxidation of light alkanes. A review by Blasco *et al*. [12] covered the effects of the distribution of vanadium on various supports and their acid-base characteristics, also paying attention to the reducibility and structure of surface vanadium oxide species. Other important factors discussed were the aggregation state of the surface vanadium species and the coordination number of these. Research into VMgO catalysts in the ODH of light alkanes showed that the size of the reactant and the dispersion of the active sites had a direct impact on the selectivity of the ODH products [12, 13]. Total oxidation was found to occur when larger molecules reacted simultaneously with adjacent active sights as

opposed to using smaller molecules or reacting with isolated active sites. The re-oxidation of VMgO catalysts used in the oxidation of propane was found to be the rate limiting step [14]. Also higher reaction temperatures accelerate REDOX exchanges and enhance catalytic activity in the activation of *n*-butane [14]. Thus the rate at which redox processes occur were found to have a direct influence on catalytic activity. Friedrich and co-workers have also investigated the activation of light alkanes on vanadium catalysts [2, 15-18]. Their work has been discussed in Chapter 1. Sugiyama *et al*. [19] investigated the use of vanadate substituted HAp catalysts in the ODH of propane. Their work showed that phosphate groups in the HAp lattice could not be fully replaced, instead partial substitution was achieved at a V/P atomic ratio of 0.15. The conversion and propylene selectivity of HAp was found to be 5.9 and 1.4 mol% respectively. A vanadate substituted HAp catalyst with a V/P atomic ratio of 0.10 gave a propylene selectivity of 54.2 mol% at a conversion of 16.5 mol% under the same conditions. Recent work by Dasireddy *et al*. [20-22] discussed the use of vanadium supported on HAp, Mg-HAp, Sr-HAp and Ba-HAp catalysts in the activation of *n*-octane. Their work has been discussed at length in Chapter 1. To date no literature exists on the use of vanadium supported on iron substituted HAp catalysts in the ODH of heavier alkanes. Thus the synthesis and testing of these catalyst systems in the activation of *n*-octane and *n*-decane will also form part of the future work plan of this project.

References

[1] H.B. Friedrich, A.S. Mahomed, Applied Catalysis A: General 347 (2008) 11-22.

[2] H.B. Friedrich, N. Govender, M.R. Mathebula, Applied Catalysis A: General 297 (2006) 81-89.

[3] F. Cavani, F. Trifirò, Catalysis Today 51 (1999) 561-580.

[4] G. Centi, F. Cavani, F. Trifirò, Selective Oxidation by Heterogeneous Catalysis, Springer USA, 2001.

[5] S. Zhai, M. Kanzaki, T. Katsura, E. Ito, Materials Chemistry and Physics 120 (2010) 348-350.

[6] R. Cusco, F. Guitian, S. de Aza, L. Artus, Journal of the European Ceramic Society 18 (1998) 1301 - 1305.

[7] Y. Kamiya, E. Nishikawa, A. Satsuma, M. Yoshimune, T. Okuhara, Microporous and Mesoporous Materials 54 (2002) 277-283.

[8] M. Khachani, M. Kacimi, A. Ensuque, J.-Y. Piquemal, C. Connan, F. Bozon-Verduraz, M. Ziyad, Applied Catalysis A: General 388 (2010) 113-123.

[9] S. Sugiyama, T. Shono, E. Nitta, H. Hayashi, Applied Catalysis A: General 211 (2001) 123-130.

[10] K. Elkabouss, M. Kacimi, M. Ziyaad, S. Ammar, F. Bozon-Verduraz, Journal of Catalysis 226 (2004) 16-24.

[11] S. Singh, S.B. Jonnalagadda, Bulletin of the Chemical Society of Ethiopia 27 (2013) 57-68.

[12] T. Blasco, J.M. López-Nieto, Applied Catalysis A: General 157 (1997) 117-142.

[13] J.M. López-Nieto, A. Corma, N. Paredes, A. Dejoz, M.I. Vazquez, in: V. Cortes Corberan, S.V. Bellom (Eds.), New Developments in Selective Oxidation, 1994, pp. 113-123.

[14] J.M. López-Nieto, J. Soler, P. Concepción, J. Herguido, M. Menéndez, J. Santamaría, Journal of Catalysis 185 (1999) 324-332.

[15] N. Govender, H.B. Friedrich, M.J. van Vuuren, Catalysis Today 97 (2004) 315-324.

[16] B. Pillay, M.R. Mathebula, H.B. Friedrich, Catalysis Letters 141 (2011) 1297-1304.

[17] B. Pillay, M.R. Mathebula, H.B. Friedrich, Applied Catalysis A: General 361 (2009) 57-64.

[18] T. Naicker, H.B. Friedrich, Journal of Porous Materials 20 (2013) 763-775.

[19] S. Sugiyama, T. Osaka, Y. Hirata, K.-I. Sotowa, Applied Catalysis A: General 312 (2006) 52-58.

[20] V.D.B.C. Dasireddy, S. Singh, H.B. Friedrich, Applied Catalysis A: General 456 (2013) 105-117.

[21] V.D.B.C. Dasireddy, S. Singh, H.B. Friedrich, Applied Catalysis A: General 421–422 (2012) 58-69.

[22] V.D.B.C. Dasireddy, H.B. Friedrich, S. Singh, Applied Catalysis A: General 467 (2013) 142-153.

Appendix A

Table A1: Summary of gas flow rates employed to attain GHSV and C:O ratios in testing

GHSV/ h^{-1}	C:O	*n*-octane/ mL min^{-1}	N_2/ mL min^{-1}	air/ mL min^{-1}	% *n*-octane
4000	8:2	0.05	31	36.5	11.4
6000	8:0	0.07	89	-	10.8
6000	8:2	0.07	46	51.1	11.0
6000	8:4	0.07	10	102.1	10.6
6000	8:6	0.06	0	131.3	8.2
8000	8:2	0.08	44	58.4	12.0

Copy of Spread Sheet

1-COP

C:O			8:2		
GHSV			6000		
Temperature °C (bed)	350	400	450	500	550
Time (hours)	1	1	1	1	1
Mass octane (initial)	2.59	2.59	2.59	2.59	2.59
Mass octane (final)	0.00	0.00	0.00	0.00	0.00
Mass of Octane in	2.59	2.59	2.59	2.59	2.59
Moles of Octane in	0.023	0.023	0.023	0.023	0.023
Moles of carbon in	0.181	0.181	0.181	0.181	0.181
Out gas (initial)	7344.9	7355.4	7364.5	7373.7	7382.3
Out gas (final)	7349.3	7359.7	7368.7	7377.8	7386.4
Out gas flow/ L	4.390	4.310	4.180	4.100	4.040
out gas flow/ mL	4390.0	4310.0	4180.0	4100.0	4040.0
Total mass of liquid	2.763	2.764	2.812	2.750	2.772
Mass Organic layer	2.497	2.493	2.491	2.454	2.471
Mass Aqueous layer	0.266	0.271	0.321	0.296	0.301
% water in Organic	0.000	0.000	0.000	0.000	0.000
% water in Aqeous	90.00	90.00	90.00	90.00	90.00
Actual mass organic	2.497	2.493	2.491	2.454	2.471
Actual mass aqeous	0.027	0.027	0.032	0.030	0.030
moles of water	0.001	0.002	0.002	0.002	0.002
Moles Octane in	0.023	0.023	0.023	0.023	0.023
Moles Octane out	0.021	0.021	0.021	0.021	0.021
Conversion/ mol%	8.722	9.012	8.462	8.508	8.465
Moles Carbon in	0.181	0.181	0.181	0.181	0.181
Moles Carbon out	0.177	0.177	0.177	0.174	0.175
Carbon balance	97.41	97.39	97.44	95.93	96.57

Selectivity of Product (mol%)	Temperature/ °C (bed)				
	350	400	450	500	550
Methane	0.01	0.02	0.01	0.01	0.04
Ethane/Ethylene	0.11	0.13	0.05	0.04	0.12
Propane/Propylene	1.19	1.29	0.64	0.53	1.19
Methanol	5.40	2.41	1.54	0.00	0.00
Butane	3.04	3.43	1.67	1.48	2.82
Ethanol	0.00	0.00	0.00	0.00	0.00
Acetone	2.82	7.42	12.51	18.54	16.24
2-Propanol	0.66	0.95	0.61	0.66	0.36
Pentane	0.02	0.02	0.02	0.01	0.02
Pentene isomers	0.07	0.08	0.04	0.04	0.07
Hexane	1.77	2.71	1.83	1.31	1.92
Hexene isomers	0.03	0.02	0.01	0.00	0.02
Heptane	1.07	1.45	1.29	1.27	0.02
Heptene isomers	0.00	0.00	0.00	0.00	0.00
n-Octane	1412.96	1341.72	1506.59	2011.71	1730.76
1-Octene	9.77	8.02	10.46	7.88	9.74
Trans-2-octene	15.79	15.02	15.17	14.79	14.38
2-Octene, cis+ trans	9.81	9.19	9.19	8.77	8.28
Trans-3-octene	20.90	18.61	17.90	17.07	16.40
Trans-4-octene	4.10	4.49	4.62	4.09	4.08
Eethylbenzene	0.00	0.00	0.00	0.00	0.00
Styrene	0.00	0.00	0.00	0.00	0.00
o-Xylene	0.00	0.00	0.00	0.00	0.00
Toluene	0.00	0.00	0.00	0.00	0.00
Benzene	0.00	0.00	0.00	0.00	0.00
Impurities	0.00	0.00	0.00	0.00	0.00
CO	0.00	0.00	0.00	0.00	0.00
CO_2	9.28	9.11	9.16	9.03	11.56
Total	4.75	4.91	4.37	5.46	4.86

Calibration Factors Liquid Products

Product	Carbon Number	Molar mass	Density	RRF
Methanol	1	32.04		0.3
Butane	4	58.12		1
Ethanol	2	47.08	0.801	0.5
Acetone	3	58.03	0.791	0.5
2-Propanol	3	60.03	0.785	0.5
Pentane	5	72.15	0.626	0.7
Pentene isomers	5	70.13	0.626	0.7
Hexane	6	86.18	0.659	1
Hexene isomers	6	84.16	0.678	1
Heptane	7	100.21	0.684	1
Heptene isomers	7	98.19	0.697	1
n-Octane	8	114.23	0.703	1
1-Octene	8	112.22	0.715	0.78694
Trans-2-octene	8	112.22	0.715	1.051916
2-Octene, cis+ trans	8	112.22	0.715	0.914589
Trans-3-octene	8	112.22	0.716	1.082868
Trans-4-octene	8	112.22	0.714	0.581583
Ethylbenzene	8	106.16	0.8665	0.954805
Styrene	8	104.19	0.909	0.625805
o-Xylene	8	106.16		0.863371
Toluene	7	92.14	0.87	0.8633
Benzene	6	78.11	0.87	0.8633
Cracked (RT >10)	8	75		1
Others(RT = 12-22)	8	110		1
Oxygenates(RT= 20-27)	8	128		0.9
Heavys(RT > 27)	8	140		0.8
Impurities	8	114		1

Calibration Factors Gaseous Products

Product	Carbon No	Gradient from Calibration curve
Methane	1	4.73E+12
Ethane/Ethylene	2	1.79E+13
Propene/propylene	3	2.16E+12
Methanol	1	1.78E+12
Butane	4	1.19E+12
Ethanol	2	3.53E+13
Acetone	3	4.57E+12
2-propanol	3	4.37E+12
Pentane	5	8.81E+12
Pentene isomers	5	1.00E+13
Hexane	6	1.32E+13
Hexene isomers	6	1.36E+13
Heptane	7	1.63E+13
Heptene isomers	7	1.63E+13
n-Octane	8	4.93E+14
1-octene	8	6.22E+14
Trans-2-octene	8	4.77E+14
2-Octene, cis+ trans	8	5.29E+14
Trans-3-octene	8	6.22E+14
Trans-4-octene	8	8.54E+14
Ethylbenzene	8	6.11E+14
Styrene	8	1.01E+15
o-Xylene	8	6.70E+14
Toluene	7	6.70E+14
Benzene	6	6.70E+14
Cracked (RT >10)	8	4.93E+14
Others(RT = 12-22)	8	4.93E+14
Oxygenates(RT= 20-27)	8	4.93E+14

Heavys(RT > 27)	8	4.93E+14
Impurities	1	2.90E+11
CO	1	3.36E+14
CO_2	1	3.36E+14

Gas Hourly Space Velocity

Flow rate of octane	0.07
Density of octane/ g mL^{-1}	0.703
Molar mass of octane/ g mol^{-1}	112.224
Universal gas Constant (R)/	0.08206
Temperature/ K	298
Pressure/ Atm	1
Mass of Octane	0.04921
Moles of Octane	0.00044
Volume of Octane/ mL min^{-1}	10.723
Hydrocarbon : oxygen	1
Moles of oxygen	0.00044
Volume of oxygen/ mL min^{-1}	10.723
Moles of air	0.00209
Volume of air/ mL min^{-1}	51.0618
GHSV/ h^{-1}	5823.83
Volume of Catalyst/ mL	1
Total gaseous feed/ mL min^{-1}	97.0639
Volume of Nitrogen (from air)/ mL min^{-1}	40.3388
Volume of Nitrogen (individually)/ mL min^{-1}	46
Total Volume of Nitrogen/ mL min^{-1}	86.3388
Fuel : Total feed ratio	11.0473
Fuel : air ratio	21

Appendix B

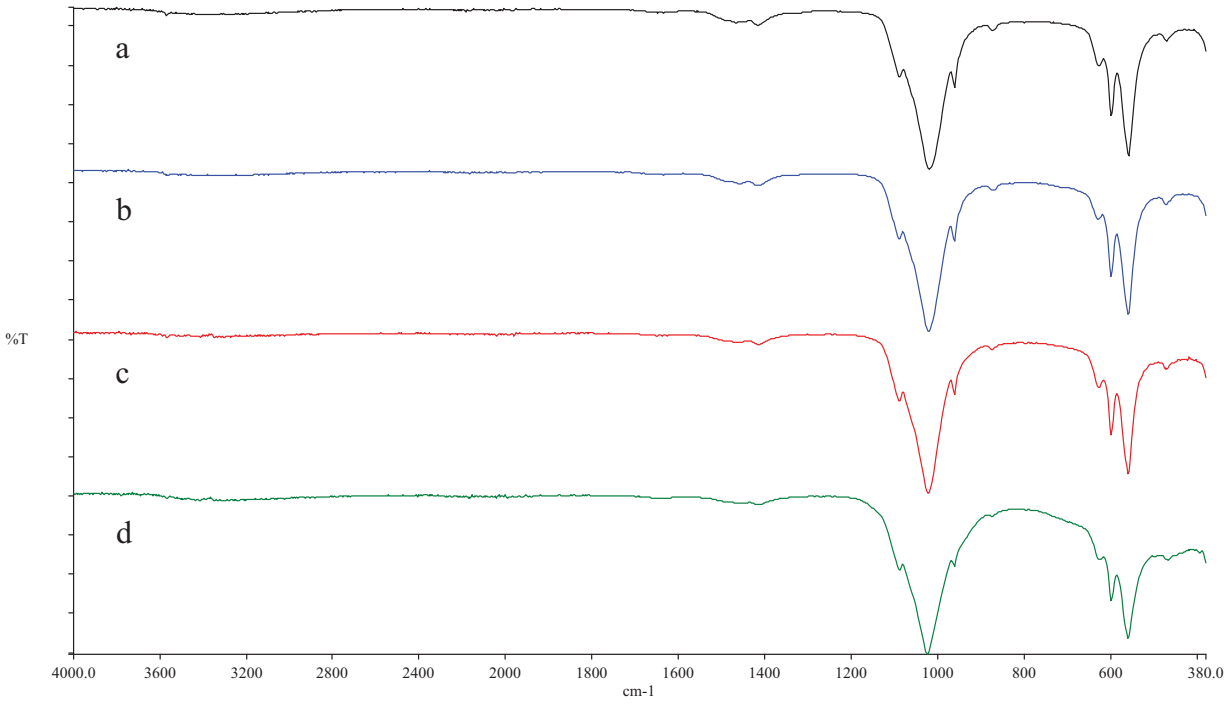

Figure B1: FTIR spectra of (a) HAp, (b) 1-WET, (c) 3-WET and (d) 9-WET

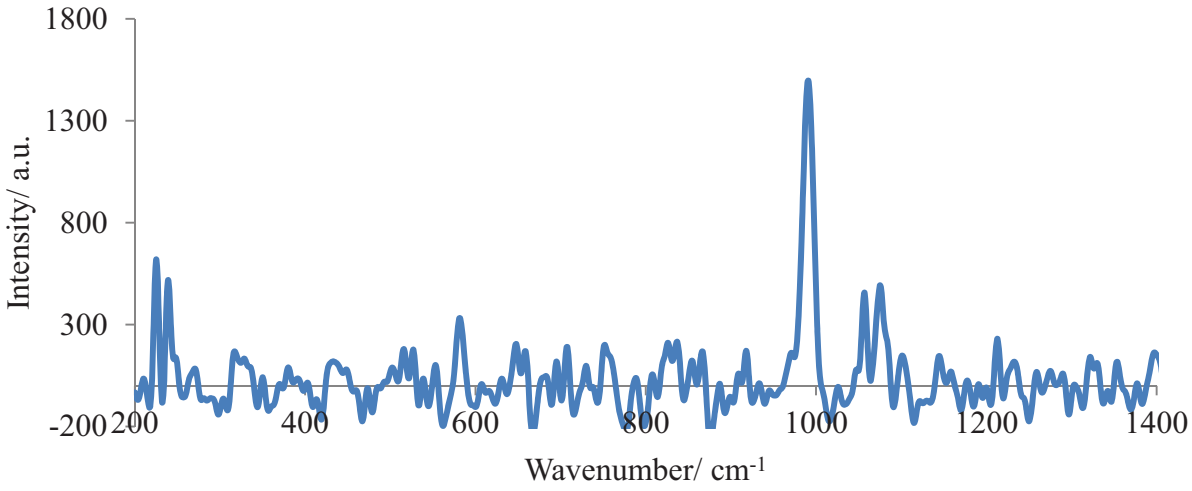

Figure B2: Raman spectrum of the 1-WET catalyst

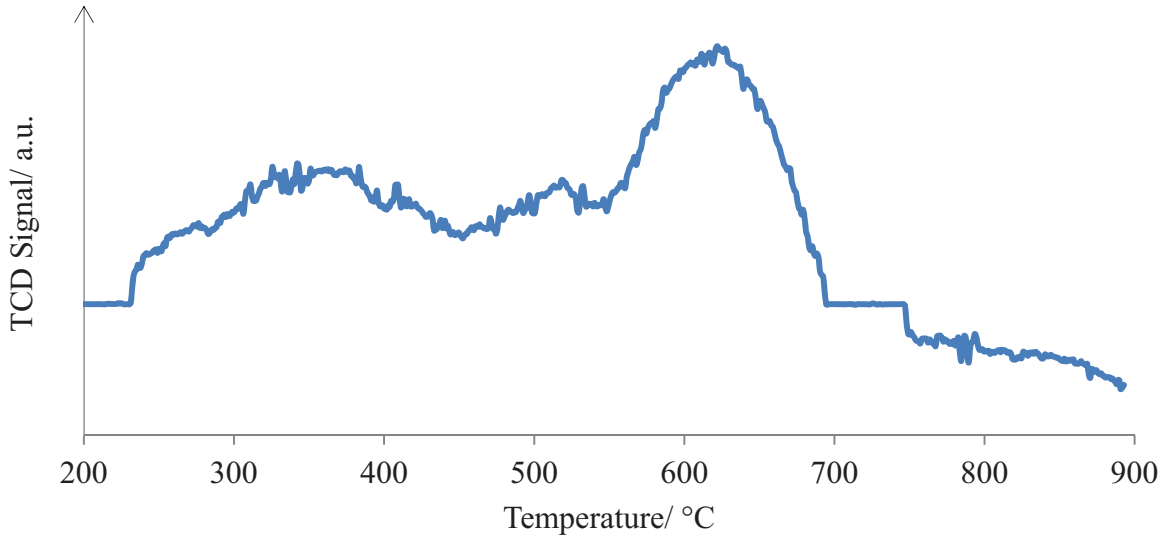

Figure B3: Temperature programmed reduction profile of the 1-WET catalyst

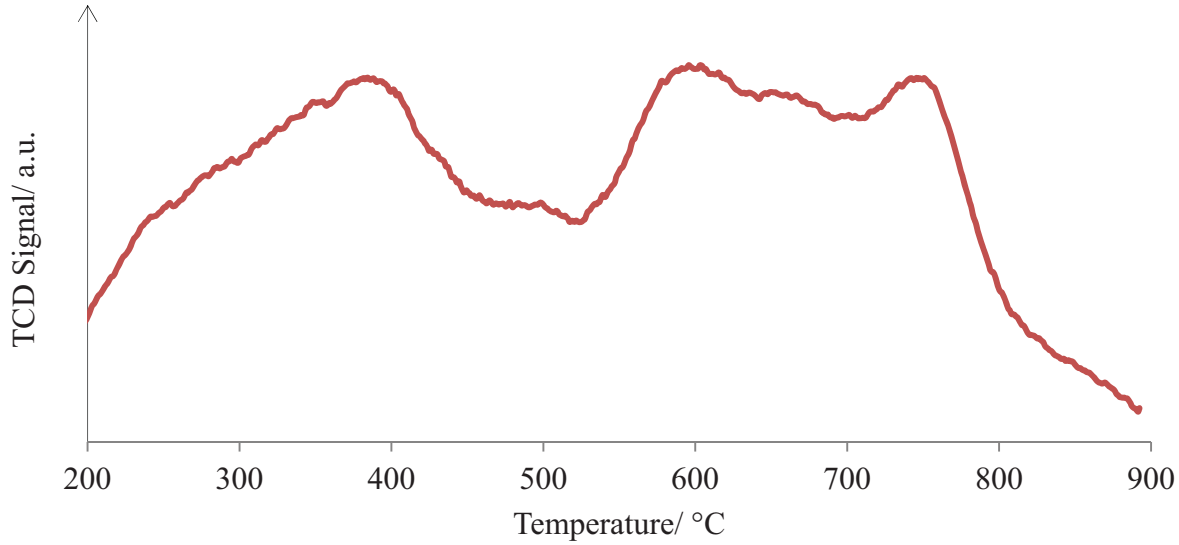

Figure B4: Temperature programmed reduction profile of the 3-WET catalyst

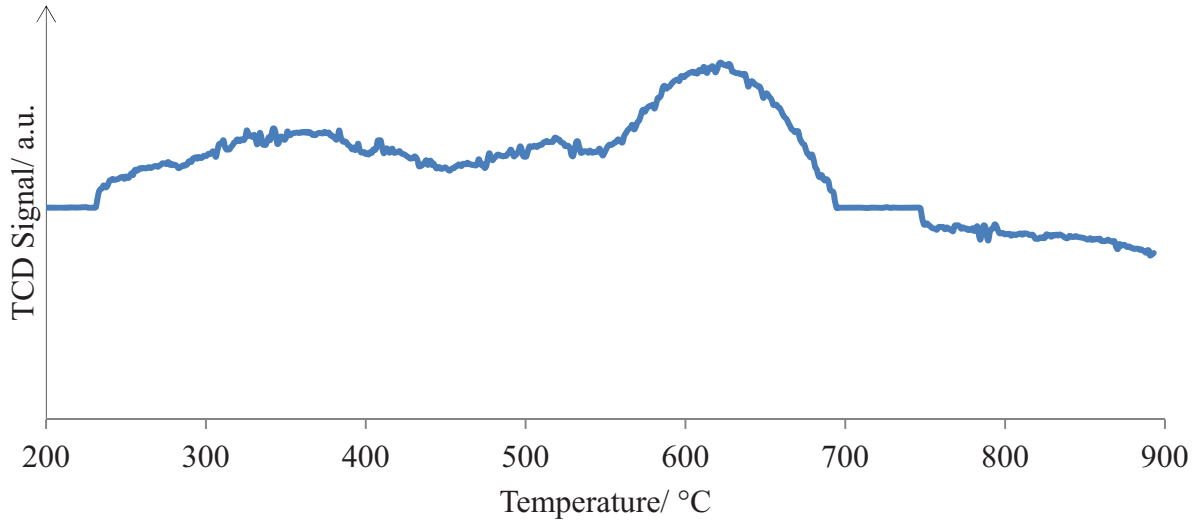

Figure B5: Temperature programmed reduction profile of the 1-COP catalyst

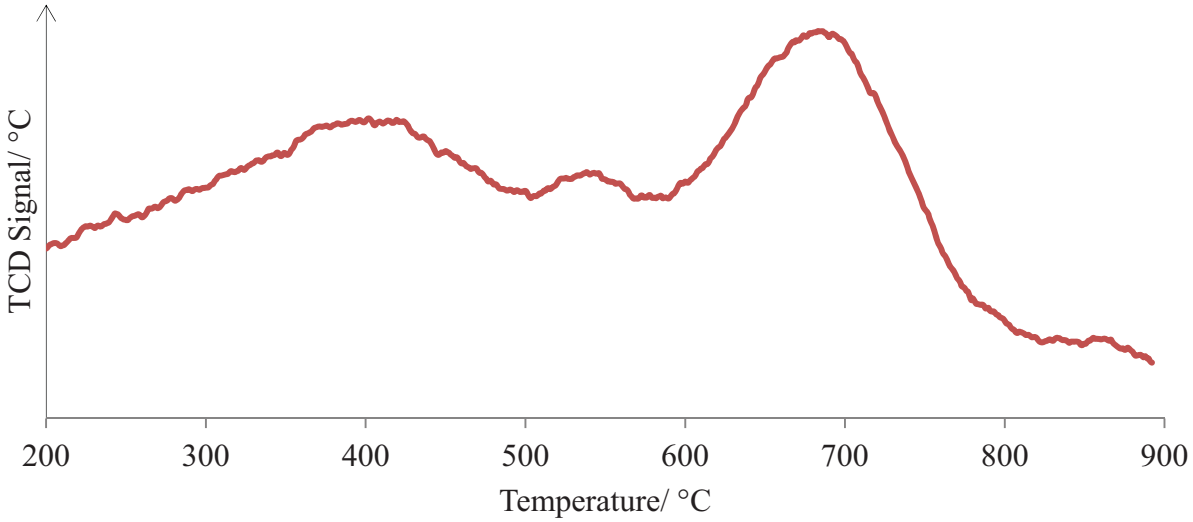

Figure B6: Temperature programmed reduction profile of the 3-COP catalyst

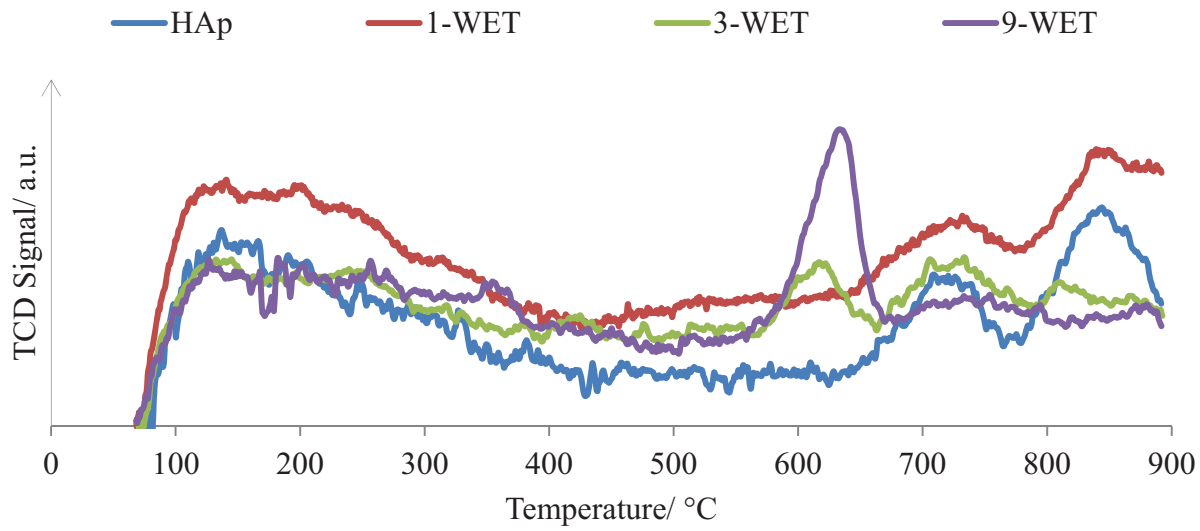

Figure B7: Temperature programmed CO_2 desorption profiles of HAp and the supported iron HAp catalysts

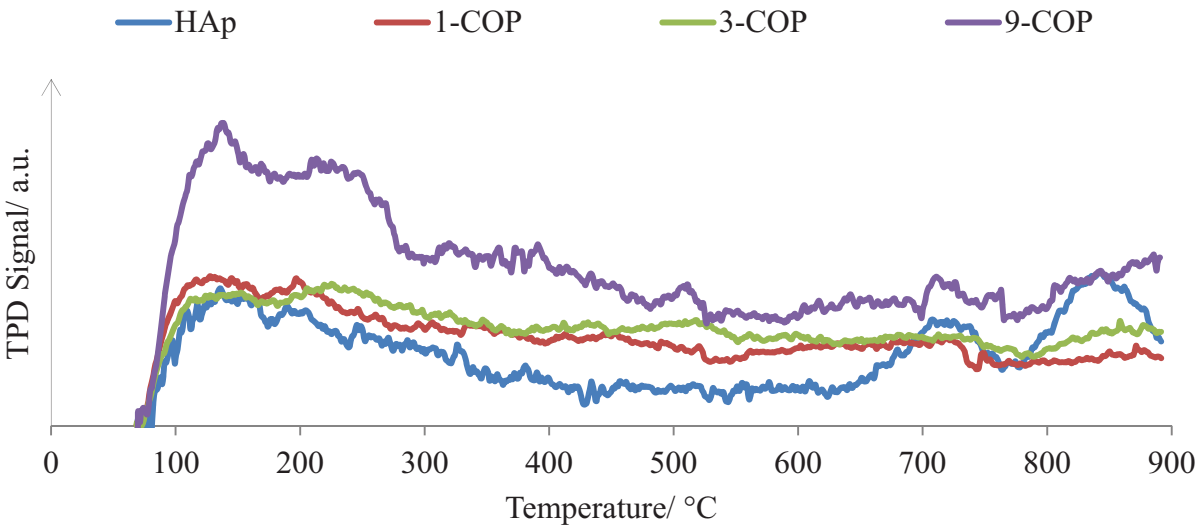

Figure B8: Temperature programmed CO_2 desorption profiles of HAp and the iron substituted HAp catalysts